Distribution Agreement

In presenting this thesis or dissertation as a partial fulfillment of the requirements for an advanced degree from Emory University, I hereby grant to Emory University and its agents the non-exclusive license to archive, make accessible, and display my thesis or dissertation in whole or in part in all forms of media, now or hereafter known, including display on the world wide web. I understand that I may select some access restrictions as part of the online submission of this thesis or dissertation. I retain all ownership rights to the copyright of the thesis or dissertation. I also retain the right to use in future works (such as articles or books) all or part of this thesis or dissertation.

Signature:

_____ _____

James W. Vickers Date

Water Oxidation by the All-Inorganic Homogeneous Catalyst $[Co_4(H_2O)_2(\alpha\text{-}PW_9O_{34})_2]^{10-}$: System Optimization, Stability Considerations, and Kinetic Analysis

By

James W. Vickers
Doctor of Philosophy

Chemistry

_____

Craig L. Hill, Ph.D.
Advisor

_____

Cora MacBeth, Ph.D.
Committee Member

_____

Khalid Salaita, Ph.D.
Committee Member

Accepted:

_____

Lisa A. Tedesco, Ph.D.
Dean of the Graduate School

_____

Date

Water Oxidation by the All-Inorganic Homogeneous Catalyst $[Co_4(H_2O)_2(\alpha\text{-}PW_9O_{34})_2]^{10-}$: System Optimization, Stability Considerations, and Kinetic Analysis

By

James W. Vickers
Bachelor of Science, Chemistry, University of North Florida, 2009

Advisor: Craig L. Hill, Ph.D.

An abstract of

A dissertation submitted to the Faculty of the James T. Laney School of Graduate Studies of Emory University in partial fulfillment of the requirements for the degree of

Doctor of Philosophy in Chemistry

2015

Abstract

Water Oxidation by the All-Inorganic Homogeneous Catalyst $[Co_4(H_2O)_2(\alpha\text{-}PW_9O_{34})_2]^{10-}$: System Optimization, Stability Considerations, and Kinetic Analysis

By James W. Vickers

Since the initial report of homogeneous water oxidation activity from the polyoxometalate complex $[Co_4(H_2O)_2(\alpha\text{-}PW_9O_{34})_2]^{10-}$ (**Co_4PPOM**) in 2010 it has been cited over 500 times, with studies examining its activity in a wide variety of systems under various conditions. Immediately following this publication, we show incorporation of the complex into a light-driven system where it maintains its activity and produces a turnover frequency several times faster than other homogeneous water oxidation catalysis (WOC) complexes to date under optimized conditions. Although this study reported several control experiments, supplemental to the seven in its initial report, work examining this catalyst in different systems suggested that the complex was not responsible for the WOC activity observed, but that this activity was instead derived from dissociation or decomposition products of the parent structure. Here we developed a series of experiments providing strong evidence that under the conditions initially reported for water oxidation using **Co_4PPOM** it functions as a molecular catalyst, not a precursor for cobalt oxide (CoO_x). Specifically, we quantify the amount of Co^{2+}(aq) released from **Co_4PPOM** by two methods, cathodic adsorptive stripping voltammetry and inductively coupled plasma mass spectrometry, and show that this amount of cobalt – whatever speciation state it may exist in – cannot account for the observed water oxidation. We document that water oxidation catalyzed by **Co_4PPOM**, Co^{2+}(aq), and CoO_x have different dependences on buffers, pH, and WOC concentration. Extraction of **Co_4PPOM**, but not Co^{2+}(aq) or CoO_x into toluene from water, and other experiments further confirm that **Co_4PPOM** is the dominant WOC. However, problems persist in studying some of the most basic aspects of WOCs including acquisition of satisfactory early-reaction-time kinetics and rapid quantification of O_2 formation. To this end, two new methods for evaluating homogeneous WOCs by reaction with a stoichiometric oxidant are presented which eliminate problems of incomplete fast mixing and O_2 measurement response time. These methods generate early-reaction-time kinetics that have previously been unavailable, and the data they produce is used to develop and evaluate mechanistic aspects of WOCs.

Water Oxidation by the All-Inorganic Homogeneous Catalyst $[Co_4(H_2O)_2(\alpha\text{-}PW_9O_{34})_2]^{10-}$: System Optimization, Stability Considerations, and Kinetic Analysis

By

James W. Vickers
Bachelor of Science, Chemistry, University of North Florida, 2009

Advisor: Craig L. Hill, Ph.D.

A dissertation submitted to the Faculty of the James T. Laney School of Graduate Studies of Emory University in partial fulfillment of the requirements for the degree of

Doctor of Philosophy in Chemistry

2015

Acknowledgments

I would like to first thank my advisor, Dr. Craig Hill. He has taught me the crucial importance of being careful and through above all else. He has been my advisor not only in chemical concepts, but in navigating my academic path. I greatly appreciate all of the members of the Hill lab past and present. It is a testament to Dr. Hill how collaborative his lab is. The guidance of Dr. Yurii Geletii has been monumental in my development as a chemist. He showed me the benefit of the occasional 'kitchen chemistry' before you get serious, and always kept my best interests in mind. Dr. Kevin O'Halloran for his mentorship and precise synthetic technique, Jordan Sumliner for his unique perspective and electrochemical prowess, Elliot Glass for his appreciation of good-quality crystals, Hongjin Lv for his diligence and demand for perfection, Dr. Jie Song, Dr. Zhen Lou, Dr. John Fielden, Dr. Guibo Zhu, Dr. Chongchao Zhao, Weiwei Guo, Kevin Sullivan, Sarah Lauinger, Mooeung Kim, Daniel Collins-Wildman, Marika Wieliczko, Yimu Hu, as well as Dr. Djamaladdin G. Musaev, Dr. Tim Lian, Dr, D. Khalid Salita, and Bryan Dyer.

No one at Emory has been more welcoming to me than Dr. Cora MacBeth. She would always include me in group activities and would always make time to answer my questions, science or otherwise. Dr. Teddy Huang has been a true mentor to me from my first day in lab to the present. He helped me understand that there is a time to study and a time for action. He is a natural born leader both in and outside of the classroom and I would follow him in any pursuit. Ben Yin is perhaps the most intelligent graduate student that I have ever had the pleasure of working with as anyone whom has spoken with him for five minutes can attest, and always game for a spirited conversation. I would like to thank Ann Dasher for always keeping me on track, and always looking out for me.

I would like to acknowledge Dr. Brandon Green for introducing me to the work of John Dwyer, Dr. Kevin Yehl for teaching me the importance of a good trick, Pi Alpha Vice President Eric Miller, Dr. Omar Villanueva of the 5th floor crew, Dr. Jen Bon, Dr. Erin Schuler, Dr. Brooke Katzman, Pravin Muthu, and Matt Lindale for their friendship. I would like to thank Robin Higgins for helping me through some of the thick of it. I would like to thank Kennedy C. McCullough, John C. Cutworm, Lolly C. Beck-Pancer, Ian Goldlust, Ciara Cordasco, Dr. Marcus Bagnell, Max Boyajian, Zarak Khan, Adam Lipus, Richard Barfield, Kellie Vinal, Chris Chenot, Matt Five, Ashley Ellis, Beca Grimm, Radric Davis, Keith Morris, Maria Corrigan, and John Steen for their friendship and council, without which this process would have been much less enjoyable.

I would like to thank my mother, Laura Vickers for her continued support in all of my endeavors, I would not have made it half this far without her encouragement; and my brother Grayum Vickers.

I would like to thank my employers and friends at EIE Materials, Inc. Rob Nordsell, Dr. Jonathan Melman, and Dr. Mike Holmes for their leadership and showing me how things get done in industry.

I would like to acknowledge the U.S. DOE, Office of Basic Energy Sciences, Solar Photochemistry Program, and the ARCS Foundation for funding my research.

Dedication

To my late father, Grayum Vickers, who reportedly, would be so proud his shirt buttons would be popping off his chest.

Table of Contents

List of Figures

List of Tables

List of Schemes

List of Abbreviations

A	sacrificial electron acceptor
bpy	2,2’-bipyridine
bpy'	partially oxidized 2,2’-bipyridine
CAdSV	cathodic adsorptive stripping voltammetry
CAPS	*N*-cyclohexyl-3-aminopropanesulfonic acid
Co_{app}	cobalt containing species including: aqueous Co^{2+}, a Co(II)-POM fragment, or any other Co(II)-containing species
Co_4PPOM	$Na_{10}[Co_4(H_2O)_2(\alpha\text{-}PW_9O_{34})_2]$
Co_4VPOM	$Na_{10}[Co_4(H_2O)_2(VW_9O_{34})_2]$
CoO_x	cobalt oxide
DLS	dynamic light scattering
DMG	dimethylglyoxime
DPV	differential pulse voltammetry
E^0	standard cell potential
$E_{1/2}$	half-cell potential
e^-	electron
EA	elemental analysis
ET	electron transfer
FT-IR	Fourier transform infrared spectroscopy
FTO	fluorine doped tin oxide
GC	gas chromatography
HEPES	2-[4-(2-hydroxyethyl)piperazin-1-yl]ethanesulfonic acid
HG	Yin, *et al. Science* **2010**, *328*, 342

I	emission intensities of $[Ru(bpy)_3]^{2+*}$ in the presence of persulfate
I_0	emission intensities of $[Ru(bpy)_3]^{2+*}$ in the absence of persulfate
ICP-MS	inductively coupled plasma mass spectrometry
i_p	voltammogram peak current
IrPPOM	$K_{14}[(IrCl_4)KP_2W_{20}O_{72}]$
ITO	indium tin oxide
l	optical path length
LMCT	metal-to-ligand charge transfer
k_n	rate constant for reaction n
K_n	equilibrium constant for reaction n
LoD	limit of detection
M_3	group of three MO_6 units
MO_6	octahedra with approximate octahedral symmetry
NaB_i	sodium borate buffer
NaP_i	sodium phosphate buffer
NHE	normal hydrogen electrode
Ni_5SiPOM	$K_{10}H_2[Ni_5(OH)_6(OH_2)_3(SiW_9O_{33})_2]$
OEC	oxygen evolving center
PCET	proton-coupled electron transfer
PEC	photoelectrochemical
PIPES	piperazine-*N,N*′-bis(2-ethanesulfonic acid)
POM	polyoxometelate
PS	photosensitiser
PSII	Photosystem II
PW_{12}	plenary Keggin $[PW_{12}O_{40}]^{3-}$

RPM	revolutions per minute
$[Ru(bpy)_3]^{2+}$	Tris(2,2'-bipyridyl)dichlororuthenium(II) hexahydrate
$[Ru(bpy)_3]^{3+}$	Tris(2,2′-bipyridyl)triperchlororuthenium(III)
Ru_4PPOM	$Cs_9[(\gamma\text{-}PW_{10}O_{36})_2Ru_4O_5(OH)(OH_2)_4]$
Ru_4SiPOM	$Rb_8K_2[\{Ru_4O_4(OH)_2(H_2O)_4\}(\gamma\text{-}SiW_{10}O_{36})_2]$
Ru_2ZnPOM	$Na_{14}[Ru_2Zn_2(H_2O)_2(ZnW_9O_{34})_2]$
SF	Stracke and Finke *J. Am. Chem. Soc.*, **2011**, *133*, 14872
SSB	Scandola, Sartorel, Bonchio *et al.*, *Chem. Commun.*, **2012**, *48*, 8808
SYS-114	magnetically-coupled stirring system SPECTROCELL
THpABr	tetra-*n*-heptylammonium bromide
TMS-POM	transition-metal-substituted polyoxometalate
TOF	turnover frequency
TON	turnover number
UV-Vis	ultraviolet-visible
WOC	water oxidation catalyst
XO_4	tetrahedral heteroatom of a polyoxometalate
$\Delta\text{-}PW_9O_{34}$	mixture of A- and B-type $Na_9[A\text{-}PW_9O_{34}]\cdot 4H_2O$
ε	molar extinction (or absorption) coefficient
ε_n	molar extinction coefficient at wavelength n
λ	wavelength
λ_{max}	wavelength where maximum absorbance occurs
ν	scan rate
ϕ_r	yield of the oxidation of $[Ru(bpy)_3]^{2+}$ to $[Ru(bpy)_3]^{3+}$ by sulfate radical ions $SO_4^{-\cdot}$

ϕ_c	yield of O_2 produced from $[Ru(bpy)_3]^{3+}$ in the presence of the catalyst
ϕ_q	quenching efficiency, or electron transfer efficiency
Φ_{CY}	chemical yield
Φ_{QY}	quantum yield

Chapter 1

Introduction:

Polyoxometalates as Water Oxidation Catalysts: A Step Towards Energy Sustainability

Hongjin Lv, Yurii V. Geletii, Chongchao Zhao, James W. Vickers, Guibo Zhu, Zhen Luo, Jie Song, Tianquan Lian, Djamaladdin G. Musaev and Craig L. Hill. *Chem. Soc. Rev.*, **2012**, *41*, 7572 – 7589 - Reproduced in part by permission of The Royal Society of Chemistry

1.1 Motivation – Earth in trouble

We are swiftly approaching a point where our global energy demands outweigh conventional production. There are many scientific models which point to the need to rapidly develop an energy economy based on renewable sources.[1-3] The problem with our current petroleum-based energy usage is two-fold. On the one hand petroleum fuels are becoming increasingly scarce as it took millions of years to create the reserves that we are rapidly depleting. If we continue to consume these fuels at our current rate we will shortly run out of them.[4-6] On the other hand, the more pressing question is not how much of these energy reserves remain, but the effect that extracting and consuming them will have on the planet. The consumption of petroleum fuels is having a massive effect on the global climate, largely due to production of the greenhouse gas CO_2. Scientific models suggest that unless there is a major shift in CO_2 production within this century, there will be irreversible damage to the Earth's climate.[1-6]

Exacerbating the situation, governments refuse to take meaningful action to mitigate this problem either through the implementation of policy or to properly fund efforts to produce a sustainable fuel source. For example, the United States allocates only 3% of its annual budget for energy and environment while spending well more than half on the military, making it not only the nation that spends the most on defense, but spends more than the next ten countries combined(**Figure 1-1**).[7]

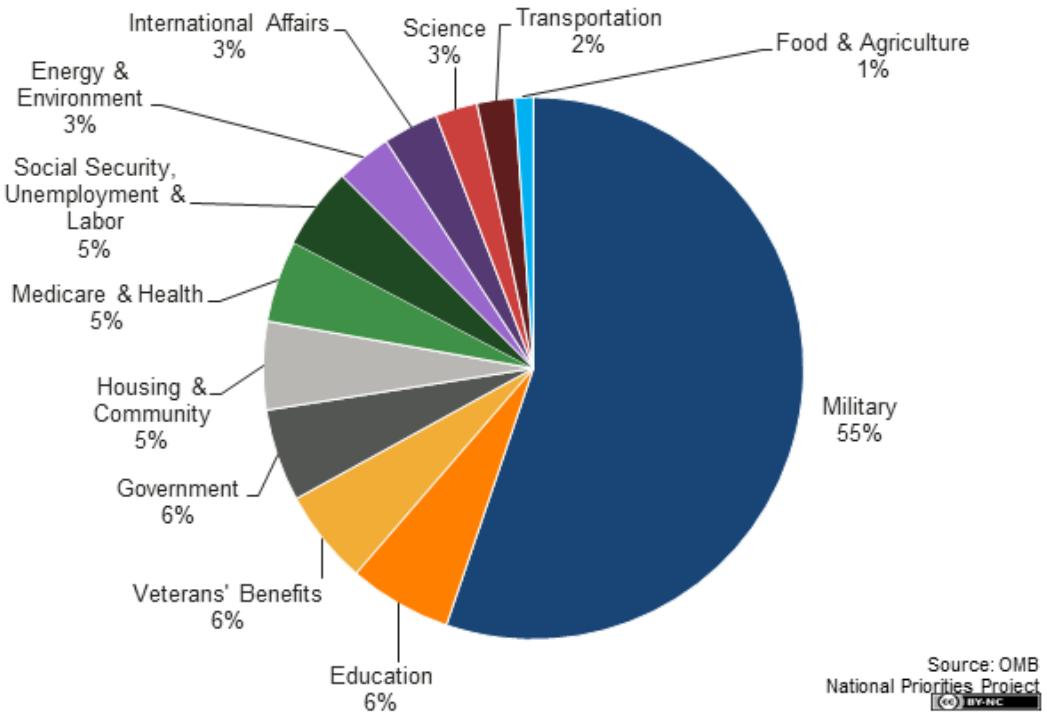

Figure 1-1. United States of America president's proposed discretionary spending for the 2015 fiscal year.[8]

Various alternative energy sources are being explored as potential replacements to our current energy infrastructure including biomass, wind, hydro-thermal, and solar. One thing that each of these sources share is that the energy they provide is ultimately derived from the sun. Plants burned as biomass power their growth with sunlight, the winds move from temperature gradients produced from the sun's heat, and photovoltaics capture certain wavelengths of the sun's radiant energy directly. Only solar energy and nuclear energy have the capabilities to meet our high usage demands. Even so, nuclear energy has several shortcomings which will prevent it from being adopted on a global scale. Aside from public distrust, there is no way of disposing of the waste from these reactors. Finally nuclear fission is widely thought to be unobtainable in the near future due to a number of

scientific and engineering challenges.[9-12] Thus the only seemingly viable option for a global scale renewable source of energy involves capture and transformation of solar energy.[13,14]

Sunlight offers very promising potential as a global energy source. A tremendous amount of sunlight that reaches the Earth's surface. While the current global energy demand is approximately 16 TW, well over 100 TW arrives as harvestable light.[15-17] Thus the problem lies not in the availability of energy, but in harnessing and storing sunlight energy in a useful form. While photovoltaics are convenient, they must be coupled with an energy storage system since the sun is an intermittent power source. There have been recent efforts to promote batteries as energy storage systems, however, batteries are expensive, must be charged, wear out over time, and lack the energy density to power large boats or planes.[18] The alternative is to store solar energy in chemical bonds, i.e. as a fuel. There are two general pathways to store energy in chemical bonds: the reduction of water to hydrogen gas (**Equation 1-1**) where the hydrogen can be consumed by burning or as a feedstock directly for industrial processes, or the reduction of carbon dioxide into a fuel such as methane or methanol (**Equations 1-2**, **1-3**). Hydrogen gas is a promising fuel in that it produces only water as a waste product from its combustion. However, many challenges remain in procuring and distributing the large quantities of hydrogen that would be required to support our growing global needs. There are known catalytic cycles for the production of H_2 but all fall short of being applicable on a large scale.[19]

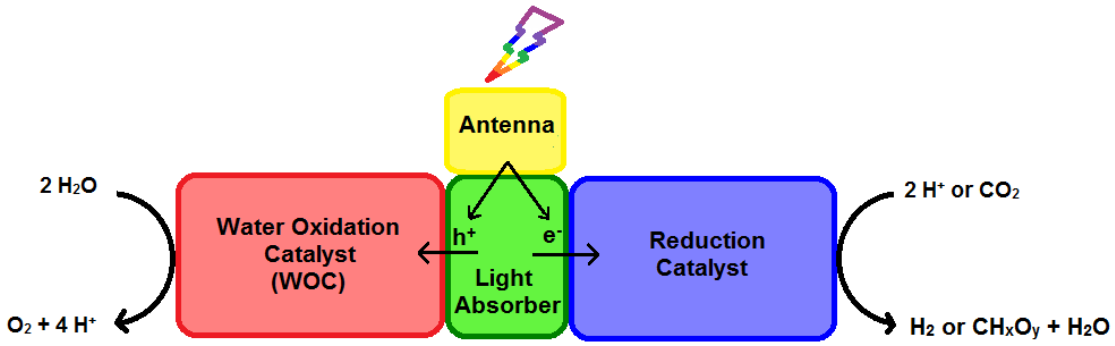

Scheme 1-1. Solar fuel production overview where the capture of light results in a charge-separated excited state. Electrons are funneled towards the reduction side where a catalyst reduces protons to water or CO_2 to methane or methanol, and holes are funneled towards a water oxidation catalyst that oxidizes water to dioxygen.

Several examples of complete water splitting systems powered by visible light and free of an external driving force have been reported which largely rely on semiconductors. Known systems include those based on amorphous silicon,[20,21] II-V semiconductors,[22] dye-sensitized solar cells,[23] among others.[24-27] The efficientreduction of carbon dioxide is often referred to as the holy grail of artificial photosynthesis, as it is also part of a carbon neutral cycle and the fuels produced are easier to store than hydrogen. To date, no complete system for CO_2 reduction by visible light has been reported, but a few systems employing UV light have.[28-32] The low potentials for CO_2 reduction are misleading as they do not reflect the kinetic concerns associated with multiple proton-coupled-electron-transfer events, as such, much work still remains before such processes are applicable on a global scale. One feature these two distinct fuel-production possibilities share is that they both require an oxidation process to complete the photosynthetic cycle, namely, the oxidation of water into dioxygen (**Equation 1-4**). This process has been identified as a bottleneck for a sustainable energy system requiring its own catalyst. Coupling of **Equations 1-1** and **1-4** plus sunlight results in **Equation 1-**

5 and constitutes the complete cycle referred to as water splitting. An overview of a complete cycle is presented in **Scheme 1-1**.

$2\ H^+ + 2\ e^- \rightarrow H_2$ $E^0 = 0.00$ V (**1-1**)

$CO_2 + 8\ H^+ + 8\ e^- \rightarrow CH_4 + 2\ H_2O$ $E^0 = -0.24$ V (**1-2**)

$CO_2 + 6\ H^+ + 6\ e^- \rightarrow CH_3OH + H_2O$ $E^0 = -0.38$ V (**1-3**)

$H_2O \rightarrow 2\ H^+ + ½\ O_2 + 2\ e^-$ $E^0 = 1.23 + 0.059$ V/pH (**1-4**)

$H_2O + \text{sunlight} \rightarrow H_2 + ½\ O_2$ (**1-5**)

1.2 Water oxidation considerations

Water oxidation catalysts (WOCs) are generally classified as either homogeneous or heterogeneous, each having their own advantages and disadvantages. Both areas constitute active fields of research. Heterogeneous catalysts are predominantly more stable and are cheaper and easier to produce in large quantities. However, this comes at the cost of being less selective, and slower on a per atom basis. Homogeneous catalysts tend to be faster, with higher selectivity and perhaps most importantly, can be studied far more easily. The ease of quantitative investigation for soluble homogeneous catalysts includes elucidation of their geometric and electronic structures as well as their turnover mechanism. Such detailed molecular-level information leads to more rational optimization of turnover rates, interface chemistry with photosensitizers and stability.

For a homogeneous WOC to be effective it must satisfy several conditions. The catalyst must be able to accumulate four oxidizing equivalents and do so with redox

leveling. Most redox processes in organic synthesis and biology are one or two-electron processes. Processes involving more than two electrons are rare, but among the outliers are photosynthetic water oxidation catalyzed by the oxygen-evolving center (OEC) in Photosystem II (PSII), a four-electron process,[33-39] and nitrogen reduction to ammonia, a six-electron process.[40-42] Redox leveling describes multi-electron processes that proceed over a narrow potential range. In other words, the initial and successive redox events, all of which are needed for the net transformation, take place at closely spaced potentials. Redox leveling is facilitated most prominently in systems that involve coupling of proton transfer events to electron transfer events. Using the four-electron oxidation of water by the OEC as an example, as each successive electron is removed from the Mn_4CaO_4 catalytic core, a proton is also removed to counteract the increase in charge induced by the oxidation. Neutralization of the charge is crucial to keep the energy low. In general, the overall charge on a redox active structure is a major determinant of the ground and excited state potentials of that structure,[43] and without proton-coupled electron transfer (PCET) or some other mechanism to neutralize accumulating charge, the energies for the subsequent electron transfers increase dramatically. This largely precludes energetically facile catalysis of most multi-electron transfer events. The central importance of PCET in multi-electron transfer processes, and in particular the catalysis of such reactions, has been one factor in the popularity of this topic in recent years. There have been numerous recent experimental[44-51] and theoretical[52-56] studies on PCET, and this phenomenon has been addressed in regard to POM systems.[57]

Another requirement in context with artificial photosynthesis is that the WOC must be amenable to interfacing with a photosensitizer without sacrificing any of the other

essential attributes noted above. Additionally, in order to be practical given the projected costs and the potential global scale of solar fuel production, the WOC must be inexpensive to make in bulk. This demands that the WOC and other components be devoid of rare and expensive elements.

While it is known that the only transition metal utilized by PSII to perform its water oxidation is Mn, synthetic WOCs frequently employ other metals in its place, most successfully Ru and Co. The first active molecular catalyst for water oxidation was published by Meyer *et al.*[58] about 30 years ago and the only transition metal it contains is ruthenium. His "blue dimer", $[(bpy)_2(H_2O)RuORu(H_2O)(bpy)_2]^{4+}$ (bpy = 2,2'-bipyridine), bears little to no resemblance to the OEC and undergoes rapid deactivation, however, this work was seminal in establishing the field of synthetic, molecular WOCs.

In order to thoroughly study WOCs without the complications of evaluating the performance of a larger device, the water oxidation reaction is commonly examined by its half reaction (**Equation 1-4**), with sacrificial reagents serving to mimic the reduction reactions necessary to complete the oxidative cycle. Generally there are three types of synthetic water oxidation systems. One class, referred to as "dark" systems makes use of a sacrificial oxidant (Ox) which is consumed during the course of the reaction. The oxidant is used to oxidize the WOC which in turn oxidizes water molecules (**Figure 1-2a)**. Common oxidants include $[Ru(bpy)_3]^{3+}$ (tris(2,2'-bipyridyl)triperchlororuthenium(III)) and Ce(IV). Another class referred to as "light-driven" systems employs a photosensitiser (PS) which is able to capture photons to create a charge separated excited state PS^* (**Figure 1-2b**). The excited PS^* which is typically the triplet metal-to-ligand charge

transfer (LMCT) excited state of $[Ru(bpy)_3]^{2+}$ or a derivative thereof, is then quenched by a sacrificial electron acceptor (A), frequently sodium persulfate ($Na_2S_2O_8$), which

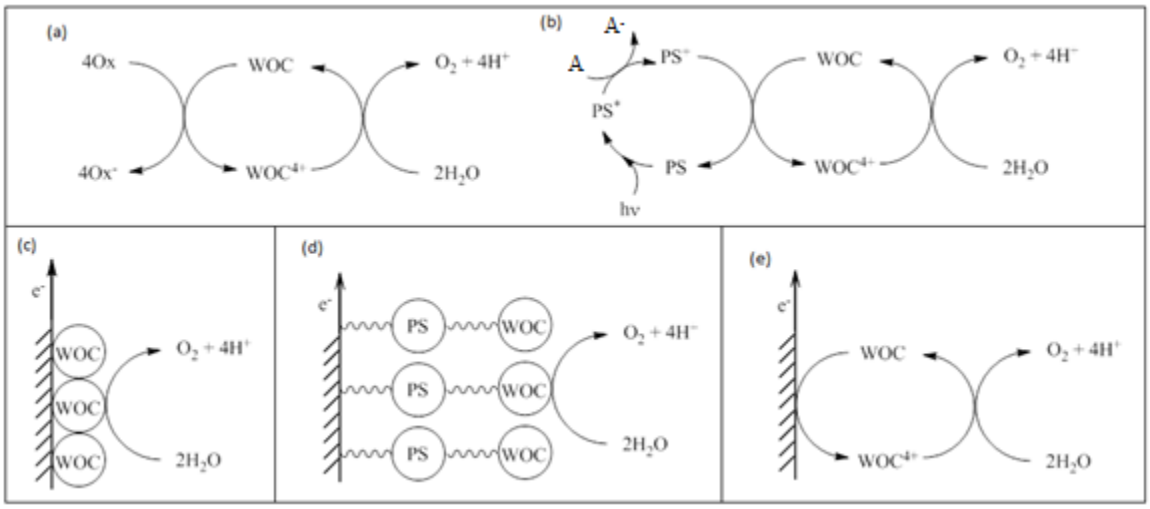

Figure 1-2. Synthetic water oxidation systems (a) "dark" system with sacrificial oxidant (Ox) consumed during reaction. (b) "light-driven" system with (PS) to capture photons and create excited state PS^* quenched by a sacrificial electron acceptor (A), oxidizing the PS^* by one electron to PS^+, oxidizes the WOC. An electrochemical system with (c) heterogeneous catalyst. (d) catalyst connected by linker. (e) homogenenous catalyst.

oxidizes the PS^* by one electron to PS^+. Then as in the dark system, the PS^+ oxidizes the WOC, which in turn oxidizes water molecules. The PS may simply interact with the catalyst electrostally, be attached to the WOC by a linker group to create a supramolecular or dyadic WOC (**Figure 1-2d)**, or as in the case of the blue dimer, the PS may also be the WOC. These two classes generally fall into the wider category of multi-component homogeneous systems. The third class called electrochemical or photoelectrochemical (PEC) systems include a diverse group of catalytic systems. The catalyst may be a heterogeneous metal oxide directly deposited on the surface of the

working electrode (**Figure 1-2c**), a molecular catalyst connected to the electrode by a linker or contained in a porous matrix (**Figure 1-2d**), or a homogeneous molecular catalyst that is freely diffusing in solution (**Figure 1-2e**). The commonality of these systems is that instead of requiring a sacrificial electron acceptor or oxidant, the electrons flow due to an applied bias from the working electrode, oxidizing the catalyst, which in turn oxidizes water molecules. In PEC systems, the working electrode is a photoanode such as TiO_2 or α-Fe_2O_3 where the absorption of photons generates a photocurrent. This current is often not sufficient to drive the system alone and a bias must be applied. Additionally, a PS may be complexed with a WOC deposited on the electrode surface to facilitate electron flow and thus redox processes.

1.3 General POM background

POMs are early transition metal oxygen anion clusters that spontaneously form in water when either soluble, molecular monomeric transition metal precursors such as $[WO_4]^{2-}$ or insoluble metal hydroxides or oxides such as WO_3 hydrate or V_2O_5 are adjusted to the appropriate pH.[59-69] The most abundant POMs are based on W(VI), Mo(VI), V(V), V(VI), Nb(V) or Ta(V) in that order. Thousands of polyoxotungstates (polytungstates) have been reported, yet examples of polytantalates are rare. The fundamental acid-base and hydrolytic properties of these POM-forming elements dictate that polytungstates, polymolybdates and polyvanadates form in and are compatible with lower pH values, while the polyniobates and polytantalates form in and are compatible with higher pH values.[70,71] Mixing these elements in an appropriate synthesis, for example, to prepare polytungstoniobates makes the resulting POM hydrolytically stable

in intermediate pH values. Most POMs contain one or more heteroatoms, typically p or d block elements found in one or more positions internal to the polyanion unit. These "heteropolyanions" tend to be stable hydrolytically over wider pH ranges than the isopolyanions which contain only the metal and oxygen atoms as exemplified by $[W_{10}O_{32}]^{4-}$, $[Mo_7O_{24}]^{6-}$, and $[V_{10}O_{28}]^{6-}$.[69]

There are many classes of POMs that are categorized by their overall structure, the most known and studied of which are the Keggin and Wells-Dawson structures. The Keggin structure (of which there are several isomers) is utilized in this work and is of the general formula $[XW_{12}O_{40}]^{n-}$. In the α isomer the heteroatom X (typically P, Si, or Ge although many elements in the periodic table have been reported including many transition metals) is in the center with tetrahedral geometry surrounded by four oxygen atoms. The overall structure is based around this unit and has T_d symmetry. This central unit is surrounded by twelve MO_6 octahedra, each with approximate O_h symmetry which are grouped into units of three (M_3 units). Each of these M_3 units shares an oxygen atom with the central XO_4 unit, and is linked to itself and the others units by oxygen atoms shared at the corners (**Figure 1-3**). Rotation of a M_3 groups by 60º (or a C_3) results in the β isomer, rotation of adjacent M_3 groups results in the γ, δ, and finally the ε isomer in which all of the M_3 group have been rotated. POMs such as the Keggin structure are referred to as "plenary" because they are complete polyhedral, i.e. no atoms have been removed. Like most plenary POMs, the Keggin structure is soluble in water, stable in air, and stable toward oxidation or reduction.

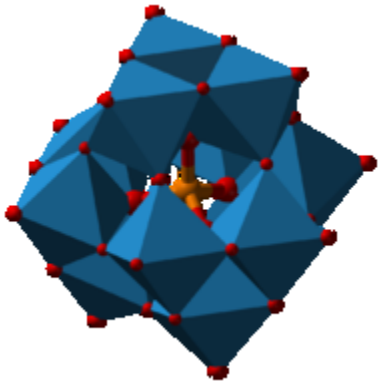

Figure 1-3. Keggin-type α-isomer POM. Blue polyhedral, MO_6 units; red balls, oxygen atoms; orange ball and stick, XO_4 tetrahedral heteroatom.[72]

Figure 1-3 illustrates the common plenary Keggin structure. Removing one or more of the MO groups results in what is referred to as a lacunary structure. Lacunary structures of the Keggin type can be experimentally prepared from the corresponding plenary structure by cleaving some of the MO groups or prepared directly from starting oxides. While these lacunary structures are sometimes of interest themselves, they are mostly utilized as ligands to incorporate other transition metals forming transition-metal-substituted polyoxometalates (TMS-POMs). It is common in the literature for these to simply be referred to as POMs as well. The PW_9 lacunary Keggin type structure is formed by the removal of three octahedral WO_6 units from the $[PW_{12}O_{40}]^{3-}$ (PW_{12}) plenary Keggin by treatment with base and is thus referred to as trivacant. If the three WO_6 units removed compose a M_3 unit, the resulting lacunary PW_9 Keggin is B-Type, if instead, one WO_6 unit is removed from three separate M_3 units, the structure is A-type; each of these structures also have α, β, and γ isomers. Thus the thousands of polytungstates made to date barely[73] scratch the surface of the structures that are, in principal, possible and synthetically accessible. Many of the polytungstates are prepared

in one-pot condensation reactions at the right pH and ionic strength, however, many POMs in recent years are made by multi-step reactions as in conventional, serial organic synthesis.[59,72]

POMs have applications in several areas including medicine,[74-87] magnetism,[88-92] high performance materials, chirality,[93-102] and others.[103] However, the dominant use of POMs is in catalysis.[72,104-118] Several processes have been commercialized where the POM serves either as an acid catalyst or as an oxidation catalyst.

1.4 Background on POMs as WOCs

POMs possess many physical and chemical properties that make them ideal candidates for water oxidation catalysts. As mentioned above, they can coordinate a number of transition metals making their structural and electronic properties highly tunable. As POMs are typically highly negatively charged, there is favorable electrostatic interaction with the common positively charged oxidants. POMs exhibit the best features of both heterogeneous and homogeneous compounds while avoiding many of the disadvantages.[119] They are generally soluble in water, thermally stable, and perhaps most importantly, stable towards oxidation. This is precisely because early transition metals are present in their fully oxidized states with d^0 and in some cases d^1 electronic configurations.[72,120] Since the catalysts and reactants are dissolved in solution, separation of products is often a consideration, however, with water oxidation the product is a gas and is thus easily collected. Stability is the most crucial issue that plagues homogenous

catalysts, however, POMs contain no organic ligands and are incredibly stable, although the specifics of stability will be addressed in a later chapter.[120]

POMs represent a fairly new class of compounds for WOCs. Since the initial report of a POM WOC, these complexes have been examined in a variety of systems including electrochemical, and homogeneous with a variety of oxidants in both the presence and absence of light. The differences in these systems and even the conditions utilized in similar systems can be subtle but produce drastically different results, the effects of which will be discussed in a later chapter. In 2004, Shannon and co-workers reported the first example of water oxidation via a transition-metal-substituted POM, $Na_{14}[Ru^{III}_2Zn_2(H_2O)_2(ZnW_9O_{34})_2]$ (**Ru_2ZnPOM**, **Figure 1-4a**).[121] Electrochemical production of oxygen was observed using pulsed voltammetry in 0.1 M sodium phosphate buffer (pH 8.0) solution. A catalytic current corresponding to oxygen production was observed when the working electrode potential was stepped repeatedly to a positive value. The calculated $E_{1/2}$ of ~0.750 V for electrocatalytic oxygen evolution approaches the thermodynamic value of ~0.760 V *vs.* NHE for water oxidation. The **Ru_2ZnPOM** structure is adapted from earlier work by Tourné *et al.* which produced a series of chiral POMs based on the structure $[WZn_3(H_2O)_2(ZnW_9O_{34})_2]^{12-}$ containing the WZn_3 in a near planar "belt", sandwiched between two identical $[ZnW_9O_{34}]^{12-}$ units. The Shannon work also reported the mono-ruthenium complex, $[Ru^{III}(H_2O)PW_9O_{39}]^{4-}$ which was inactive for water oxidation under the same conditions.

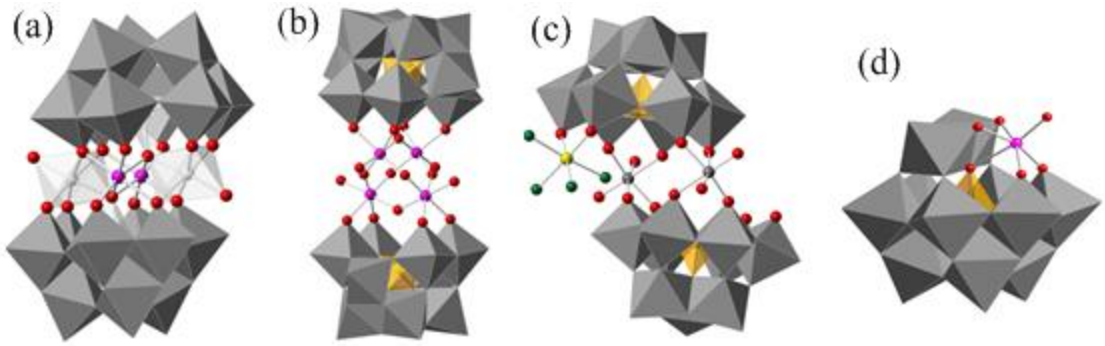

Figure 1-4. X-ray crystal structure of polyoxometalates in combined ball-and-stick and polyhedral representations Red: O; magenta: Ru; yellow: Ir; green: Cl; orange polyhedra: PO_4/SiO_4/GeO_4 as denoted; white polyhedra: ZnO_4/ZnO_6; grey polyhedra: WO_6. (a) $Na_{14}[Ru^{III}{}_2Zn_2(H_2O)_2(ZnW_9O_{34})_2]$ (**Ru_2ZnPOM**), (b) $Rb_8K_2[Ru_4O_4(OH)_2(H_2O)_4(\gamma\text{-}SiW_{10}O_{36})_2]$ (**Ru_4SiPOM)** and $Cs_9[Ru^{IV}{}_4O_5(OH)(OH_2)_4(\gamma\text{-}PW_{10}O_{36})_2]$ (**Ru_4PPOM)** (c) $K_{14}[(IrCl_4)KP_2W_{20}O_{72}]$ (**IrPPOM)**, (d) $Cs_5[Ru^{III}(H_2O)SiW_{11}O_{39}]$ and $Cs_5[Ru^{III}(H_2O)GeW_{11}O_{39}]$

A major breakthrough in POM WOC development was achieved in 2008, when two groups simultaneously reported the synthesis albeit, by different routes, solid state and solution characterization, and homogeneous catalytic water oxidation activity of the tetra-ruthenium polytungstate, $[Ru_4(\mu\text{-}O)_4(\mu\text{-}OH)_2(H_2O)_4(\gamma\text{-}SiW_{10}O_{36})_2]^{10-}$ (**Ru_4SiPOM**). **Figure 1-4b** shows the X-ray crystal structure of **Ru_4SiPOM** where a Ru_4 core is not planar as in **Ru_2ZnPOM**, and the Ru atoms can be described as, "out-of-pocket" in that they are not ligated to the central SiO_4 unit as is typical of POMs of this type.[122,123] The structure has overall D_{2d} symmetry where the two di lucanary γ-$[SiW_{10}O_{36}]$ units are rotated 90º relative to each other around the central C_2 axis of the structure. The large rigid POM ligands are thought to stabilize the redox active Ru_4 core, lowering the reorganization energy for the observed redox process.[124,125] Subsequently **Ru_4SiPOM** was shown to catalyze the oxidation of water with visible light using $[Ru(bpy)_3]^{2+}$ as a

photosensitizer and $S_2O_8^{2-}$ as a sacrificial electron acceptor.[126] The mechanism of **Ru_4SiPOM** catalyzed water oxidation by $[Ru(bpy)_3]^{3+}$ or Ce(IV) oxidants has also been studied in depth:[127-130] **Ru_4SiPOM** was shown to undergo sequential oxidation from $Ru(IV)_4$ resting state to the active $Ru(V)_4$ state.

To take advantage of the tunability of POMs, an isostructural phosphorus **Ru_4SiPOM** analogue, $[Ru_4(\mu\text{-}O)_4(\mu\text{-}OH)_2(H_2O)_4(\gamma\text{-}PW_{10}O_{36})_2]^{n-}$ (**Ru_4PPOM**), was prepared.[131] Two P(V) centers replace the two Si(IV) positions in the central orange XO_4 tetrahedra of **Ru_4SiPOM** (**Figure 1-4b**), resulting in a different charge on the WOC polyanion, which in turn changes the redox potentials of the complex. **Ru_4PPOM** is also an effective WOC albeit with 20% less catalytic activity as a WOC under the same conditions in light-driven water oxidation relative to **Ru_4SiPOM**. Notably, of the multitude of experiments conducted by either the Hill or Bonchio group, under either thermal or photo-driven water oxidation conditions; **Ru_4SiPOM** showed no evidence of hydrolytic decomposition to metal oxides RuO_2 or WO_3

Ru_4SiPOM has been examined in a wide variety of systems and conditions. It was shown to be an effective WOC when electrostatically associated with dendrimers containing amide and amine functionality and bound to conductive multiwalled carbon nanotube scaffolds on indium tin oxide (ITO) elctrodes.[132,133] The oxidation of **Ru_4SiPOM** by photogenerated Ru^{III} oxidants was investigated both in homogeneous and heterogeneous systems.[134] Another study confirmed the formation of a 1:4 stoichiometric ratio ion pair between the highly anionic **Ru_4SiPOM** catalyst and the cationic $[Ru(bpy)_3]^{2+}$ sensitizer.[135] A light-driven WOC study was performed using a tetranuclear Ru(II) dendrimer photosensitizer with red-shifted excitation wavelength.[136] **Ru_4SiPOM**

was also found to function as a molecular propeller associated with bottom-up control of chemically-induced dynamics in nano-devices and functional systems by catalyzing the disproportionation of H_2O_2.[137]

The oxygen evolution activity of **Ru_4SiPOM** examined by flash photolysis shows that a single molecule can catalyze the reduction of about 45 equivalents of $[Ru(bpy)_3]^{3+}$ in 40 ms, corresponding to a very high TOF of 280 s^{-1}. This TOF, however, was calculated assuming that one oxygen molecule is released after four hole-scavenging events instead of using actual oxygen yields generated during experiments.[135] Thus, as will be highlighted in **Chapter 3**, the experimental system and conditions must be the same, or account for differences, if meaningful comparisons of a catalyst are to be made.

The Ir-containing POM, $[(IrCl_4)KP_2W_{20}O_{72}]^{14-}$ (**IrPPOM),** was prepared in which an $IrCl_4$ unit is anchored to a $[KP_2W_{20}O_{72}]^{13-}$ polyanion through two O atoms (**Figure 1-4c**).[138] However, **IrPPOM** slowly decomposes in aqueous solution to $[IrCl_4(H_2O)_2]^-$ and $[KP_2W_{20}O_{72}]^{13-}$. The rate of its first-order dissociation is $1.5\pm0.1 \times 10^{-4}$ s^{-1}, ca. two orders of magnitude slower than the rate of catalyzed water oxidation, and **IrPPOM** catalyzes water oxidation much faster than authentic IrO_2 nanoparticles[139,140] under otherwise identical conditions. These stability considerations are of great importance in a catalytic system, as will be discussed in detail in **Chapter 3**.

There are also many documented single-metal-site WOCs despite the fact that water oxidation is a four-electron process.[141-148] Mononuclear Ru-substituted Keggin-type POMs $[Ru^{III}(H_2O)SiW_{11}O_{39}]^{5-}$ and $[Ru^{III}(H_2O)GeW_{11}O_{39}]^{5-}$ were demonstrated as active WOCs (**Figure 1-4d**).[144]

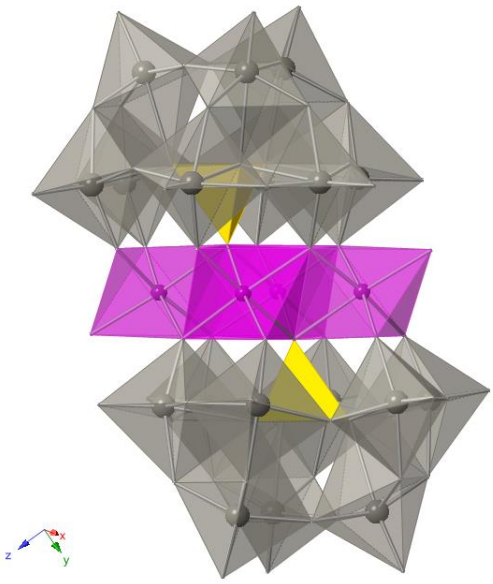

Figure 1-5. Crystal structure of $[Co_4(H_2O)_2(PW_9O_{34})_2]^{10-}$ (**Co_4PPOM)** where purple ball, Co; grey polyhedra, WO_6; yellow polyhedra, PO_4.

Another significant breakthrough was achieved in 2010, with a tetracobalt-substituted polytungstate, $[Co_4(H_2O)_2(PW_9O_{34})_2]^{10-}$ (**Co_4PPOM**; **Figure1-5)**.[149] The structure was first reported in 1973[150] and later with an improved synthesis in 1986,[151] however, no catalytic activity was assessed. This structure, like that of other Tourné type compounds, contains four planar Co atoms in the belt and is sandwiched by two lacunary B-type α-PW_9O_{34} ligands. Interestingly, this compound also bears structural resemblance to the OEC.[152] **Co_4PPOM** is the first example of an all-inorganic complex, free of rare-earth metals, demonstrated to catalyze water oxidation. In the absence of light, using $[Ru(bpy)_3]^{3+}$ as a chemical oxidant in aqueous phosphate buffer solution at pH 8.0, **Co_4PPOM** produced the highest TON per active site metal of any WOC at that time:

over 1000 in 3 min affording a TOF of 5 s^{-1}. Oxygen evolution yields were found to be highly pH and buffer dependent.

1.5 Goals of this work and outline

The objective of this dissertation is to investigate the water oxidation activity, stability, and mechanistic aspects of POMs, namely, **Co_4PPOM. Chapter 2** reports the design and optimization of a light-driven system for water oxidation utilizing **Co_4PPOM**, **t**his includes systematic study of each parameter including catalyst concentration, buffer concentration, light wavelength and power, stirring rate, reaction chamber size and shape among others. The catalytic performance was also thoroughly evaluated in this system by turnover number, chemical yield, and quantum yield. Stability studies, supplemental to those in the initial publication of **Co_4PPOM** we also performed. Two subsequent papers, one by the Finke group[153] and one a collaboration between the Scandola, Bonchio and Campagna groups,[155] were published calling claims made in these previous Hill group **Co_4PPOM** publications into question. The thesis of these publications can be summed up as stability issues of **Co_4PPOM** under reaction conditions. The claims in these papers are addressed in **Chapter 3** along with additional evidence for stability of **Co_4PPOM**. Several new control experiments are conducted showing thoroughly that **Co_4PPOM** is a stable and active catalyst for water oxidation. Through studies of the kinetic considerations of **Co_4PPOM**, both theoretical and experimental, are presented in **Chapter 4** along with the development of two new systems for evaluation of WOCs in general.

1.6 References

(1) Chow, J., Kopp, R. J. & Portney, P. R. *Science* **2003**, *302*, 1528.

(2) State, U. S. D. o. *Climate Action Report* **2015**.

(3) Energy, U. S. D. o. *Annual Energy Outlook* **2015**.

(4) Lewis, N. S. *MRS Bulletin* **2007**, *32*, 208.

(5) Pimentel, D., Hurd, L. E., Bellotti, A. C., Forster, M. J., Oka, I. N., Sholes, O. D. & Whitman, R. J *Science* **1973**, *182*, 443.

(6) Turner, J. A. *Science* **1999**, *285*, 687.

(7) *International Institute for Strategic Studies* **2015**, *The Military Balance. London: Routledge*, ISBN 1857437667.

(8) *National Priorities Project, President's Proposed Discretionary Spending* **2015**, *https://media.nationalpriorities.org (accessed June, 10 2015)*.

(9) Whittell, G. In *The Times* Wapping, 2010.

(10) Survey, G., Ed.; U.S. Geological Survey Open File Report 80-375 ed.: Washington, DC: U.S. , 1980.

(11) Bloom, E. E. *Journal of Nuclear Materials* **1998**, *258-263*, 7.

(12) Bloom, E. E., Zinkle, S. J. & Wiffen, F. W. *Journal of Nuclear Materials* **2004**, *329-333*, 12.

(13) Barnham, K. W. J., Mazzer, M. & Clive, B. *Nat Mater* **2006**, *5*, 161.

(14) Balzani, V., Credi, A. & Venturi, M. *ChemSusChem* **2008**, *1*, 26.

(15) Lewis, N. S.; Nocera, D. G. *Proc. Natl. Acad. Sci.* **2006**, *103(43)*, 15729.

(16) *World Energy Assessment Report: Energy and the Challenge of Sustainability, U. N. D. Program*, **2015**, *United Nations, New York*.

(17) Froehlich, C. *Space Science Reviews* **2006**, *125*, 53.

(18) Tarascon, J. M. A., M. *Nature* **2001**, 359.

(19) Serpone, N. P., E.; Grätzel, M. *Coordin. Chem. Rev.* **1985**, *64*, 225.

(20) R. E. Rocheleau, E. L. M. a. A. M. *Energy Fuels* **1998**, *12*.

(21) S. Y. Reece, J. A. H., K. Sung, T. D. Jarvi, H. J. Esswein, J. J. H. Pijpers and D. G. Nocera *Science* **2011**, *334*.

(22) Khaselev, O.; Turner, J. A. *Science* **1998**, *280*, 425.

(23) J. Brillet, J. H. Y., M. Cornuz, T. Hisatomi, R. Solarska, J. Augustynski, M. Gratzel and K. Sivula *Nature Photonics* **2012**, *6*.

(24) Abdi, F. F.; Han, L.; Smets, A. H. M.; Zeman, M.; Dam, B.; van de Krol, R. *Nat. Commun.* **2013**, 4:2195.

(25) Liu, C.; Tang, J.; Chen, H. M.; Liu, B.; Yang, P. *Nano Lett.* **2013**, *13*, 2989.

(26) Hu, S.; Shaner, M. R.; Beardslee, J. A.; Lichterman, M.; Brunschwig, B. S.; Lewis, N. S. *Science* **2014**, *344*, 1005.

(27) Maeda, K.; Teramura, K.; DalingLu; Takata, T.; Saito, N.; Inoue, Y.; Domen, K. *Nature* **2006**, *440*, 295.

(28) J. C. Hemminger, R. C. a. G. A. S. *Chem. Phys. Lett.* **1978**, *57*.

(29) Inoue, T.; Fujishima, A.; Konishi, S.; Honda, K. *Nature* **1979**, 637.

(30) Yamashita, H.; Fujii, Y.; Ichihashi, Y.; Zhang, S. G.; Ikeue, K.; Park, D. R.; Koyano, K.; Tatsumi, T.; Anpo, M. *Catal. Today* **1998**, *45*, 221.

(31) Lin, W.; Han, H.; Frei, H. *J. Phys. Chem. B* **2004**, *108*, 18269.

(32) S. Sato, T. A., T. Morikawa, K. Uemura, T. M. Suzuki, H. Tanaka and T. Kajino *Journal of the American Chemical Society* **2011**, *133*.

(33) Szalai, V. A.; Brudvig, G. W. *American Scientist* **1998**, *86*, 542.

(34) McEvoy, J. P.; Brudvig, G. W. *Chem. Rev.* **2006**, *106*, 4455.

(35) Ferreira, K. N.; Iverson, T. M.; Maghlaoui, K.; Barber, J.; Iwata, S. *Science* **2004**, *303*, 1831.

(36) Barber, J. *Chem. Soc. Rev.* **2009**, *38*, 185.

(37) Dau, H.; Zaharieva, I. *Acc. Chem. Res.* **2009**, *42*, 1861.

(38) Siegbahn, P. E. M. *Acc. Chem. Res.* **2009**, *42*, 1871.

(39) Umena, Y.; Kawakami, K.; Shen, J.-R.; Kamiya, N. *Nature* **2011**, *473*, 55.

(40) Yandulov, D. V.; Schrock, R. R. *Science* **2003**, *301*, 76.

(41) Schrock, R. R. *Acc. Chem. Res.* **2005**, *38*, 955.

(42) Weare, W. W.; Dai, X.; Byrnes, M. J.; Chin, J. M.; Schrock, R. R.; Mueller, P. *Proc. Natl. Acad. Sci.* **2006**, *103*, 17099.

(43) Hill, C. L. In *Comprehensive Coordination Chemistry-II: From Biology to Nanotechnology*; Wedd, A. G., Ed.; Elsevier Ltd.: Oxford, UK, 2004; Vol. 4, p 679.

(44) Huynh, M. H. V.; Meyer, T. J. *Chem. Rev.* **2007**, *107*, 5004.

(45) Mayer, J. M.; Hrovat, D. A.; Thomas, J. L.; Borden, W. T. *J. Am. Chem. Soc.* **2002**, *124*, 11142.

(46) Dempsey, J. L.; Winkler, J. R.; Gray, H. B. *Chem. Rev.* **2010**, *110*, 7024.

(47) Su, Q.; Klinman, J. P. *Biochem.* **1998**, *37*, 12513.

(48) Cukier, R. I. *J. Phys. Chem.* **1996**, *100*.

(49) Cukier, R. I.; Nocera, D. G. *Annu. Rev. Phys. Chem.* **1998**, *49*, 337.

(50) Shafirovich, V. Y.; Courtney, S. H.; Ya, N.; Geacintov, N. E. *J. Am. Chem. Soc.* **1995**, *117*, 4920.

(51) Weinberg, D. R.; Gagliardi, C. J.; Hull, J. F.; Murphy, C. F.; Kent, C. A.; Westlake, B. C.; Paul, A.; Ess, D. H.; Granville, D.; McCafferty; Meyer, T. J. *Chem. Rev.* **2012**, *112*, 4016.

(52) Hammes-Schiffer, S. *Acc. Chem. Res.* **2001**, *34*, 273.

(53) Cukier, R. I. *J. Phys. Chem.* **1999**, *103*, 5989.

(54) Hammes-Schiffer, S. *Acc. Chem. Res.* **2009**, *42*, 1881.

(55) Hammes-Schiffer, S. *Chem. Rev.* **2010**, *110*, 6937.

(56) Hammes-Schiffer, S.; Stuchebrukhov, A. A. *Chem. Rev.* **2010**, *110*, 6939.

(57) Prenzler, P. D.; Boskovic, C.; Bond, A. M.; Wedd, A. G. *Anal. Chem.* **1999**, *71*, 3650.

(58) Collin, J. P.; Sauvage, J. P. *Inorg. Chem.* **1986**, *25*, 135.

(59) Pope, M. T. *Heteropoly and Isopoly Oxometalates*; Springer-Verlag: Berlin, 1983.

(60) Day, V. W.; Klemperer, W. G. *Science* **1985**, *228*, 533.

(61) Pope, M. T. In *Comprehensive Coordination Chemistry*; Wilkinson, G., Gillard, R. D., McCleverty, J. A., Eds.; Pergamon Press: New York, 1987; Vol. 3, p Chapter 38.

(62) Pope, M. T.; Müller, A. *Angew. Chem. Int. Ed.* **1991**, *30*, 34.

(63) *Polyoxometalates: From Platonic Solids to Anti-retroviral Activity*; Pope, M. T.; Müller, A., Eds.; Kluwer Academic Publishers: Dordrecht, Netherlands, 1993.

(64) *Special Thematic Issue on Polyoxometalates*; Hill, C. L., Ed., 1998; Vol. 98, No. 1.

(65) Hill, C. L. *Chem. Rev.* **1998**, *98*, 1.

(66) Borrás-Almenar, J. J.; Coronado, E.; Müller, A.; Pope, M. T. *Polyoxometalate Molecular Science. Proceedings of the NATO Advanced Study Institute, Tenerife, Spain from 25 August to 4 September 2001*; Kluwer Academic Publishers: Dordrecht, 2003; Vol. 98.

(67) Kortz, U.; Müller, A. *J. Cluster Sci.* **2006**, *17*, 139.

(68) Long, D.-L.; Tsunashima, R.; Cronin, L. *Angew. Chem. Int. Ed.* **2010**, *49*, 1736.

(69) Pope, M. T. In *Comprehensive Coordination Chemistry II: From Biology to Nanotechnology*; Wedd, A. G., Ed.; Elsevier Ltd.: Oxford, UK, 2004; Vol. 4, p 635.

(70) Besecker, C. J.; Klemperer, W. G. *J. Am. Chem. Soc.* **1980**, *25*, 7598.

(71) Day, V. W.; Klemperer, W. G.; Schwartz, C. *J. Am. Chem. Soc.* **1987**, *109*, 6030.

(72) Hill, C. L.; Prosser-McCartha, C. M. *Coord. Chem. Rev.* **1995**, *143*, 407.

(73) Hill, C. L. *J. Mol. Catal. A: Chem. Special Issue* **2007**, *262*, 1.

(74) Barnard, D. L.; Hill, C. L.; Gage, T.; Matheson, J. E.; Huffman, J. H.; Sidwell, R. W.; Otto, M. I.; Schinazi, R. F. *Antiviral Res.* **1997**, *34*, 27.

(75) Hill, C.; Weeks, M.; Schinazi, R. F. *J. Med. Chem.* **1990**, *33*, 2767.

(76) Schinazi, R. F.; Sijbesma, R.; Srdanov, G.; Hill, C. L.; Wudl, F. *Antimicrob. Agents Chemother.* **1993**, *37*, 1707.

(77) Shigeta, S.; Mori, S.; Watanabe, J.; Baba, M.; Khenkin, A. M.; Hill, C. L.; Schinazi, R. F. *Antiviral Chem. Chemother.* **1995**, *6*, 114.

(78) Judd, D. A.; Nettles, J. H.; Nevins, N.; Snyder, J. P.; Liotta, D. C.; Tang, J.; Ermolieff, J.; Schinazi, R. F.; Hill, C. L. *J. Am. Chem. Soc.* **2001**, *123*, 886.

(79) Yamase, T.; Fukuda, N.; Tajima, Y. *Biol. Pharm. Bull.* **1996**, *19*, 459.

(80) Fukuda, N.; Yamase, T. *Biol. Pharm. Bull.* **1997**, *20*, 927.

(81) Shigeta, S.; Mori, S.; Watanabe, J.; Soeda, S.; Takahashi, K.; Yamase, T. *Antimicrob. Agents Chemother.* **1997**, *41*, 1423.

(82) Shigeta, S.; Mori, S.; Kodama, E.; Kodama, J.; Takahashi, K.; Yamase, T. *Antiviral Res.* **2003**, *58*, 265.

(83) Hasenknopf, B. *Front. Biosci.* **2005**, *10*, 275.

(84) Rhule, J. T.; Hill, C. L.; Judd, D. A.; Schinazi, R. F. *Chem. Rev.* **1998**, *98*, 327.

(85) Clayette, P.; Dormont, D. *Topics in Molecular Organization and Engineering* **1994**, *10*, 387.

(86) Lee, I. S.; Long, J. R.; Prusiner, S. B.; Safar, J. G. *J. Am. Chem. Soc.* **2005**, *127*, 13802.

(87) Wille, H.; Shanmugam, M.; Murugesu, M.; Ollesch, J.; Stubbs, G.; Long, J. R.; Safar, J. G.; Prusiner, S. B. *Proc. Natl. Acad. Sci.* **2009**, *106*, 3740.

(88) Kögerler, P.; Tsukerblat, B.; Müller, A. *Dalton Trans.* **2010**, *39*, 21.

(89) Coronado, E.; Gómez-García, C. J. *Chem. Rev.* **1998**, *98*, 273.

(90) Coronado, E.; Day, P. *Chem. Rev.* **2004**, *104*, 5419.

(91) Clemente-Juan, J. M.; Coronado, E. *Chem. Rev.* **1999**, *193-195*, 361.

(92) Speldrich, M.; Schilder, H.; Lueken, H.; Kögerler, P. *Isr. J. Chem.* **2011**, *51*, 215.

(93) Hasenknopf, B.; Micoine, K.; Lacôte, E.; Thorimbert, S.; Malacria, M.; Thouvenot, R. *Eur. J. Inorg. Chem.* **2008**, 5001.

(94) Hou, Y.; Fang, X.; Hill, C. L. *Chem. Eur. J.* **2007**, *13*, 9442.

(95) Fang, X.; Anderson, T. M.; Hill, C. L. *Angew. Chem. Int. Ed.* **2005**, *44*, 3540.

(96) Fang, X.; Anderson, T. M.; Hou, Y.; Hill, C. L. *Chem. Commun.* **2005**, 5044.

(97) Yan, L.; López, X.; Carbó, J. J.; Sniatynsky, R.; Duncan, D. C.; Poblet, J. M. *J. Am. Chem. Soc.* **2008**, *130*, 8223.

(98) Carraro, M.; Modugno, G.; Sartorel, A.; Scorrano, G.; Bonchio, M. *Eur. J. Inorg. Chem.* **2009**, 5164.

(99) Jahier, C.; Cantuel, M.; McClenaghan, N. D.; Buffeteau, T.; Cavagnat, D.; Agbossou, F.; Carraro, M.; Bonchio, M.; Nlate, S. *Chem. Eur. J.* **2009**, *15*, 8703.

(100) Lu, M.; Kang, J.; Wang, D.; Peng, Z. *Inorg. Chem.* **2005**, *44*, 7711.

(101) An, H.-Y.; Wang, E.-B.; Xiao, D.-R.; Li, Y.-G.; Su, Z.-M.; Xu, L. *Angew. Chem. Int. Ed.* **2006**, *45*, 904.

(102) Long, D.-L.; Kögerler, P.; Farrugia, L. J.; Cronin, L. *Chem. Asian J.* **2006**, *1*, 352.

(103) Katsoulis, D. E. *Chem. Rev.* **1998**, *98*, 359.

(104) Harrup, M. K.; Hill, C. L. *Inorg. Chem.* **1994**, *33*, 5448.

(105) Weinstock, I. A.; Atalla, R. H.; Reiner, R. S.; Moen, M. A.; Hammel, K. E.; Houtman, C. J.; Hill, C. L.; Harrup, M. K. *J. Mol. Catal. A: Chem.* **1997**, *116*, 59.

(106) Weinstock, I. A.; Barbuzzi, E. M. G.; Wemple, M. W.; Cowan, J. J.; Reiner, R. S.; Sonnen, D. M.; Heintz, R. A.; Bond, J. S.; Hill, C. L. *Nature* **2001**, *414*, 191.

(107) Neumann, R. *Prog. Inorg. Chem.* **1998**, *47*, 317.

(108) Neumann, R. *Mod. Oxidation Methods* **2004**, 223.

(109) Neumann, R. In *Transition Metals for Organic Synthesis (2nd Edition)*; Beller, M., Bolm, C., Eds.; Wiley-VCH: Weinheim, 2004; Vol. 2, p 415.

(110) Vazylyev, M.; Dorit, S.-R.; Haimov, A.; Maayan, G.; Neumann, R. *Top. Catal.* **2005**, *34(1-4)*, 93.

(111) Mizuno, N.; Misono, M. *Chem. Rev.* **1998**, *98*, 199.

(112) Misono, M.; Ono, I.; Koyano, G.; Aoshima, A. *Pure Appl. Chem.* **2000**, *72*, 1305.

(113) Okuhara, T.; Mizuno, N.; Misono, M. *Appl. Catal., A* **2001**, *222*, 63.

(114) Okuhara, T.; Mizuno, N.; Misono, M. *Advances in Catalysis* **1996**, *41*, 113.

(115) Kozhevnikov, I. V. *Catalysis by Polyoxometalates*; Wiley: Chichester, England, 2002; Vol. 2.

(116) Kozhevnikov, I. V. *Chem. Rev.* **1998**, *98*, 171.

(117) Moffat, J. B. *Metal-Oxygen Clusters: The Surface and Catalytic Properties of Heteropoly Oxometalates.*; Kluwer Academic/Plenum Publishers: New York, 2001; Vol. 9.

(118) Hill, C. L. *Synlett* **1995**, 127.

(119) Hurst, J. K. *Coord. Chem. Rev.* **2005**, *249*, 313.

(120) Hill, C. L. *J. Mol. Catal. A: Chem.* **2007 Special Issue**, *262*, 1.

(121) Howells, A. R.; Sankarraj, A.; Shannon, C. *J. Am. Chem. Soc.* **2004**, *126*, 12258.

(122) Botar, B.; Geletii, Y. V.; Kögerler, P.; Musaev, D. G.; Morokuma, K.; Weinstock, I. A.; Hill, C. L. *J. Am. Chem. Soc.* **2006**, *128*, 11268.

(123) Botar, B.; Kögerler, P.; Hill, C. L. *J. Am. Chem. Soc.* **2006**, *128*, 5336.

(124) Geletii, Y. V.; Botar, B.; Kögerler, P.; Hillesheim, D. A.; Musaev, D. G.; Hill, C. L. *Angew. Chem. Int. Ed.* **2008**, *47*, 3896.

(125) Sartorel, A.; Carraro, M.; Scorrano, G.; Zorzi, R. D.; Geremia, S.; McDaniel, N. D.; Bernhard, S.; Bonchio, M. *J. Am. Chem. Soc.* **2008**, *130*, 5006.

(126) Geletii, Y. V.; Huang, Z.; Hou, Y.; Musaev, D. G.; Lian, T.; Hill, C. L. *J. Am. Chem. Soc.* **2009**, *131*, 7522.

(127) Geletii, Y. V.; Besson, C.; Hou, Y.; Yin, Q.; Musaev, D. G.; Quinonero, D.; Cao, R.; Hardcastle, K. I.; Proust, A.; Kögerler, P.; Hill, C. L. *J. Am. Chem. Soc.* **2009**, *131*, 17360.

(128) Kuznetsov, A. E.; Geletii, Y. V.; Hill, C. L.; Morokuma, K.; Musaev, D. G. *J. Am. Chem. Soc.* **2009**, *131*, 6844.

(129) Quiñonero, D.; Kaledin, A. L.; Kuznetsov, A. E.; Geletii, Y. V.; Besson, C.; Hill, C. L.; Musaev, D. G. *J. Phys. Chem. A* **2010**, *114*, 535.

(130) Sartorel, A.; Miro, P.; Salvadori, E.; Romain, S.; Carraro, M.; Scorrano, G.; Valentin, M. D.; Llobet, A.; Bo, C.; Bonchio, M. *J. Am. Chem. Soc.* **2009**, *131*, 16051.

(131) Besson, C.; Huang, Z.; Geletii, Y. V.; Lense, S.; Hardcastle, K. I.; Musaev, D. G.; Lian, T.; Proust, A.; Hill, C. L. *Chem. Commun.* **2010**, 2784.

(132) Toma, F. M.; Sartorel, A.; Iurlo, M.; Carraro, M.; Parisse, P.; Maccato, C.; Rapino, S.; Gonzalez, B. R.; Amenitsch, H.; Ros, T. D.; Casalis, L.; Goldoni, A.; Marcaccio, M.; Scorrano, G.; Scoles, G.; Paolucci, F.; Prato, M.; Bonchio, M. *Nature Chem.* **2010**, *2*, 826.

(133) Toma, F. M.; Sartorel, A.; Carraro, M.; Bonchio, M.; Prato, M. *Pure Appl. Chem.* **2011**, *83*, 1529.

(134) Orlandi, M.; Argazzi, R.; Sartorel, A.; Carraro, M.; Scorrano, G.; Bonchio, M.; Scandola, F. *Chem. Commun.* **2010**, *46*, 3152.

(135) Natali, M.; Orlandi, M.; Berardi, S.; Campagna, S.; Bonchio, M.; Sartorel, A.; Scandola, F. *Inorg. Chem.* **2012**, *51*, 7324.

(136) Puntoriero, F.; Ganga, G. L.; Sartorel, A.; Carraro, M.; Scorrano, G.; Bonchio, M.; Campagna, S. *Chem. Commun.* **2010**, *46*, 4725.

(137) Sartorel, A.; Truccolo, M.; Berardi, S.; Gardan, M.; Carraro, M.; Toma, F. M.; Scorrano, G.; Prato, M.; Bonchio, M. *Chem. Commun.* **2011**, *47*, 1716.

(138) Cao, R.; Ma, H.; Geletii, Y. V.; Hardcastle, K. I.; Hill, C. L. *Inorg. Chem.* **2009**, *48*, 5596.

(139) Cook, T. R.; Dogutan, D. K.; Reece, S. Y.; Surendranath, Y.; Teets, T. S.; Nocera, D. G. *Chem. Rev.* **2010**, *110*, 6474.

(140) Youngblood, W. J.; Lee, S.-H. A.; Kobayashi, Y.; Hernandez-Pagan, E. A.; Hoertz, P. G.; Moore, T. A.; Moore, A. L.; Gust, D.; Mallouk, T. E. *J. Am. Chem. Soc.* **2009**, *131*, 926.

(141) Chen, Z.; Concepcion, J. J.; Meyer, T. J. *Dalton Trans.* **2011**, *40*, 3789.

(142) An, J.; Duana, L.; Sun, L. *Faraday Discuss.* **2012**, *155*, 267.

(143) Kaveevivitchai, N.; Zong, R.; Tseng, H.-W.; Chitta, R.; Thummel, R. P. *Inorg. Chem.* **2012**, *51*, 2930.

(144) Murakami, M.; Hong, D.; Suenobu, T.; Yamaguchi, S.; Ogura, T.; Fukuzumi, S. *J. Am. Chem. Soc.* **2011**, *133*, 11605.

(145) Concepcion, J. J.; Tsai, M.-K.; Muckerman, J. T.; Meyer, T. J. *J. Am. Chem. Soc.* **2010**, *132*, 1545.

(146) Tong, L.; Wang, Y.; Duan, L.; Xu, Y.; Cheng, X.; Fischer, A.; Ahlquist, M. S. G.; Sun, L. *Inorg. Chem.* **2012**, *51*, 3388.

(147) Concepcion, J. J.; Jurss, J. W.; Templeton, J. L.; Meyer, T. J. *J. Am. Chem. Soc.* **2008**, *130*, 16462.

(148) Romain, S.; Vigara, L.; Llobet, A. *Acc. Chem. Res.* **2009**, *42*, 1944.

(149) Yin, Q.; Tan, J. M.; Besson, C.; Geletii, Y. V.; Musaev, D. G.; Kuznetsov, A. E.; Luo, Z.; Hardcastle, K. I.; Hill, C. L. *Science* **2010**, *328*, 342.

(150) Weakley, T. J. R.; Evans, H. T., Jr.; Showell, J. S.; Tourné, G. F.; Tourné, C. M. *J. Chem. Soc., Chem. Commun.* **1973**, *4*, 139.

(151) Evans, H. T.; Tourné, C. M.; Tourné, G. F.; Weakley, T. J. R. *J. Chem. Soc., Dalton Trans.* **1986**, 2699.

(152) Swiegers, G. F.; Clegg, J. K.; Stranger, R. *Chem. Sci.* **2011**, *2*, 2254.

(153) Stracke, J. J.; Finke, R. G. *J. Am. Chem. Soc.* **2011**, *133*, 14872.

(154) Vickers, J. W.; Lv, H.; Sumliner, J. M.; Zhu, G.; Luo, Z.; Musaev, D. G.; Geletii, Y. V.; Hill, C. L. *J. Am. Chem. Soc.* **2013**, *135*, 14110.

(155) Natali, M.; Berardi, S.; Sartorel, A.; Bonchio, M.; Campagna, S.; Scandola, F. *Chem. Commun.* **2012**, *48*, 8808.

Chapter 2

Efficient Light-Driven Carbon-Free Cobalt-Based Molecular Catalyst for Water Oxidation

2.1 Introduction

Water oxidation is a key step in the production of fuel from water by photochemical, electrochemical, and other approaches.[1-3] The development of efficient WOCs remains a major scientific challenge despite considerable progress in recent years.[4-21] A series of molecular, carbon-free, soluble, and fast ruthenium and cobalt based POM WOCs, including $[Ru_4O_4(OH)_2(H_2O)_4(\gamma\text{-}SiW_{10}O_{36})_2]^{10-}$ (**Ru_4SiPOM**) and $[Co_4(H_2O)_2(PW_9O_{34})_2]^{10-}$ (**Co_4PPOM**), have been reported.[22-31] **Co_4PPOM**, which is based on earth-abundant Co, exhibits a turnover frequency for homogeneous catalytic water oxidation using $[Ru(bpy)_3]^{3+}$ as a sacrificial oxidant at pH 8 that is as high as any WOC reported at its publication date, estimated to be about 20 times higher than that

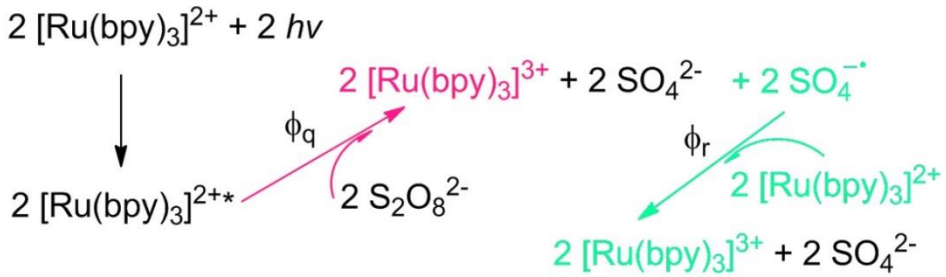

Scheme 2-1. Principal processes of O_2 evolution in a homogeneous light-driven water oxidation system

of **Ru_4SiPOM** at pH 7.2 (5 vs 0.25 s^{-1}).[22,31] It was previously demonstrated that **Ru_4SiPOM** and its isostructural phosphorus-centered analogue, **Ru_4PPOM,** catalyze oxygen evolution in a homogeneous light-driven water-oxidation system (**Scheme 2-1**)

using $[Ru(bpy)_3]^{2+}$ as a photosensitizer and $S_2O_8^{2-}$ as a sacrificial electron acceptor.[24,28] It is reported here that **Co_4PPOM** does the same (**Scheme 2-1**) but exhibits substantially higher rates and O_2 evolution quantum yields ($\sim$ 30%) than **Ru_4SiPOM** and all other POM-based WOCs to date. Significantly, **Co_4PPOM** and **Ru_4SiPOM** have different kinetic features (elaborated in **Chapter 4**), indicating that the reactivities of one POM WOC are not necessarily operable for others.[22-31]

$$4\,[Ru(bpy)_3]^{3+} + 2\,H_2O \xrightarrow{\phi_C,\mathbf{Co_4PPOM}} 4\,[Ru(bpy)_3]^{2+} + O_2 + 4\,H^+ \qquad (\mathbf{2\text{-}1})$$

$$2\,S_2O_8^{2-} + 2\,H_2O + 2\,h\upsilon \xrightarrow{\Phi_{CY},\Phi_{QY}} 4\,SO_4^{2-} + O_2 + 4\,H^+ \qquad (\mathbf{2\text{-}2})$$

2.2 Experimental

2.2.1 Instrumentation

UV-Vis spectra were acquired using Agilent 8453 spectrophotometer equipped with a diode-array detector and an Agilent 89090A cell temperature controller unit. Steady state luminescence quenching was studied using a SPEX® FluoroLog®-3 self-contained and fully automated spectrofluorometer. Analysis of dioxygen in the reaction headspace was performed using Agilent 7890a gas-chromatography (GC) system equipped with a thermoconductivity detector and a HP-MOLESIEVE capillary column (30m x 0.535 mm x 25.00 μm) with Argon as a carrier gas. A Hamamatsu Xe-lamp (model C2577) was used as a light source and the desired wavelength range was created with a 420-470 nm band pass filter. A magnetically-coupled stirring system (SYS-114, SPECTROCELL) was used for reaction solutions. The stirring rate in revolutions per

minute (RPM) was determined by a home-built set-up consisting of a helium-neon laser (IMATTRONIC), a magnetic stick (VP 736-1, V&P scientific), a photo-diode detector (PDA 55, ThorLabs), and an oscilloscope (LT262, LeCroy). Power measurements were made with a Molectron, model Max 500A laser power meter. The fast reactions were studied using a Hi-Tech KinetAsyst Stopped Flow SF-61SX2 instrument equipped with a diode array detector operating in wavelength range 400-700 nm. Headspace was sampled with 1010 TLL Gastight Hamilton syringes.

2.2.2 Materials and synthesis

Water for the preparation of solutions was obtained from a Barnstead Nanopure water-purification system, and all other chemicals and salts used were of the highest purity available from commercial sources. Tris(2,2'-bipyridyl)dichlororuthenium(II) hexahydrate $[Ru(bpy)_3]^{2+}$, and sodium persulfate (98+%) were purchased from Aldrich. $[Ru(bpy)_3]^{2+}$ was recrystallized before use: 1 g of $[Ru(bpy)_3]^{2+}$ was dissolved in about 5 mL of deionized H_2O, and filtered through a Millipore Millex-FX Phobic PTFE 0.45 μm syringe filter, then brought to 80 ^oC in the dark. After cooling to room temperature, the sample was collected by filtration and air dried with 50% yield.

(a) Tris(2,2′-bipyridyl)triperchlororuthenium(III) was prepared as reported[25] by oxidation of the recrystallized $[Ru(bpy)_3]Cl_2$. $[Ru(bpy)_3]Cl_2$ (375 mg) was dissolved in 10 mL of 0.5 M H_2SO_4. PbO_2 was added in small amounts until the solution went from a bright orange to a dark green over approximately 5 minutes. The mixture was filtered to remove PbO_2 and concentrated $HClO_4$ was added to the filtrate until no additional

precipitate was formed. The green crystals were separate by filtration over a fine frit and dried under reduced pressure for several hours.

(b) $Rb_8K_2[Ru_4O_4(OH)_2(H_2O)_4(\gamma\text{-}SiW_{10}O_{36})_2]$ (**Ru_4SiPOM)** was prepared as published previously.[22] The precursor potassium γ-decatungstosilicate, $K_8[\gamma\text{-}SiW_{10}O_{36}]\cdot 12H_2O$ was prepared according to literature methods,[32] and its identity and purity were checked by infrared spectroscopy. **Ru_4SiPOM**: A solid sample of $RuCl_3\cdot H_2O$ (0.60 g, 2.67 mmol) was quickly added to a freshly prepared solution of $K_8[g\text{-}SiW_{10}O_{36}]\cdot 12H_2O$ (4.00 g, 1.33 mmol) dissolved in 65 mL of H_2O. The solution immediately turned brown and the pH dropped to ca. 2.6. The solution pH was adjusted to 1.6 by drop-wise addition of 6M HCl. After additional stirring for 5 min, a solution of RbCl (2.4 g, 20 mmol) dissolved in 10-15 mL of H_2O was added to the mixture in small portions. The mixture was filtered and the filtrate left to stand at room temperature. Brown plate crystals began to form after 24 h. Yield *ca.* 1.8 g (*ca.* 40% based on W)**.**

(c) $Na_{10}[Co_4(H_2O)_2(\alpha\text{-}PW_9O_{34})_2]$ (**Co_4PPOM**) was prepared as previously reported.[33] $Na_2WO_4\cdot 2H_2O$ (35.62 g, 0.108 mol), $Na_2HPO_4\cdot 7H_2O$ (3.22 g, 0.012 mol), and $Co(NO_3)_2\cdot 6H_2O$ (6.98 g, 0.024 mol) were added to 100 mL of distilled water. This corresponds to the Co:W:P ratio that is found in the product 2:9:1. The pH was adjusted to 7.0 by dropwise addition of HCl (0.1M). The resulting purple reaction mixture was refluxed at 100 ^oC or two hours. After reflux, the solution was removed from heat, saturated with NaCl, and allowed to cool to room temperature. Purple crystals were

collected by filtration and the final product was obtained by recrystallization from deionized water. The identity of the compound was checked by FT-IR. and UV-Vis.

2.2.3 Light-driven system

The light driven reaction is summarized in **Scheme 2-1**. Two molecules of the photosensitizer $Ru(bpy)_3^{2+}$ each absorb a photon of light and are promoted to an excited state $[Ru(bpy)_3]^{2+*}$. These excited state molecules then each react with the sacrificial electron acceptor sodium persulfate ($Na_2S_2O_8$), oxidizing the $[Ru(bpy)_3]^{2+}$ by one electron to $[Ru(bpy)_3]^{3+}$ and producing two molecules of both sulfate, and sulfate radical which is extremely oxidizing (~2.4 V). The sulfate radicals then react with another two molecules of $[Ru(bpy)_3]^{2+}$ again oxidizing them by one electron to $[Ru(bpy)_3]^{3+}$ and yielding another two molecules of sulfate. The four molecules of $[Ru(bpy)_3]^{3+}$ then each undergo a one-electron reduction to return to $[Ru(bpy)_3]^{2+}$ while converting two molecules of water into one molecule of O_2 and four protons by coupling to the WOC. The system also contains a buffer to maintain pH while generating four protons per dioxygen molecule. The overall reaction for this process based on oxidant is presented in **Equation 2-1**, and based on sacrificial agents (electron acceptor, persulfate) in **Equation 2-2**.[25] The conditions are as follows unless otherwise noted: 1.0 mM $[Ru(bpy)_3]^{2+}$, 5.0 mM $Na_2S_2O_8$, 80 mM sodium borate buffer (NaB_i), initial pH 8.0, total reaction volume 2 mL, vigorous stirring (5×10^3 RPM). Illumination: 16.8 mW, 420-470 nm with a beam diameter of 0.75 cm.

2.2.4 Quantum yield measurements

The amount of O_2 formed was quantified as described above at the reaction time of less than 2 min. The total amount of photons absorbed for a given reaction time was calculated from the irradiation power and the absorbance of the reaction solution. The irradiation power was measured directly in front of the reaction vessel using a laser power meter as 16.8 mW. The spectrum of light emitted by the Xe-lamp in the 420-470 nm range as well as the absorption spectra of cutoff filter was considered to be flat in this spectral region. During illumination, the reaction solution remained orange in color indicating the photosensitizer was mostly present in its reduced form, $[Ru(bpy)_3]^{2+}$. The optical density of the reaction solution was calculated as nearly 30 in the 420-470 nm range thus all light entering the reaction solution was considered to be absorbed by Beer's Law. The amount of absorbed light was determined from the measured power in front of the reaction vessel, the absorption loss (18%) by the optical glass (NSG cuvette manual, and by UV-Vis spectrometer) and reflection loss (4%) at the glass/air interface.

2.2.5 Steady state luminescence quenching

The general procedure to measure the steady state fluorescence can be found in a previous report.[24] The solutions of $[Ru(bpy)_3]^{2+}$, $S_2O_8^{2-}$, and their mixtures were prepared and stored in the absence of light to avoid photoreaction. All solutions were purged with Ar before measurements. A 10x1 mm dual-path-length quartz cuvette and 1.8-nm excitation and emission slits were used in all steady-state luminescence measurements. Samples were excited at 450 nm, and emission intensity data were collected at 20 °C at 617-620 nm. Integration time was set at 0.05 s. To minimize light induced reactions during the measurements, the acquisition time was kept to less than 1 s. Repetitive

measurements showed that the emission intensity decreased by less than 2% during this acquisition time.

2.2.6 Stopped-flow

One of the feeding syringes was filled with $[Ru(bpy)_3]^{3+}$ solution and the other with a freshly prepared solution of the catalyst in buffer. The $[Ru(bpy)_3]^{3+}$ solution was prepared in 0.1 mM HCl to avoid self-reduction to $[Ru(bpy)_3]^{2+}$ at basic pH and filtered before use. Each data set included 200 spectra collected with different timescales: from 0-0.4 s up to 0-400 s. Typically, the consumption of $[Ru(bpy)_3]^{3+}$ was followed by a decrease in absorbance at 670 nm (ε_{670} = 420 $M^{-1}cm^{-1}$) with optical path length l = 10 mm. The data were acquired and treated using KinetAsyst™ 3.0 software.

2.3 System design

2.3.1 System quantification

In order to quantitatively gauge the catalytic performance of a catalyst in a given system the turnover number (TON), chemical yield (Φ_{CY}), and quantum yield (Φ_{QY}) are calculated. TON is defined the final number of moles of product, O_2 in this case, produced per mole of catalyst (**Equation 2-3**).

$$TON = (O_2 \text{ yield at end of run}) / (\text{moles catalyst}) = [O_2]_f/[\text{catalyst}] \quad \textbf{(2-3)}$$

Generally, TON reflects the long term stability of a catalyst, demonstrating how many times it is able to catalyze a reaction before being rendered inactive. However, this

system is limited in overall TON by the amount of the sacrificial electron acceptor ($Na_2S_2O_8$). Thus, TON as described here does not say anything about catalyst stability, but because the experiments reported herein are under identical conditions it is a useful metric for direct comparisons. The chemical yield, however, is based on the overall stoichiometry of the reaction from **Equation 2-2** in which two molecules of persulfate produce one molecule of O_2.

$$\Phi_{CY} = 2\frac{[O_2]_f}{[Na_2S_2O_8]_0} = 0.5(1 + \phi_r)\phi_c \qquad \textbf{(2-4)}$$

where $[O_2]_f$ and $[Na_2S_2O_8]_0$ are the final yield of O_2 and the initial concentration of persulfate, respectively, ϕ_r is the yield of the oxidation of $[Ru(bpy)_3]^{2+}$ to $[Ru(bpy)_3]^{3+}$ by sulfate radical ions $SO_4^{-\cdot}$, and ϕ_c is the yield of O_2 produced from $[Ru(bpy)_3]^{3+}$ in the presence of the catalyst (**Scheme 2-1**).

Since Φ_{CY} is based on the initial amount of persulfate it is a good measure of reaction completion. It does not however, adequately reflect the long-term stability of the catalyst. The quantum yield for a photochemical reaction is defined as the amount of product formed per photon absorbed. In this system, two photons are required to produce one molecule of O_2 and thus the photon-to-O_2 quantum yield is multiplied by 2 as in **Equation 2-5**.

$$\Phi_{QY}(t) = 2\left[\frac{\Delta(O_2)}{\Delta(h\upsilon)}\right]_t = 0.5\,\phi_q(t)(1 + \phi_r)\phi_c \qquad \textbf{(2-5)}$$

The quantities $\Delta(O_2)$ and $\Delta(h\upsilon)$ are the change in the total amount of O_2 produced and the number of photons absorbed, respectively. Each of the values reported has been

corrected for the control experiment with no catalyst. Here, the quenching efficiency, or electron transfer efficiency, ϕ_q, is defined as,

$$\phi_q = \frac{I_0 - I}{I_0} \quad \textbf{(2-6)}$$

where I_0 and I are the emission intensities of $[Ru(bpy)_3]^{2+*}$ in the absence and presence of persulfate respectively. The quantum yield as a function of time can be described in terms of quenching efficiency as in **Equation 2-7**.

$$\Phi_{QY}(t) = \phi_q(t)\Phi_{QY} \quad \textbf{(2-7)}$$

The value of $\Phi_{QY}(t)$ can also be calculated from the ratio of the rates of O_2 generation and photon absorption and is related to the slope of the plot of O_2 versus illumination time. The yield in the dark system was previously calculated from **Equation 2-1** by:

$$\text{Yield} = \frac{4[O_2]_f}{[Ru(bpy)_3]^{3+}{}_0} \quad \textbf{(2-8)}$$

2.3.2 Optimization

The procedure for the light-driven reaction was adapted from a previous report[24] where light induced water oxidation was performed in the round bottom-reaction vessel with a diameter of about 3 cm and with a total volume of about 15 mL equipped with a side arm stopcock and 14/20 outer joint. The vessel was filled with 8 mL of solution with the desired concentrations of $[Ru(bpy)_3]^{2+}$, $Na_2S_2O_8$, catalyst, and buffer. The reaction vessel was then sealed with a rubber septum, carefully deaerated and filled with Ar. All

procedures were performed with minimum exposure to ambient light. The reaction was initiated by turning on the Xe-lamp. The output of the Xe-Lamp was filtered with a 420-520 nm band-pass filter and was focused onto the reaction vessel. Light intensity was adjusted by varying the beam size at the sample (by an aperture) and/or applying a neutral density filter (50% transmission). At high light intensity (28 mW/cm^2), the reaction in solution proceeded very fast and the O_2 concentration in the head space was not in equilibrium with O_2 formed in solution. Therefore, to follow the kinetics of O_2 formation, the reaction was stopped after the desired illumination time by blocking the lamp. The reaction vessel was then vigorously shaken to equilibrate dioxygen concentrations in liquid and gas phases, and the headspace was analyzed for O_2 content. The O_2 yield was quantified by withdrawing 0.1 mL of the gas in the headspace of the reaction vessel through a septum using a deaerated gas-tight syringe and injected into gas chromatograph. Contamination of the head-space by air was corrected by quantification of N_2 present in the head-space by GC. Typically, contamination was very small and the area under the O_2 peak was much larger than that of the N_2 peak. The peak area from the chromatograph corresponding to O_2 was then adjusted for contamination from air by subtracting half of the peak from the chromatograph corresponding to N_2 (less than 0.07 μmol O_2). This is a conservative estimate since the chromatograph of air exhibits an oxygen to nitrogen ratio of 1 : 2.8.

To improve on this procedure, the efficiency of light-driven water-oxidation was optimized by testing three vessels with different sizes and shapes (A, B and C), as shown in **Figure 2-1**. The reaction conditions were kept the same for direct comparison: 1 mM $[Ru(bpy)_3]^{2+}$, 5 mM $[S_2O_8]^{2-}$, 20 mM sodium phosphate buffer (NaP_i) with initial pH 7.2,

and 5 μM **Ru_4SiPOM**. Reaction vessels were filled with 8, 16, and 2 mL solutions, leaving 5, 8, and 0.9 mL sampling headspaces for vessels A, B, and C, respectively. The reaction vessel was then sealed with a rubber septum, carefully deaerated, and filled with Ar. All procedures were performed with a minimum exposure to ambient light.

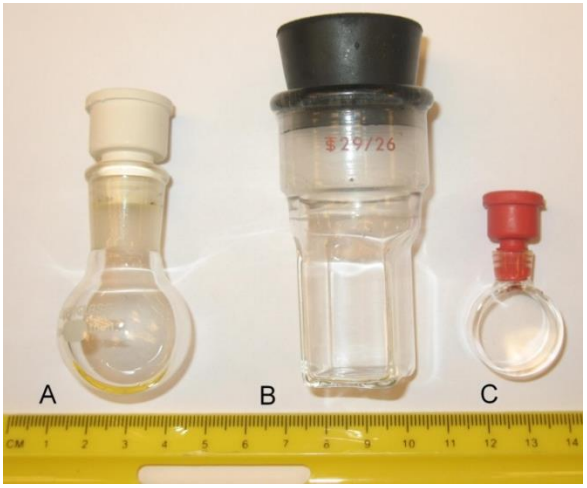

Figure 2-1. Three cells selected for optimizing the O_2 formation efficiency. A: glass round bottom flask. B: glass photoelectrochemical cell, square bottom with flat illumination windows. C: cylindrical quartz cuvette with a light path of 1 cm.

The reaction was initiated by unblocking the Xe-lamp. Cutoff filters (420-520 nm for cell A, 420-470 nm combined with another 300-720 filters for cell B and C) were applied to block light outside of the $[Ru(bpy)_3]^{2+}$ absorption range. The light intensity was measured with a power meter to be 50 mW for vessel A and 16.8 mW for vessels B and C. The procedure was followed as described above.

Figure 2-2 shows the O_2 evolution kinetics measured in each of the three cells. Efficiency of each cell was compared by considering the O_2 yields per unit volume of reaction solution and per unit of incident light power. As seen from **Figure 2-2**, the reaction carried out in cell C harnesses the light most efficiently. Additionally, the TON,

and chemical yields based on persulfate were calculated, and the initial quantum yield was estimated from the initial slope of the dependence O_2 yield versus total number of photons consumed. These results are reported in **Table 2-1**.

For the cells A and C, the TONs and chemical yields are close to each other, but almost twice of those for the cell B, which is probably due to the difference in volumes of solutions that were exposed to light. At 1 mM $[Ru(bpy)_3]^{2+}$, only ~0.1% of light can penetrate the 2 mm solution layer. Thus, most of solution actually remains in dark and serves as a reservoir of reactants. A thinner cell with small volume therefore seems ideal for the light driven reactions.

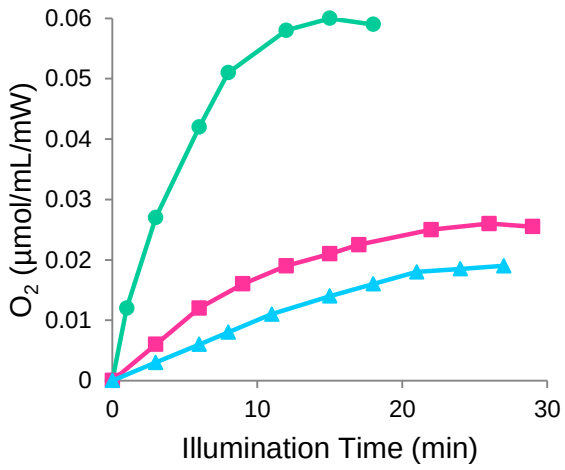

Figure 2-2. Kinetics of O_2 formation (expressed as the O_2 yield per unit volume of reaction solution and per unit of illumination power in different cells. A (blue triangles), B (pink squares) and C (teal circles). Conditions: 1.0 mM $[Ru(bpy)_3]^{2+}$, 5.0 mM $Na_2S_2O_8$, 5.0 µM **Ru_4SiPOM**, 20 mM sodium phosphate buffer, initial pH 7.2, total reaction volume 8, 16, 2 mL for cell A, B and C, respectively. Illumination: 50 mW, 420-520 nm for A; 16.8 mW, 420-470 nm for B and C.

On the other hand, the quantum efficiency for cell A is far lower than that for cells B and C. Cell A is a round bottom flask made from borosilicate glass with non-polished

and curved surface, resulting in a loss of light on the vessel surface due to reflection, refraction, and scattering while cells B and C have flat and polished surfaces to facilitate the light harnessing. As such, the experimental accuracy for determining quantum yield is better for cells B and C. Additionally, the higher quantum yield in cell B than in C indicates that the overall solution volume can also affect the rate of O_2 evolution. Considering the three factors (TON, chemical yield, and quantum yield) together, cell C was chosen as the ideal reaction vessel for further studies.

Table 2-1. Turnover Numbers, chemical yields ($2O_2/Na_2S_2O_8$) and Quantum Yields ($2O_2/h\nu$) of reaction performed in the cells A, B and C. Experimental conditions in **Figure 2-2**.

Cell	TON (O_2/ **Ru_4SiPOM**)	Chemical Yield ($2O_2/Na_2S_2O_8$)	Quantum Yield ($2O_2/h\nu$)
A	192	39%	8.5%
B	88	18%	35%
C	200	40%	27%

Calibration of the cuvette was conducted with the same general procedure as above except in the absence of the reactants substituted with equal volume of deionized water. After degassing, an amount of O_2 was injected into the cuvette. The cuvette was then stirred for about 1 min to allow equilibration of O_2 between the aqueous and gas phases before the headspace was sampled. This process was repeated for volumes of 0, 23.5, 47, and 70.5 μL of O_2 corresponding to 0, 1, 2, and 3 μmol of O_2 respectively. The peak area from the chromatograph corresponding to O_2 was then adjusted for contamination from air by subtracting half of the peak from the chromatograph corresponding to N_2 (less than 0.07 μmol O_2). The adjusted O_2 peak was then plotted against the amount of O_2 injected. This entire process was repeated twice more and each data point averaged.

2.3.3 Dependence on stirring rate

In the photocatalytic reaction with **Co_4PPOM** as a catalyst carried out in cell A and using a Scienceware* Cell Spinbar* stir bar, increasing the stirring rate was shown to facilitate the O_2 formation, resulting in higher TON, chemical yield, and quantum yield. For the light-driven reaction with **Co_4PPOM** as a catalyst in cell C using a VWP 8 x 1.5 mm flea micro spinbar, similar effects of stir rate on the O_2 formation were observed, as shown in **Figure 2-3.** Using cell C and SYS-114 system to stir the solution, the stir bar does not stably spin when the RPM is higher than 5000 rpm. Based on the trend observed in **Figure 2-3** where increased stirring rate results in increased amounts of dioxygen, a faster stirring rate may produce even greater amounts of dioxygen, however, if the stirring is too fast, the agitated solution fills up all the headspace, resulting in difficulties for gas sampling. Thus the ideal stirring rate for vessal C at the given conditions was set to 5000 rpm (level 10 on stirring meter) for our further experiments.

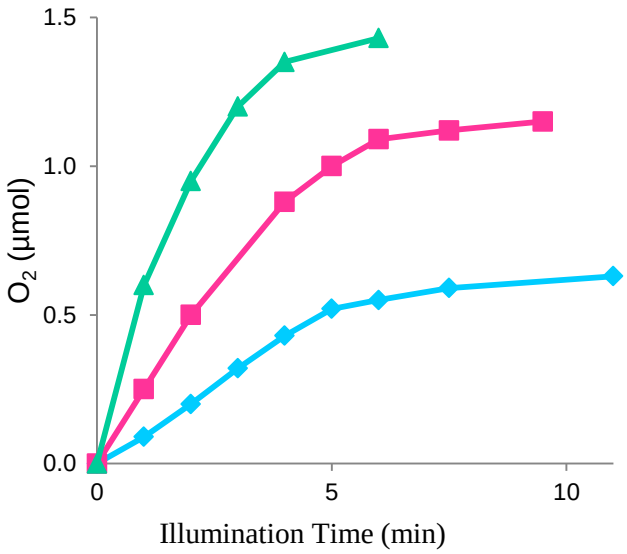

Figure 2-3. Kinetics of O_2 formation at stirring rate: 5000 (teal triangles), 3000 (pink squares), and 1200 rpm (blue diamonds). Experiments were carried out in the cell C using a VWP 8 x 1.5 mm flea micro spinbar. Conditions: 1.0 mM $[Ru(bpy)_3]^{2+}$, 5.0 mM $Na_2S_2O_8$, 5.0 µM **Co_4PPOM**, 20 mM sodium borate buffer, initial pH 8.0, total reaction volume 2 mL. Illumination: 16.8 mW, 420-470 nm, beam size 0.75 in diameter.

Optimization for this light-driven system was also carried out with respect to buffer. For reasons that will be elaborated in **Chapter 3**, the nature of buffer also affected the efficiency of O_2 formation (**Figure 2-4**). In this work, 80 mM borate buffer was found to maintain the pH well, with a pH decrease of only 0.1−0.3 pH unit by the end of the reaction.

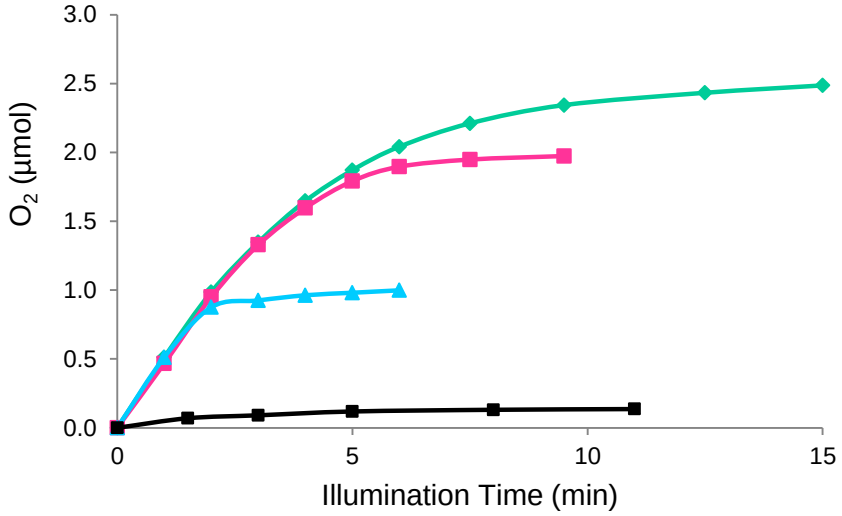

Figure 2-4. Kinetics of O_2 formation with pH 8 buffer: 20 mM NaP_i; black squares, final pH 6.5, 20 mM NaB_i: blue triangles, final pH 2.0, 40 mM NaB_i pink squares, final pH 5.3, and 80 mM NaB_i teal diamonds, final pH 7.9. Conditions: 1.0 mM $[Ru(bpy)_3]^{2+}$, 5.0 mM $Na_2S_2O_8$, 5.0 µM **Co_4PPOM**.

2.4 Results and discussion

Dioxygen was formed quickly under visible-light illumination (420−470 nm) catalyzed by even 1.5 µM **Co_4PPOM** (**Figure 2-5**). A series of control experiments confirmed that fast O_2 generation requires the presence of all four components: photons, $[Ru(bpy)_3]^{2+}$, persulfate, and **Co_4PPOM**. In the absence of **Co_4PPOM**, the maximum O_2 yield after 15 min of illumination was about 0.2 µmol; 12 times lower than in catalytic runs using 5 µM **Co_4PPOM**. After 10−15 min of illumination, the amount of O_2 reached a plateau value, the concentration of $S_2O_8^{2-}$ decreased from its initial value of 5.0 mM to less than the limit of detection of 0.2 mM as quantified by a method discussed previously.[24,34] The concentration of $[Ru(bpy)_3]^{2+}$ was found to be about 15% as has been shown to be the case in other WOC systems[35] as quantified by absorbance at 450 nm. The spectra of $[Ru(bpy)_3]^{2+}$ before and after catalytic runs is shown in **Figure 2-6**.

Significantly, photosensitizer decomposition decreases as concentration of the catalyst increases (**Figure 2-6** insert), indicating that the photosensitizer is protected from decomposition by the presence of the catalyst. Furthermore, catalytic oxidation of water resumed upon the addition of $S_2O_8^{2-}$ (**Figure 2-7**), suggesting that the catalyst remains active and that significant $[Ru(bpy)_3]^{2+}$ remains intact. Thus, the final amount of O_2 formed and the TON (**Table 2-2)** at the end of each run was limited mainly by depletion of the sacrificial electron acceptor.

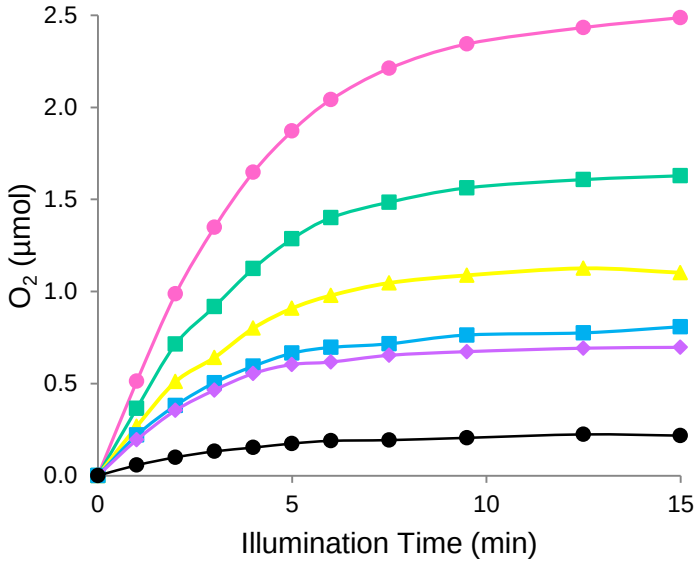

Figure 2-5. Kinetics of O_2 formation in the light-driven system at different concentrations of **Co_4PPOM**: 0 (black circles), 1.5 (purple diamonds), 2 (blue squares), 3 (yellow triangles), 4 (teal squares), and 5 µM (pink circles). 1.0 mM $[Ru(bpy)_3]^{2+}$, 5.0 mM $Na_2S_2O_8$, 80 mM sodium borate buffer initial pH 8.0.

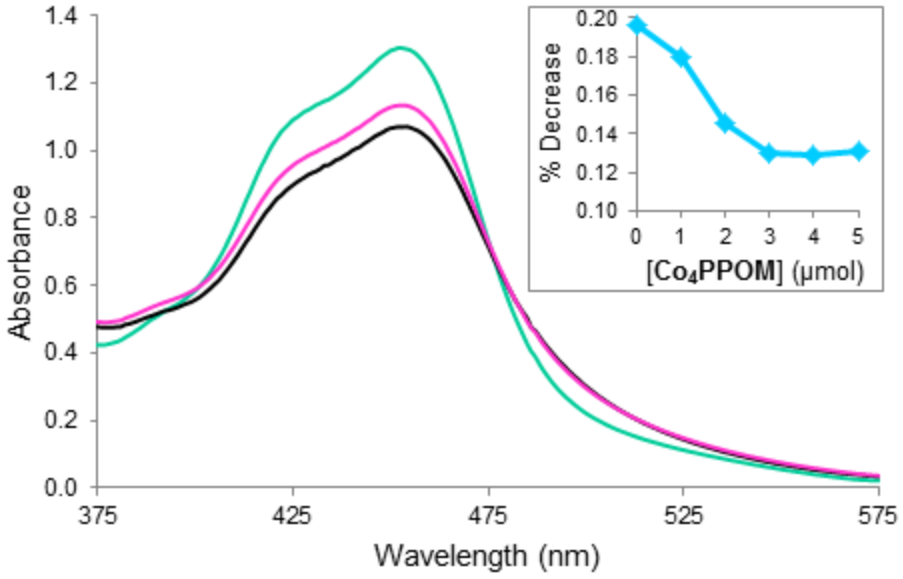

Figure 2-6. UV-Vis of $[Ru(bpy)_3]^{2+}$ before reaction (teal), and after catalysis with: no catalyst (black), and 5 uM **Co_4PPOM** (pink). Insert shows absorbance at 450 nm as a function of **Co_4PPOM** concentration after catalytic reaction. 1.0 mM $[Ru(bpy)_3]^{2+}$, 5.0 mM $Na_2S_2O_8$, 80 mM sodium borate buffer initial pH 8.0.

Although the stability of **Co_4PPOM** under thermal (dark) catalytic water oxidation conditions was assessed previously by seven distinct and complementary techniques as elaborated in **Chapter 1**,[1] the conditions in the light-driven reactions reported in this study are sufficiently different than in the absence of light, thus additional catalyst stability experiments were conducted. Further experiments and analysis of **Co_4PPOM** stability across light-driven, dark, and electrochemical systems will be addressed in **Chapter 3**. Careful assessment of the pre- and post-catalysis solutions showed no evidence of nanoparticle formation by dynamic light scattering or Tyndall effect. Second, the kinetics of O_2 evolution using **Co_4PPOM** after one use showed very similar kinetics (similar curvature and rate; **Figure 2-7**). These arguments and all the

work assessing the stability of **Co_4PPOM** under dark catalytic water oxidation conditions provide good evidence that the catalyst is stable under these photochemical conditions up to the number of turnovers in these studies: TON = 220 per run. The kinetics (curvatures in **Figure 2-5**) and the turnover numbers were solely limited by the amount of sacrificial electron acceptor, persulfate, present in the system.

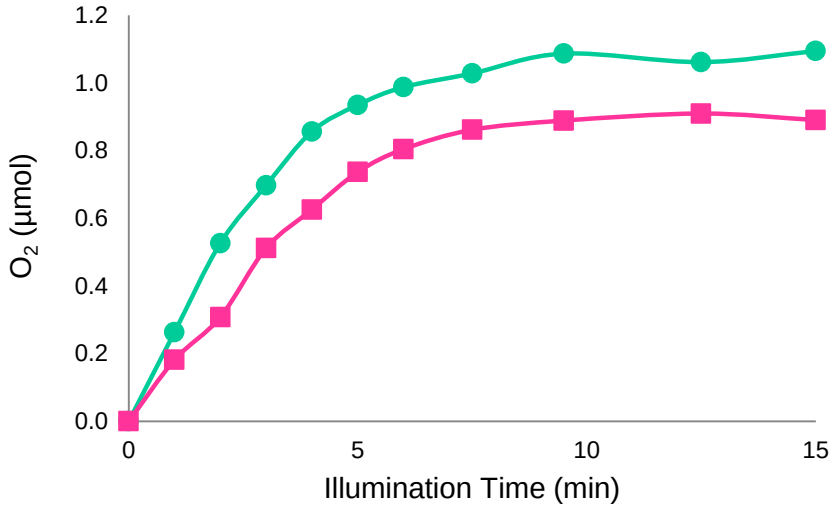

Figure 2-7. O_2 formation kinetics of the first run (teal circles) and the second run (pink squares). After first run, another 0.05 mL of $Na_2S_2O_8$ was added (the persulfate concentration was the same as at the outset of the first run), the contents degassed and a second run was conducted under otherwise identical conditions. Conditions for the first run: 1.0 mM $[Ru(bpy)_3]^{2+}$; 5.0 mM $Na_2S_2O_8$; 130 mM NaB_i (initial pH 8.0); 5 µM catalyst.

At the end of the second run, the pH was reduced to 7.3 from initial pH 8.0, and the TON and chemical yield decrease about 20%. At the end of the second run, the $[Ru(bpy)_3]^{2+}$ concentration decreases by about 28%. For these reuse runs 130 mM buffer was used because higher buffer capacity was required although at this buffer

concentration, the TON, Φ_{CY} and Φ_{QY}(t) all decrease to about half their measured values in 80 mM buffer.

Table 2-2. Turnover Numbers (TON), Chemical Yields, and Initial Quantum Yields for Homogeneous Visible-Light-Driven Water Oxidation Catalyzed by **Co_4PPOM**. TONs and chemical yields were averaged for results at 12.5 and 15 min. (a) 5 μM **Ru_4SiPOM**; reported values, excluding 0 μM, were corrected for the amount of O_2 generated in absence of catalyst. 1.0 mM $[Ru(bpy)_3]^{2+}$, 5.0 mM $Na_2S_2O_8$, 80 mM sodium borate buffer initial pH 8.0.

Catalyst (μM)	TON	Chemical Yield	Quantum Yield
0	N/A	0.04 ± 0.01	0.03 ± 0.01
1.5	158 ± 15	0.09 ± 0.01	0.09 ± 0.01
2.0	143 ± 03	0.11 ± 0.01	0.10 ± 0.01
3.0	149 ± 15	0.18 ± 0.02	0.14 ± 0.01
4.0	175 ± 06	0.28 ± 0.01	0.20 ± 0.01
5.0	224 ± 11	0.45 ± 0.02	0.30 ± 0.05
5.0[a]	136 ± 05	0.27 ± 0.01	0.24 ± 0.01

To quantify the photocatalytic performance, the average stoichiometric dioxygen chemical yields and the initial photon-to-O_2 generation quantum yields were compared. According to **Equation 2-2** and **Scheme 2-1**, two photons and two $S_2O_8^{2-}$ ions lead to the evolution of one O_2 molecule in the absence of loss pathways. The value of $\Phi_{QY}(t)$ can also be calculated from the ratio of the rates of O_2 generation and photon absorption and is related to the slope of the plot of O_2 versus illumination time shown in **Figure 2-5**. It is clear that $\Phi_{QY}(t)$ is largest at the onset of the reaction and decreases with time, approaching zero at ~15 min. It was shown previously that the ratio of O_2 formed to $Na_2S_2O_8$ consumed changes negligibly throughout the course of the catalytic runs with **Ru_4SiPOM** in a similar system.[24] Only the average value of $2[O_2]/[Na_2S_2O_8]$ (over the course of the reaction) was measured in this study. The values of Φ_{CY} and $\Phi_{QY}(0)$ as

functions of catalyst concentration are plotted in **Figure 2-8** and listed in **Table 2-2**. In calculating these values the maximal contribution of O_2 generated from noncatalytic pathways, obtained from the control experiment without catalyst, was subtracted from the observed value.[35] Both the chemical yield and the initial quantum yield were found to increase with catalyst concentration.

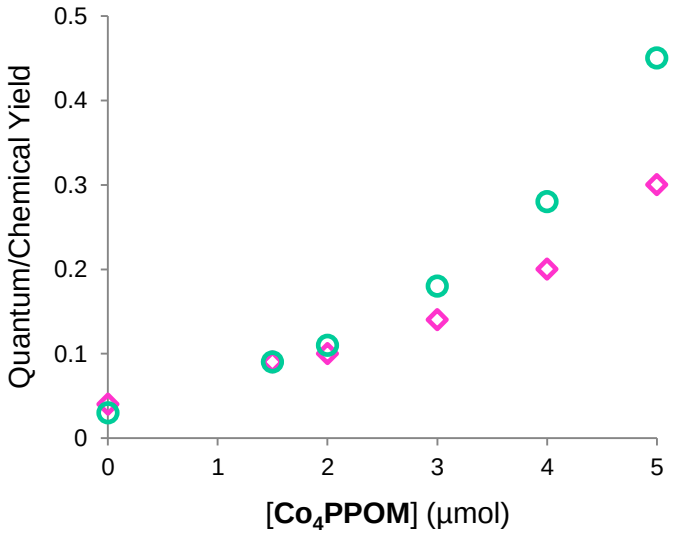

Figure 2-8. Dependence of chemical yield (teal square) and initial quantum yield (pink circles) on catalyst concentration, **Co_4PPOM**. 1.0 mM $[Ru(bpy)_3]^{2+}$, 5.0 mM $Na_2S_2O_8$, 80 mM sodium borate buffer initial pH 8.0.

The photocatalytic O_2 evolution in this system is believed to follow the well-established reaction mechanism presented in **Scheme 2-1**.[24,27,28] The reaction is initiated upon the absorption of two photons by two $[Ru(bpy)_3]^{2+}$ complexes. Because of the large extinction coefficient ($\varepsilon_{454} = 1.4 \times 10^4\ M^{-1}\ cm^{-1}$) and high relative concentration of

$[Ru(bpy)_3]^{2+}$ (1 mM), all of the incident photons are captured by $[Ru(bpy)_3]^{2+}$ in the solution. Following photoexcitation, the excited $[Ru(bpy)_3]^{2+*}$ is quenched by $S_2O_8^{2-}$ through both bimolecular and unimolecular electron transfer (ET) pathways.[36-38] The quenching, or ET efficiency (ϕ_q) increases with the $S_2O_8^{2-}$ concentration (as shown in **Figure 2-9**) and is 67% at 5.0 mM $Na_2S_2O_8$, the initial concentration used in the catalytic runs. The photoinduced ET results in the generation of two $[Ru(bpy)_3]^{3+}$ complexes and two $SO_4^{-\bullet}$ radical anions. The latter subsequently oxidize two additional $[Ru(bpy)_3]^{2+}$ to give two $[Ru(bpy)_3]^{3+}$, with a yield of ϕ_r. Finally, four $[Ru(bpy)_3]^{3+}$ complexes oxidize water to make one O_2 with a yield of ϕ_c.

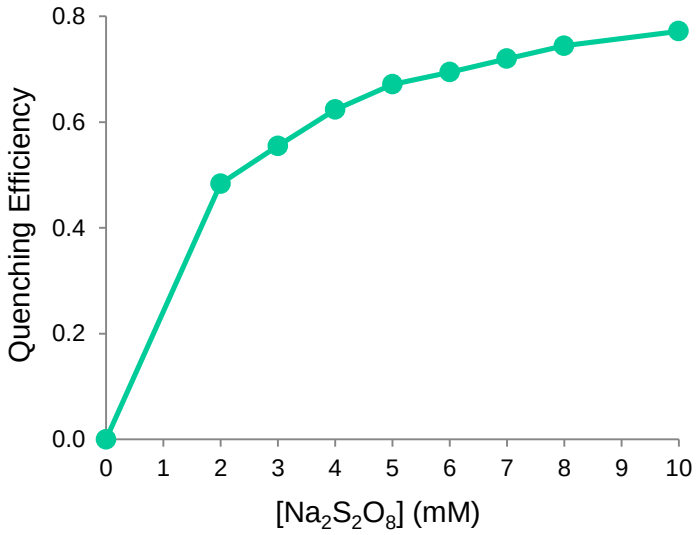

Figure 2-9. Quenching efficiency of $[Ru(bpy)_3]^{2+*}$ emission by the addition of $[Na_2S_2O_8]$. Conditions: 1.0 mM $[Ru(bpy)_3]^{2+}$, 80 mM sodium borate buffer initial pH 8.0.

The relationship in **Equation 2-7** agreed well with our experimental data (**Table 2-2**) and accounts for the observed decrease in the rate (quantum yield) of O_2 formed as a function of time and the catalyst concentration. For example, with the

measured initial ϕ_q of 0.67 (**Figure 2-8**) and Φ_{CY} of 0.45 (**Table 2-2)**, for 5 μM **Co_4PPOM**, the initial Φ_{QY} is 0.30, which agrees well with the measured value (0.30). As the reaction proceeds, $\phi_q(t)$ and therefore $\Phi_{QY(t)}$ decrease as a result of the depletion of $S_2O_8^{2-}$. In measurements with different catalyst concentrations, the initial quenching efficiency ϕ_q should be identical (67%) because it is based solely on initial concentrations of $[Ru(bpy)_3]^{2+}$ and $S_2O_8^{2-}$. According to **Equation 2-7**, the reduced initial quantum yield for O_2 generation can be attributed to the decrease in the chemical yield at lower catalyst concentrations, consistent with the experimental observations shown in **Figure 2-5** and **Table 2-2**.

Our results suggests that a key factor that limits the quantum yield is the chemical yield Φ_{CY}, which is significantly less than unity in the current system. According to **Equation 2-4**, Φ_{CY} is determined by both ϕ_r and ϕ_c. The ϕ_r is generally taken to be near unity, although several reports have indicated that it is less than unity and highly dependent on the solution environment.[39-41] In a previous study, it was determined that ϕ_c = 67% for **Co_4PPOM** at pH 8 in stoichiometric water oxidation in the dark by $[Ru(bpy)_3]^{3+}$.[31] From the measured Φ_{CY} (0.45 at 5 μM **Co_4PPOM**), the minimal ϕ_c (when ϕ_r = 1) can be estimated to be 0.45, consistent with the previously reported ϕ_c value.[31] Φ_{CY} and hence ϕ_c increase with the catalyst concentration, implying a competition between catalytic (see **Scheme 2-1**) and noncatalytic pathways involving the photogenerated $[Ru(bpy)_3]^{3+}$.

To gain further insight into the factors limiting the quantum and chemical yields for catalytic O_2 generation, we also compared the catalytic activities

of **Ru_4SiPOM** and **Co_4PPOM** under identical conditions. As shown by both **Figure 2-10** and **Table 2-2**, the chemical yield and TON in the reactions catalyzed by **Co_4PPOM** are about 1.7 fold higher than those catalyzed by **Ru_4SiPOM**, with a 1.25 higher quantum yield. These three criteria demonstrate that **Co_4PPOM**, an abundant-metal-based material, catalyzes visible-light-driven water oxidation more rapidly than **Ru_4SiPOM**, which contains a precious metal, ruthenium. Furthermore, the photochemical reactions using **Ru_4SiPOM** and **Co_4PPOM** have the same charge, and were carried out under the same conditions, thus ϕ_r should be the same in both systems. Therefore, a higher Φ_{CY} for **Co_4PPOM** suggests a higher ϕ_c using this catalyst. These data suggest that **Co_4PPOM** has a higher selectivity toward water oxidation than **Ru_4SiPOM**, which is consistent with a higher TOF for dark water oxidation by **Co_4PPOM** than by **Ru_4SiPOM**.[31]

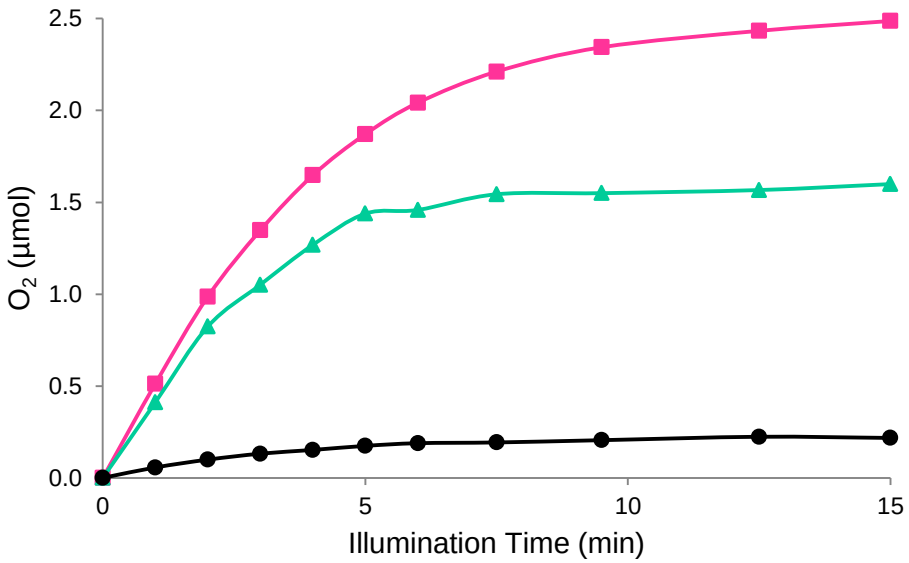

Figure 2-10. Kinetics of O_2 formation in the light-driven system using different catalysts: **Ru_4SiPOM** (teal triangles), **Co_4PPOM** (pink squares) and control (no catalyst, black circles). Conditions: 1.0 mM $[Ru(bpy)_3]^{2+}$; 5.0 mM $Na_2S_2O_8$; 80 mM sodium borate buffer initial pH 8.0; 5 µM catalyst.

Light-driven water oxidation utilizes $[Ru(bpy)_3]^{3+}$ as an intermediate oxidant (**Equation 2-1** and **Scheme 2-1**). A higher ϕ_c indicates a faster conversion of $[Ru(bpy)_3]^{3+}$ to $[Ru(bpy)_3]^{2+}$ in the presence of the catalyst. The concentration of $[Ru(bpy)_3]^{3+}$ can be followed by the absorption at 670 nm, where $[Ru(bpy)_3]^{2+}$ has a very low extinction coefficient (ε_{670} = 20 $M^{-1}cm^{-1}$). Hence, the catalytic efficiencies of **Ru_4SiPOM** and **Co_4PPOM** for water oxidation can also be compared using the kinetics of the disappearance of $[Ru(bpy)_3]^{3+}$ in the stoichiometric dark water oxidation system. These kinetics traces (**Figure 2-11**) were measured by the stopped-flow technique, in which solutions containing $[Ru(bpy)_3]^{3+}$ and the catalysts, respectively, were rapidly mixed. It was found that $[Ru(bpy)_3]^{3+}$ is consumed via two competing pathways: catalytic water oxidation (**Equation 2-1**) and the self-decomposition reaction.[25] At pH 8, the $[Ru(bpy)_3]^{3+}$ half-life of about 30 s in the absence of catalyst was reduced to 11 and 1.3 s upon addition of **Ru_4SiPOM** and **Co_4PPOM**, respectively. Here, the half-life, defined as the time at which the concentration has decreased to one-half of the initial value, was used to compare the relative decay rates of $[Ru(bpy)_3]^{3+}$ because the kinetics are complex (not single-exponential) and will be expanded on in detail in **Chapter 4**. While oxidative catalysis of the bpy ligand cannot be ruled out as a pathway for the consumption of $[Ru(bpy)_3]^{3+}$,[35] this along with the results in **Figure 2-3** and **Figure 2-10** suggest that **Ru_4SiPOM** and **Co_4PPOM** are both efficient WOCs. This result shows that **Co_4PPOM** is almost 10 times more efficient than **Ru_4SiPOM** in catalyzing the dark reaction (**Equation 2-1**), suggesting that **Co_4PPOM** should also be a more efficient catalyst in the light-driven systems. Indeed, the O_2 formation kinetics shows this to be the case.

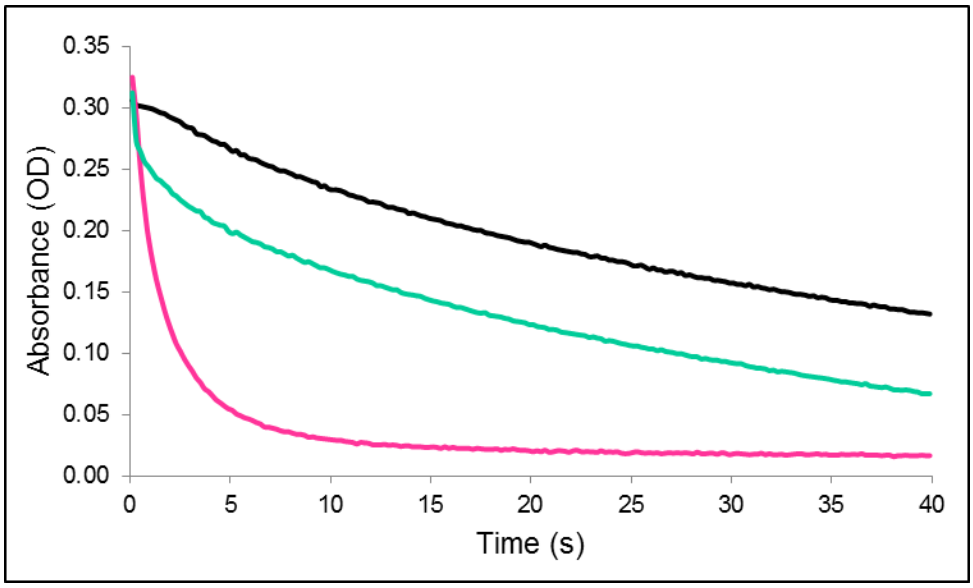

Figure 2-11. Kinetics of $[Ru(bpy)_3]^{3+}$ reduction to $[Ru(bpy)_3]^{2+}$, measured as the decrease in absorbance at 670 nm for the noncatalytic reaction (black, no catalyst), 5 μM **Ru_4SiPOM** (teal), and 5 μM **Co_4PPOM** (pink). Conditions: 1 mM $[Ru(bpy)_3]^{3+}$ (initial), 80 mM sodium borate buffer, pH 8.0, 20 °C.

In summary, it has been demonstrated that **Co_4PPOM**, a carbon-free molecular WOC consisting of only earth-abundant metals, is a very efficient and stable molecular catalyst for light-driven water oxidation. Under the same conditions (pH 8), **Co_4PPOM** is more efficient than **Ru_4SiPOM** in oxidizing water, and this finding can be attributed to the higher turnover frequency of **Co_4PPOM** relative to **Ru_4SiPOM**.

2.5 References

(1) Barber, J. *Chem. Soc. Rev.* **2009**, *38*, 185.

(2) Lewis, N. S.; Nocera, D. G. *Proc. Natl. Acad. Sci.* **2006**, *103(43)*, 15729.

(3) Gray, H. B. *Nature Chem.* **2009**, *1*, 7.

(4) Binstead, R. A.; Chronister, C. W.; Ni, J.; Hartshorn, C. M.; Meyer, T. J. *J. Am. Chem. Soc.* **2000**, *122*, 8464.

(5) Yagi, M.; Kaneko, M. *Chem. Rev.* **2001**, *101*, 21.

(6) Hurst, J. K. *Coord. Chem. Rev.* **2005**, *249*, 313.

(7) Zong, R.; Thummel, R. *J. Am. Chem. Soc.* **2005**, *127*, 12802.

(8) Eisenberg, R. *Science* **2009**, *324*, 44.

(9) Du, P.; Eisenberg, R. *Energy Environ. Sci.* **2012**, *5*, 6012.

(10) Tinker, L. L.; McDaniel, N. D.; Bernhard, S. *J. Mater. Chem.* **2009**, *19*, 3328.

(11) Robinson, D. M.; Go, Y. B.; Greenblatt, M.; Dismukes, G. C. *J. Am. Chem. Soc.* **2010**, *132*, 11467.

(12) Tamaki, Y.; Vannucci, A. K.; Dares, C. J.; Binstead, R. A.; Meyer, T. J. *J. Am. Chem. Soc.* **2014**, *136*, 6854.

(13) Faunce, T.; Styring, S.; Wasielewski, M. R.; Brudvig, G. W.; Rutherford, A. W.; Messinger, J.; Lee, A. F.; Hill, C. L.; deGroot, H.; Fontecave, M.; MacFarlane, D. R.; Hankamer, B.; Nocera, D. G.; Tiede, D. M.; Dau, H.; Hillier, W.; Wang, L.; Amal, R. *Energy Environ. Sci.* **2013**, *6*, 1074.

(14) Badiei, Y. M.; Polyansky, D. E.; Muckerman, J. T.; Szalda, D. J.; Haberdar, R.; Zong, R.; Thummel, R. P.; Fujita, E. *Inorg. Chem.* **2013**, *52*, 8845.

(15) Llobet, A. *Molecular Water Oxidation Catalysis: A Key Topic for New Sustainable Energy Conversion Schemes*; John Wiley & Sons, Ltd., 2014.

(16) Cao, R.; Ma, H.; Geletii, Y. V.; Hardcastle, K. I.; Hill, C. L. *Inorg. Chem.* **2009**, *48*, 5596.

(17) Yang, J.; Walczak, K.; Anzenberg, E.; Toma, F. M.; Yuan, G.; Beeman, J.; Schwartzberg, A.; Lin, Y.; Hettick, M.; Javey, A.; Ager, J. W.; Yano, J.; Frei, H.; Sharp, I. D. *J. Am. Chem. Soc.* **2014**, *136*, 6191.

(18) Young, K. J.; Martini, L. A.; Milot, R. L.; III, R. C. S.; Batista, V. S.; Schmuttenmaer, C. A.; Crabtree, R. H.; Brudvig, G. W. *Coord. Chem. Rev.* **2012**, *256*, 2503.

(19) Kuznetsov, A. E.; Geletii, Y. V.; Hill, C. L.; Morokuma, K.; Musaev, D. G. *J. Am. Chem. Soc.* **2009**, *131*, 6844.

(20) Duan, L.; Araujo, C. M.; Ahlquist, M. S. G.; Sun, L. *Proc. Natl. Acad. Sci.* **2012**, *109*, 15584.

(21) Nakazono, T.; Parent, A. R.; Sakai, K. *Chem. Commun.* **2013**, *49*, 6325.

(22) Geletii, Y. V.; Botar, B.; Kögerler, P.; Hillesheim, D. A.; Musaev, D. G.; Hill, C. L. *Angew. Chem. Int. Ed.* **2008**, *47*, 3896.

(23) Sartorel, A.; Carraro, M.; Scorrano, G.; Zorzi, R. D.; Geremia, S.; McDaniel, N. D.; Bernhard, S.; Bonchio, M. *J. Am. Chem. Soc.* **2008**, *130*, 5006.

(24) Geletii, Y. V.; Huang, Z.; Hou, Y.; Musaev, D. G.; Lian, T.; Hill, C. L. *J. Am. Chem. Soc.* **2009**, *131*, 7522.

(25) Geletii, Y. V.; Besson, C.; Hou, Y.; Yin, Q.; Musaev, D. G.; Quinonero, D.; Cao, R.; Hardcastle, K. I.; Proust, A.; Kögerler, P.; Hill, C. L. *J. Am. Chem. Soc.* **2009**, *131*, 17360.

(26) Sartorel, A.; Miro, P.; Salvadori, E.; Romain, S.; Carraro, M.; Scorrano, G.; Valentin, M. D.; Llobet, A.; Bo, C.; Bonchio, M. *J. Am. Chem. Soc.* **2009**, *131*, 16051.

(27) Puntoriero, F.; Ganga, G. L.; Sartorel, A.; Carraro, M.; Scorrano, G.; Bonchio, M.; Campagna, S. *Chem. Commun.* **2010**, *46*, 4725.

(28) Besson, C.; Huang, Z.; Geletii, Y. V.; Lense, S.; Hardcastle, K. I.; Musaev, D. G.; Lian, T.; Proust, A.; Hill, C. L. *Chem. Commun.* **2010**, 2784.

(29) Orlandi, M.; Argazzi, R.; Sartorel, A.; Carraro, M.; Scorrano, G.; Bonchio, M.; Scandola, F. *Chem. Commun.* **2010**, *46*, 3152.

(30) Toma, F. M.; Sartorel, A.; Iurlo, M.; Carraro, M.; Parisse, P.; Maccato, C.; Rapino, S.; Gonzalez, B. R.; Amenitsch, H.; Ros, T. D.; Casalis, L.; Goldoni, A.; Marcaccio, M.; Scorrano, G.; Scoles, G.; Paolucci, F.; Prato, M.; Bonchio, M. *Nature Chem.* **2010**, *2*, 826.

(31) Yin, Q.; Tan, J. M.; Besson, C.; Geletii, Y. V.; Musaev, D. G.; Kuznetsov, A. E.; Luo, Z.; Hardcastle, K. I.; Hill, C. L. *Science* **2010**, *328*, 342.

(32) Tézé, A.; Hervé, G. In *Inorg. Synth.*; Ginsberg, A. P., Ed.; John Wiley and Sons: New York, 1990; Vol. 27, p 85.

(33) Qiushi Yin, J. M. T., Claire Besson, Yurii V. Geletii, Djamaladdin G. Musaev,; Aleksey E. Kuznetsov, Z. L., Ken I. Hardcastle, Craig L. Hill *Science* **2010**, *328*, 342.

(34) House, D. A. *Chem. Rev.* **1962**, *62*, 185.

(35) Ghosh, P. K.; Brunschwig, B. S.; Chou, M.; Creutz, C.; Sutin, N. *J. Am. Chem. Soc.* **1984**, *106*, 4772.

(36) White, H. S.; Becker, W. G.; Bard, A. J. *J. Phys. Chem.* **1984**, *88*, 1840.

(37) Kaledin, A. L.; Huang, Z.; Yin, Q.; Dunphy, E. L.; Constable, E. C.; Housecroft, C. E.; Geletii, Y. V.; Lian, T.; Hill, C. L.; Musaev, D. G. *J. Phys. Chem. A* **2010**, *114*, 6284.

(38) Quiñonero, D.; Kaledin, A. L.; Kuznetsov, A. E.; Geletii, Y. V.; Besson, C.; Hill, C. L.; Musaev, D. G. *J. Phys. Chem. A* **2010**, *114*, 535.

(39) Horváth, A.; Bakó, Z.; Papp, S.; Keszei, C. *J. Photochem. Photobiol. A: Chem.* **1990**, *52*, 271.

(40) Bolletta, F.; Juris, A.; Maestri, M.; Sandrini, D. *Inorg. Chim. Acta* **1980**, *44*, L175.

(41) Henbest, K.; Douglas, P.; Garley, M. S.; Mills, A. *J. Photochem. Photobiol. A: Chem.* **1994**, *80*, 299.

Chapter 3

Differentiating Homogeneous and Heterogeneous Water Oxidation Catalysis: Confirmation that $[Co_4(H_2O)_2(\alpha\text{-}PW_9O_{34})_2]^{10-}$ Is a Molecular Water Oxidation Catalyst

3.1 Introduction

As mentioned in **Chapter 1** the production of solar fuel is a consensus goal of the research community based on the projected need for enormous quantities of high density energy in the coming decades.[1-3] Central to the production of solar fuels, either by water splitting or carbon dioxide reduction is the oxidation of water. This four-electron process continues to be viewed as a central challenge in realizing solar fuel generating prototypes (electron-donor nanostructures, photoelectrochemical cells, etc.).[4-6] As a consequence, there continues to be exceptional research activity aimed at developing viable (fast, selective, stable) both homogeneous[7-25] and heterogeneous[26-41] water oxidation catalysts (WOCs).[31,40,42-49]

Pioneering work has provided criteria for distinguishing homogeneous catalysts from heterogeneous ones, largely for reactions under reducing conditions.[50-52] In continuation with this effort, a series of new experiments which can be used to not only differentiate a homogeneous catalyst from a heterogeneous one under oxidizing conditions, but also to distinguish particular molecular species generated in solution during turnover have been developed. Furthermore, these techniques can rule out activity from decomposition products which are known catalysts, and show which species is responsible for the observed catalytic activity. These studies can be divided into two categories: (1) those quantifying the amount of catalyst decomposition during catalytic turnover or the amount of some decomposition product that could be involved in catalysis, and (2) those assessing the kinetic behavior of each catalytically competent species as a function of the reaction variables. For reactions in aqueous media, these variables include pH, buffer and buffer concentration. The combined knowledge of the

quantities and kinetic behaviors of potential catalytic species provides a complete picture of which species is responsible for observed catalytic activity, in this case, but not limited to water oxidation.

One of the most promising classes of WOCs are polyoxometalates (POMs) because of their oxidative, thermal and tendency towards kinetic hydrolytic (over pH ranges dictated by the POM metal) stability. Some of these systems are among the fastest WOCs available to date.[53-55] Recently, several groups have reported POM WOCs based on abundant 3d elements (Co and Ni)[56-59] in addition to earlier Ru-containing POM WOCs.[60-64] After publication of the first precious-metal-free POM WOC, $[Co_4(H_2O)_2(PW_9O_{34})_2]^{10-}$ (**Co_4PPOM**) in 2010 (henceforth "HG"),[65-66] and a follow up paper examining its activity in a light-driven system, its stability, as well as the nature of the active species became the subject of multiple investigations over a range of

Table 3-1. Experimental conditions from various studies examining catalytic activity and stability of **Co_4PPOM**.

SF	SSB	HG Science	HG JACS	This Work
Electrochemical 1.1 V vs Ag/AgCl	Nanosecond Flash Photolysis	Dark (stoichiometric oxidant)	Photochemical 420-470 nm Xe lamp 16.8 mW	Photochemical 455 nm LED 17 mW
pH = 8.0 100 mM NaP_i 500 µM **Co_4PPOM**	pH = 8.0 80 mM NaP_i 50 µM **Co_4PPOM** 0.05 mM $[Ru(bpy)_3]^{2+}$ 5.0 mM $Na_2S_2O_8$	pH = 8.0 30 mM NaP_i 3.2 µM **Co_4PPOM** 1.5 mM $[Ru(bpy)_3]^{3+}$	pH = 8.0 80 mM NaB_i 5 µM **Co_4PPOM** 1.0 mM $[Ru(bpy)_3]^{2+}$ 5.0 mM $Na_2S_2O_8$	pH = 8.0 80 mM NaB_i 2 µM **Co_4PPOM** 1.0 mM $[Ru(bpy)_3]^{2+}$ 5.0 mM $Na_2S_2O_8$
TON calculated as 0.363	O_2 not measured	TON = 78.1	TON = 224	TON = 302 ± 1

experimental conditions (**Table 3-1**). The initial claim of a fast, stable, molecular WOC was first brought into question by Stracke and Finke (Stracke and Finke, *J. Am. Chem. Soc.*, **2011**, *133*, 14872, henceforth "SF") who, in electrochemical experiments, demonstrated that, the activity of **Co_4PPOM** could be explained by the formation of CoO_x films on the electrode surface. Another group (Scandola, Sartorel, Bonchio et al., *Chem. Commun*., **2012**, *48*, 8808, henceforth "SSB") studied **Co_4PPOM** by nanosecond flash photolysis experiments suggesting that the catalyst was a soluble molecular species, but that it was not **Co_4PPOM**. These three studies report on the WOC activity of **Co_4PPOM** in different systems using different techniques and draw conflicting conclusions. A follow-up paper by Finke and coworkers has revisited their previous work.[67] While **Co_4PPOM** has been well documented to be hydrolytically unstable above pH 7.5-8.0 in sodium phosphate buffer,[68-70] its kinetic stability under water oxidation conditions remains a subject of debate. A recent review noted, a general need to address in detail the fate of **Co_4PPOM** under a variety of conditions.[71] Thus **Co_4PPOM** makes a prime example of a system where there is need to differentiate an initial molecular species from its various possible decomposition products which are also known catalysts.

3.2 Experimental

3.2.1 General methods and materials

$[Ru(bpy)_3]Cl_2.H_2O$, sodium peroxydisulfate, and all other chemicals were of the highest purity available from commercial sources. $[Ru(bpy)_3]Cl_2 \cdot H_2O$ was recrystallized from 5 mL DI-water before use and $[Ru(bpy)_3](ClO_4)_3$ was prepared as previously reported.[72] Electronic absorption spectra were recorded using Agilent 8453

spectrophotometer. Infrared spectra (2 % sample in KBr pellet) were recorded with a Nicolet TM 6700 FT-IR spectrometer. The fast reactions were studied using a Hi-Tech KinetAsyst Stopped Flow SF-61SX2 instrument equipped with a diode array detector operating in wavelength range 400-700 nm. Stopped flow was performed as described in **Chapter 2**. Catalytic light-driven water oxidation was performed as described in **Chapter 2** except that the light source here was a 455 nm LED adjusted to 17 mW with a beam diameter of 0.5 cm.

3.2.2 Synthesis of Co_4PPOM from Δ-PW_9O_{34} and Co^{2+} in borate buffer

Although **Co_4PPOM** has been prepared in one pot synthesis[65] and previously in a multi-step procedure, an experiment was conducted to show that $[Co_4(H_2O)_2(PW_9O_{34})_2]^{10-}$ (**Co_4PPOM**) can form kinetically even under conditions where it is not fully stable hydrolytically. Specifically **Co_4PPOM** was prepared in NaB_i solution as follows: $Na_9[A\text{-}PW_9O_{34}]\cdot 4H_2O$ was synthesized according to the published method.[73] The Δ-PW_9O_{34} (a mixture of A- and B-type) was prepared by baking the dried solid of A-PW_9O_{34} at 140 °C for 6 hours.[66] A 116 mg sample of $Co(NO_3)_2\cdot 6H_2O$ was dissolved in 10 mL of borate buffer (0.1 M, pH 8) solution, and then 0.5 g of Δ-PW_9O_{34} was added in small portions with gentle stirring. The mixture was heated to 80 °C until a homogeneous purple solution was obtained, and then it was kept at 80 °C for an additional 10 min. Slow evaporation at room temperature resulted in 0.3 g (54.5% yield) of purple crystalline solid after about 5 days. X-ray crystallography was used to solve the crystal structure of the resulting product and its purity was checked by FT-IR and EA as in previous work. [65]

3.2.3 Cathodic adsorptive stripping voltammetry

Cathodic adsorptive stripping voltammetry (CAdSV) was performed with slight modifications to the literature method.[74] A bismuth film glassy carbon electrode was prepared by applying a -0.25 V potential (vs Ag/AgCl, 3M NaCl, BASi) for 45 s, using the clean electrode function in the software, while stirring, to a 1 M HCl solution containing 0.02 M $Bi(NO_3)_3 \bullet 5H_2O$ and 0.5 M LiBr. The electrode was then rinsed with water and immediately immersed into a solution containing the desired buffer and 0.1 mM DMG. Differential pulse voltammetry (DPV) was then performed with the following parameters: Accumulation occurred at -0.7 V, for 60 s with stirring at 300 rpm, followed by a quiet period without stirring for 15 s. The voltammogram was then recorded from -0.7 V to -1.3 V at ν = 10 mV/s, a pulse potential = 50 mV and step potential = 2 mV.

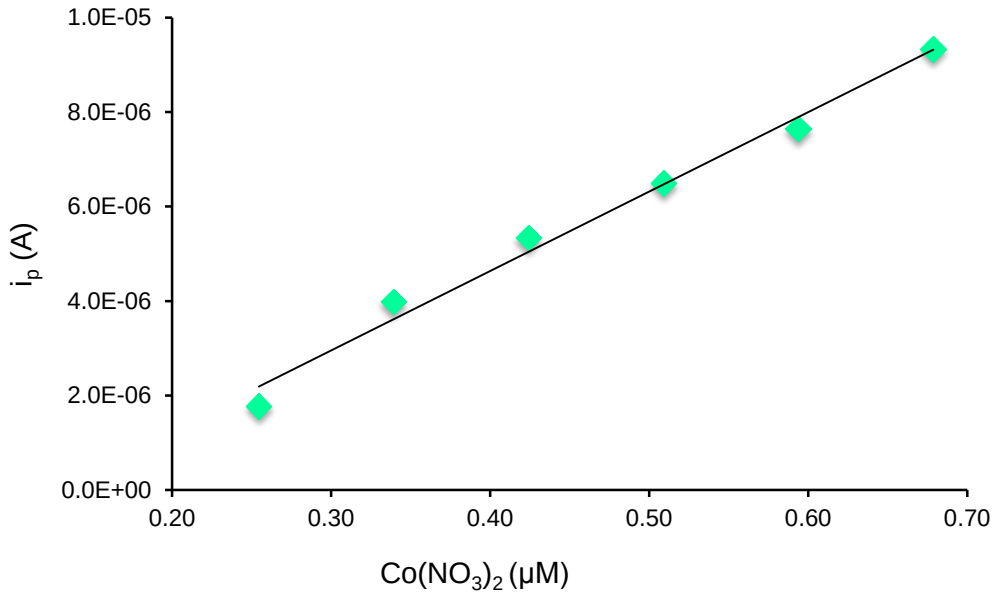

Figure 3-1. CAdSV NaP_i buffer calibration curve. Cathodic adsorptive stripping voltammetry with bismuth film glassy carbon electrode and 0.1 mM DMG. Voltammogram peak current (i_p) recorded from -0.7 V to -1.3 V at ν = 10 mV/s, pulse potential = 50 mV and step potential = 2 mV. With $Co(NO_3)_2$ in NaP_i buffer. $R^2 = 0.9871$

Calibration curves using $Co(NO_3)_2 \cdot 6H_2O$ as the source of $Co^{2+}(aq)$ were prepared for NaP_i (**Figure 3-1**) and borate buffers (**Figure 3-2**) to reduce possible interference effects from the buffer. In all cases, the peak current (i_p) was used to determine the concentration of cobalt present.

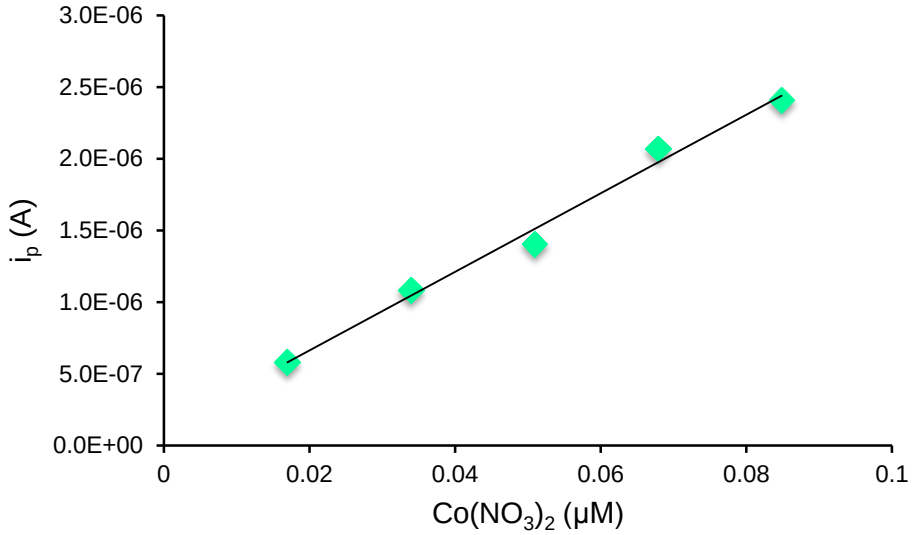

Figure 3-2. CAdSV Borate buffer calibration curve. Cathodic adsorptive stripping voltammetry with bismuth film glassy carbon electrode and 0.1 mM DMG. Voltammogram peak current (i_p) recorded from -0.7 V to -1.3 V at ν = 10 mV/s, pulse potential = 50 mV and step potential = 2 mV. With $Co(NO_3)_2$ in NaB_i. $R^2 = 0.9899$

3.2.4 Synthesis of tetraheptylammonium nitrate ($THpANO_3$) and extraction of Co_4PPOM from post-reaction solution

The $THpANO_3$ was synthesized from the reaction of tetra-*n*-heptylammonium bromide (THpABr) with $AgNO_3$. Typically, an aqueous solution (10 mL of H_2O) of $AgNO_3$ (40 mg) was added to a solution of THpABr (110 mg) in toluene. The resulting mixture was shaken vigorously forming light yellow AgBr. The colorless organic layer

was filtered to remove AgBr precipitate before use. The catalyst **Co_4PPOM** was extracted from the post-reaction solution using the resulting solution of $THpANO_3$ in toluene. The **Co_4PPOM**-free reaction solution was then recharged with 2.4 mg $Na_2S_2O_8$ before repeating the light-driven water oxidation reaction. A control experiment was conducted to ensure that the extraction did not in itself affect the O_2 yield (**Figure 3-3**). The extraction procedure was conducted on the buffer solution before the catalyst was added, solid **Co_4PPOM** was added and the reaction was conducted as normal.

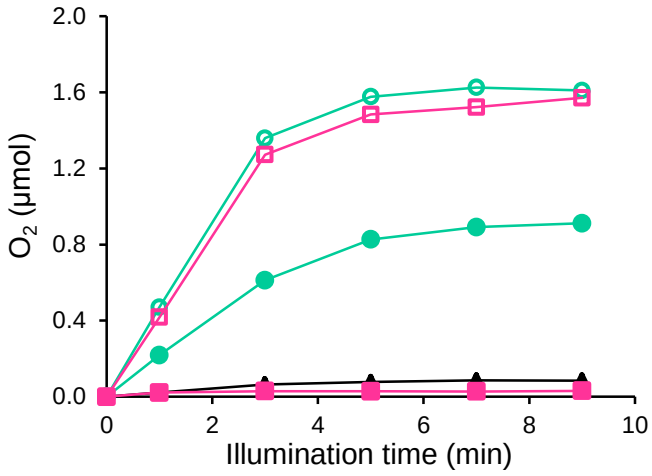

Figure 3-3. Kinetics of light-driven catalytic O_2 evolution from water catalyzed by **Co_4PPOM** in 0.12 M borate buffer at pH 8. Conditions: 5.0 mM $Na_2S_2O_8$, 1.0 mM $[Ru(bpy)_3]Cl_2$. Teal open circles, 2 µM **Co_4PPOM** initial run; teal solid circles, 2 µM **Co_4PPOM** second run; pink solid squares, extraction of the 2 µM **Co_4PPOM** solution in borate buffer with a toluene solution of $THpANO_3$, followed by addition of $[Ru(bpy)_3]Cl_2$ and $Na_2S_2O_8$; black triangles, the aqueous catalyst solution after the first run followed by extraction using a toluene solution of $THpANO_3$; pink open squares, control reaction where 2 µM **Co_4PPOM** solution in borate buffer extracted by a toluene solution of $THpANO_3$, followed by addition of 2 µM **Co_4PPOM**, $[Ru(bpy)_3]Cl_2$ and $Na_2S_2O_8$.

3.2.5 Measurement of Co^{2+}(aq) from Co_4PPOM

Co_4PPOM was aged in the desired buffer, and then a 1.5 mL aliquot of this solution was added to 1.5 mL of the same buffer containing 0.1 mM dimethylglyoxime (DMG). DPV was immediately performed as described above. The concentration determined from the calibration curve was then multiplied by 2 to account for dilution. Complete results are presented below in **Table 3-2**.

Table 3-2. Cathodic adsorptive stripping voltammetry for quantification of Co^{2+}(aq) from aged **Co_4PPOM**, in buffer at pH 8. Conditions: Bismuth film glassy carbon electrode and 0.1 mM DMG. Voltammogram peak current (i_p) recorded from -0.7 V to -1.3 V at ν = 10 mV/s, pulse potential = 50 mV and step potential = 2 mV.

Entry	[**Co_4PPOM**] (μM)	Buffer type, pH, concentration (mM)	Aging time in buffer (h)	[Co^{2+}(aq)], (μM)	Reference
1	2	NaB_i, 8, 80	3	0.07 ± 0.01	This work
2	2	NaP_i, 8, 80	3	0.54 ± 0.04	This work
3	2.5	NaP_i, 8, 100	1	0.25 ± 0.06	SF ACS Catalysis[67]
4	500	NaP_i, 8, 80	3	56 ± 2	SF JACS[75]

3.2.6 Inductively coupled plasma mass spectrometry

Inductively coupled plasma mass spectrometry (ICP-MS) was performed by Galbraith Laboratories, Inc. (Knoxville, TN, USA) with a Perkin Elmer Sciex Elan 6100 ICP Mass Spectrometer. Samples were diluted as needed, then introduced to the instrument via peristaltic pump and cross flow II nebulizer.

Samples were prepared as above for catalytic light-driven water oxidation. They were allowed to age for the desired time before the extraction procedure was performed

as above. The remaining solution was then submitted for analysis. Complete results are presented below in **Table 3-3**.

Table 3-3. Inductively coupled plasma mass spectrometry for solution with **Co_4PPOM**, in buffer at pH 8 aged as noted.

Entry	**Co_4PPOM** (μM)	Aging time (h)	Buffer	Co after extraction (μM)
1	500	16	0.1 M NaB_i	18 ± 1
2	500	16	0.1 M NaP_i	93 ± 5
3	2	3	0.08 M NaB_i	0.07 ± 0.01
4	2	3	0.08 M NaP_i	0.44 ± 0.02

3.2.7 Dynamic light scattering

Reaction solutions were prepared as in standard catalytic light driven procedure. Buffer solution was filtered prior to addition of reagents. Spectra were collected on a Zetasizer Nano ZS 90 instrument (Malvern Instruments Ltd, UK) after one run. The particle sizes suitable for measurement by this instrument range from 0.3 to 5000 nm (diameter) with a limit of detection (LoD) of 0.1 ppm.

As mentioned in previous work, the concentration of the catalyst and $[Ru(bpy)_3]Cl_2$ is limited by the formation of an insoluble adduct between **Co_4PPOM** and $[Ru(bpy)_3]^{2+}$. To quantify at what concentration an appreciable amount of this complex forms, DLS was used. To a solution containing 1.0 mM $[Ru(bpy)_3]^{2+}$, 5.0 mM $Na_2S_2O_8$ in 80 mM borate buffers filtered through a Millipore Millex-FX Phobic PTFE 0.45 μm syringe filter was added aliquots of 1.0 mM **Co_4PPOM** in water. Resulting solution was analyzed by DLS for particles above the limit of detection (**Figure 3-4**).

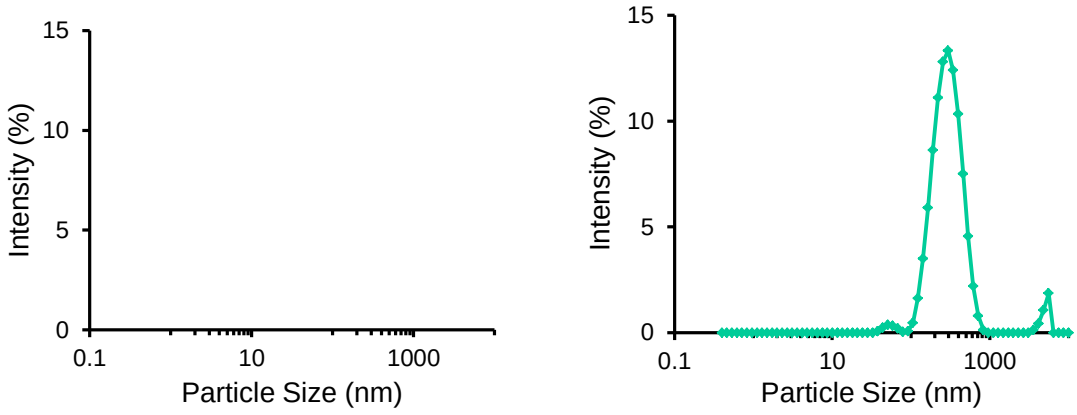

Figure 3-4. Particle size distribution (intensity %) obtained from dynamic light scattering measurement for solutions containing 1 mM $Ru(bpy)_3^{2+}$ in 80 mM NaB_i (pH = 8), 5.0 mM $Na_2S_2O_8$, with added **Co_4PPOM**. Amount added < 5.5 μM **Co_4PPOM** (left) or ≥ 5.5 μM **Co_4PPOM** (right).

3.2.8 Electronic absorption

Solutions of **Co_4PPOM** were dissolved in desired buffer solution and spectra were collected in a quartz cuvette (1 or 10 cm path length). Solutions were filtered prior to use. Absorbance at 580 nm was corrected by subtracting the absorbance at 800 nm.

3.2.9 Measurement of Co^{2+}(aq) from Co_4PPOM

Co_4PPOM was aged in the desired buffer, and then a 1.5 mL aliquot of this solution was added to 1.5 mL of the same buffer containing 0.1 mM DMG. DPV was immediately performed as described above. The concentration determined from the calibration curve was then multiplied by 2 to account for dilution. Complete results are presented below in **Table 3-2**.

3.2.10 Catalyst reusability test

After completion of the first reaction cycle, the same amount of NaS_2O_8, 2.38 mg, was added for the second run. The reaction was run with an initial buffer concentration of 120 mM such that the buffer capacity is not depleted over the second run but decreases O_2 yield.

3.2.11 Electrochemical synthesis of CoO_x

Authentic CoO_x was prepared by anodic deposition on fluorine doped tin oxide (FTO), (TEC-15 Hartford Glass Co.) at 1 V (vs Ag/AgCl, 3M NaCl) from 0.5 mM $Co(NO_3)_2$ •$6H_2O$ in 0.1 M pH 7 sodium phosphate buffer solution as previously described.[30] CoO_x was dried in air and then removed from the FTO electrode with a razor blade. Typically, 2-3 mg of CoO_x was formed during electrolysis. The CoO_x powder was suspended in water and sonicated for 10 minutes before doing a catalytic reaction.

3.2.12 Co_4PPOM decomposition

To correctly interpret the kinetics of decomposition of **Co_4PPOM** (measured as the decrease in absorbance at 580 nm, **Figure 3-5**), it is necessary to take into account the spectra of decomposition products which may overlap with the **Co_4PPOM** spectrum, and change the observed spectral shape. No such changes were observed under conditions in **Figure 3-5**. To increase the reaction conversion in order to obtain sufficient

decomposition for quantification by UV-Vis we aged the solutions of 0.5 mM **Co_4PPOM** in 80 mM borate buffer (pH 8) at 60 °C for 10 hours. The initial and final spectra (after correction for the base line) are presented in **Figure 3-6**. The analysis of these spectra showed that decomposition products absorb light in the range 450-550 nm and the contribution of Co^{2+}(aq) is negligibly small. Thus, the decrease in absorbance at 580 nm can be safely assigned to the decrease of **Co_4PPOM** concentration (ε_{580} = 170±10 $M^{-1}cm^{-1}$).

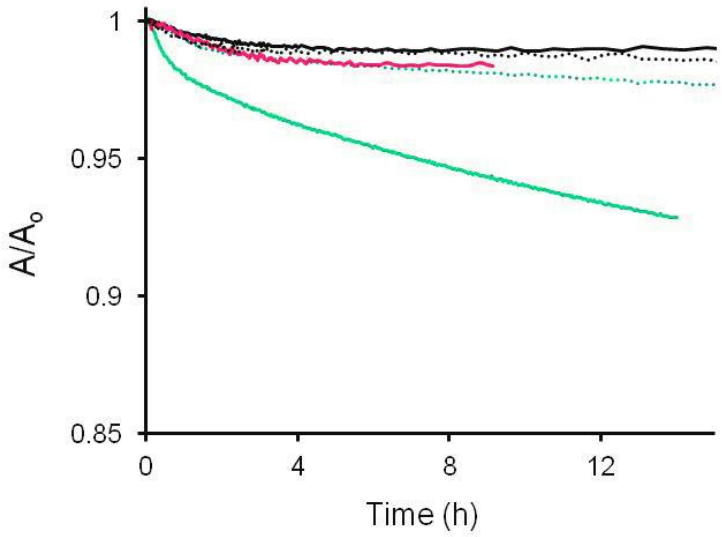

Figure 3-5. Normalized peak absorbance at 580 nm of **Co_4PPOM** as a function of time. Conditions: 0.5 mM **Co_4PPOM** in 0.03 and 0.1 M NaP_i (teal dotted and solid lines, respectively), in 0.1 M sodium borate buffer 0.45 and 0.8 mM **Co_4PPOM** at pH 8 and 9 (black solid and dotted lines, respectively); 1.15 mM **Co_4PPOM** in 0.05 M CAPS buffer at pH 10 (pink); 25 ºC.

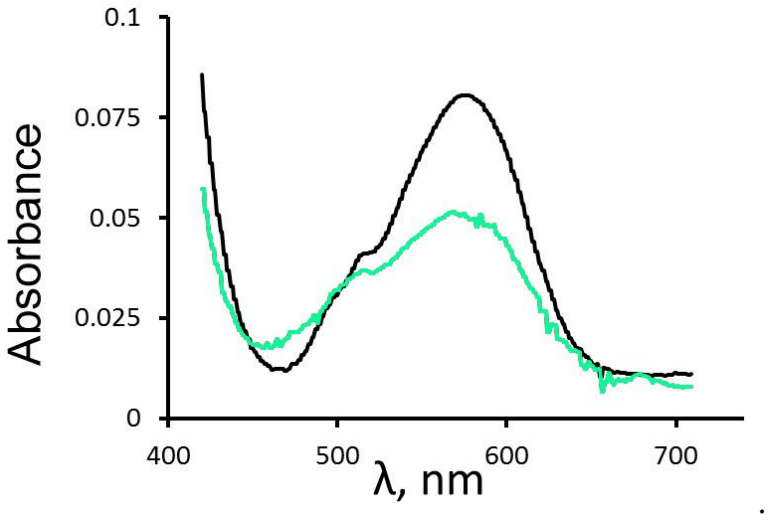

Figure 3-6. The spectra of 0.5 mM **Co_4PPOM** in 80 mM borate buffer at pH 8.0 before (black) and after 10 hours aging (teal) at 60 °C.

Summary of Experiments from Yin, Q, *et. al*. *Science* 2010, *328*, 342. (HG) that are all consistent with molecular **Co_4PPOM** being the principal WOC and not CoO_x or Co^{2+}(aq) under those conditions:

The (1) UV-Vis of **Co_4PPOM** showed no change at 30 mM NaP_i pH = 8 over a 1-month period and at pH from 3.5 to 9 showed no change over 1 day (Note, it is shown here, as has SF, that there is a small change in the UV-vis spectra as discussed in the main text). (2) The ^{31}P NMR spectrum (unique chemical shift) of **Co_4PPOM** showed no change at 30 mM NaP_i pH = 8 over a 1-month period and at pH from 3.5 to 9 showed no change over 1 day. (3) Experiments in HG were done in the presence of bpy which chelates any Co^{2+}(aq) forming coordinately saturated and catalytically inert $[Co(bpy)_3]^{2+}$ ($\log \beta_3 = 16.02$)[76] which completely eliminates water oxidation activity by Co^{2+}(aq) and has only minimal effect on **Co_4PPOM**. The (4) ^{31}P NMR spectrum and (5) FTIR spectra of **Co_4PPOM** are identical before after catalytic reaction. (6) Neither the initial rate nor

the rate behavior of the catalyst recovered after reaction was changed relative to the fresh catalyst. (7) **Co_4PPOM** shows no decrease in activity towards electrochemically generated $Ru(bpy)_3^{n+}$ after catalysis, while Co^{2+} shows a marked decrease.[65]

3.3 Results

3.3.1 Quantification of active species leached from the initial molecular catalyst

Cobalt oxides (henceforth "CoO_x") and aqueous cobalt ions are the simplest and most likely decomposition products of **Co_4PPOM** and are known WOCs.[29,30,72] Thus it was important to test the hypothesis that some cobalt containing species or cobalt oxides, in amounts that have been shown to be present, might be able to account for the O_2 yields we observe. The results herein show that they cannot. These cobalt containing species (Co_{app}) are defined in SF as,[77] "whether it is just aqueous Co^{2+}, a Co(II)-POM fragment, or conceivably some other Co(II)-containing species."

The first step in examining whether decomposition products of **Co_4PPOM** are able to account for the observed catalysis is quantifying the amount of decomposition and the decomposition products formed. To this end two techniques have been developed. We conducted an analysis showing quantitatively that the maximum amount of Co_{app} present in solutions of **Co_4PPOM** and the equivalent quantity of CoO_x formed from this Co_{app} do not account for the observed catalytic water oxidation rates. Previous work[75] estimated decomposition based on the decrease in absorbance at 580 nm from a solution of **Co_4PPOM**. Due to the low molar absorptivity of **Co_4PPOM**, high concentrations (≥500 μM) are required to obtain a sufficient absorbance. However, these experimental

conditions do not convincingly reflect conditions where **Co_4PPOM** was reported to be catalytically active (~5 μM, complete listing in **Table 3-1**). To more accurately quantify the amount of Co_{app} present in solution when **Co_4PPOM** is aged in catalytic conditions (low concentrations), CAdSV, a technique that has been recently applied to similar systems,[75] was used as described by the general procedure above. This technique has been reported to determine the amount of Co_{app} in a high **Co_4PPOM** concentration sodium phosphate buffered system,[75] as well as at 2.5 μM in the same buffer,[67] released as a function of aging time. After aging 2 μM of **Co_4PPOM** in 80 mM pH 8 borate buffer for 3 h, the concentration of Co_{app} was found to be 0.07 ± 0.01 μM. Complete results are listed in **Table 3-2**.

A second new and general method to address catalysis by soluble molecular species (POMs or otherwise) versus insoluble metal oxides or soluble hydrated metal cations as catalysts for reactions in aqueous solution has been devised and is reported here. This method is a two-step process where a soluble, anionic catalyst is separated from solution containing all species present during turnover, then the remaining Co_{app} in solution are quantified. Here, a toluene solution of $THpANO_3$ is used to extract **Co_4PPOM** from the aqueous layer. $THpA^+$ is well known to quantitatively extract most POMs from the aqueous phase to a second toluene phase.[78] This extraction technique was applied to the aqueous solution of **Co_4PPOM** after light-driven catalytic water oxidation and this removal of **Co_4PPOM** effectively stops catalysis decreasing catalytic water oxidation by ~ 98 %, (experimental section, **Figure 3-7**, and **Figure 3-3**, black triangles). Control experiments show that neither the extraction method nor the presence of residual toluene or $THpA^+$ significantly affect catalysis by Co^{2+}(aq), or CoO_x (**Figure 3-7**).

Catalysis of **Co_4PPOM** is also not significantly affected by residual toluene or $THpA^+$ (**Figure 3-3**, pink open squares). Extraction of **Co_4PPOM** before catalytic reaction reduces the O_2 yield to effectively zero.

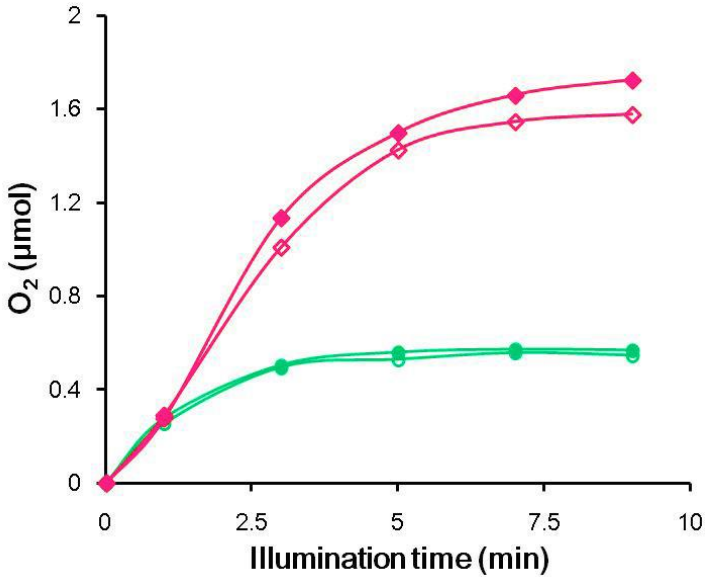

Figure 3-7. Kinetics of light-driven catalytic O_2 evolution from water catalyzed by CoO_x and $Co(NO_3)_2$ in 0.12 M borate buffer at pH 8. Conditions: 5.0 mM $Na_2S_2O_8$, 1.0 mM $[Ru(bpy)_3]Cl_2$. Pink solid diamonds: 2 µM $Co(NO_3)_2$ initial run. Pink empty diamonds: control reaction where 2 µM $Co(NO_3)_2$ solution in borate buffer extracted by a toluene solution of $THpANO_3$, followed by addition of $[Ru(bpy)_3]Cl_2$ and $Na_2S_2O_8$; Teal solid circles: CoO_x (containing 8 µM equivalents of Co^{2+}) initial run. Teal empty circles: control reaction where CoO_x suspension in borate buffer extracted by a toluene solution of $THpANO_3$, followed by addition of $[Ru(bpy)_3]Cl_2$ and $Na_2S_2O_8$ to return to starting concentrations.

After extraction of **Co_4PPOM** from solutions aged in buffer, inductively coupled ICP-MS was performed to quantify the amount of Co_{app}.[79] Aging 2 µM of **Co_4PPOM** in 80 mM pH 8 sodium borate buffer for 3 h, followed by the extraction technique, yielded a

concentration of Co_{app} at 0.07 ± 0.01 μM remaining in the reaction solution, exactly as was found by CAdSV above. Complete results and procedure reported in **Table 3-3**.

In order to gauge the catalytic role of the quantified cobalt containing species, water oxidation was conducted either by dark-reaction where reaction kinetics are monitored by decrease in absorbance of sacrificial oxidant $[Ru(bpy)_3]^{3+}$, or the light-driven method monitored by GC with $[Ru(bpy)_3]^{2+}$ as a photosensitizer and $Na_2S_2O_8$ as a sacrificial electron acceptor with visible light. Both methods were previously reported[65,80] and are fully elaborated in **Chapter 2**. To show that ~ 0.07 μM Co_{app}, the amount quantified by both CAdSV and extraction followed by ICP-MS could not account for the observed catalytic activity, several control experiments were conducted. $Co(NO_3)_2$ was used to approximate Co_{app}, as was done previously by SF. Addition of 0.10 μM $Co(NO_3)_2$, nearly twice the amount of Co_{app}, to a buffered solution of 2 μM **Co_4PPOM** produces less than 5 % increase on the overall rate of $[Ru(bpy)_3]^{3+}$ reduction (dark-reaction): compare the blue dashed curve in **Figure 3-8** and the pink solid curve which has no added $Co(NO_3)_2$. Similar results were obtained under light-driven conditions, where water oxidation by 0.15 μM $Co(NO_3)_2$, twice the amount found to be present by both techniques, gives a negligible O_2 yield and addition of 0.15 μM $Co(NO_3)_2$ to 2 μM **Co_4PPOM** shows no effect on the kinetics or yield of oxygen evolution (**Figure 3-9**). Furthermore, increasing the concentration of the added $Co(NO_3)_2$ to 0.5 μM (teal dashed curve) increases the overall rate of the reaction by ~ 15 %. Thus, the concentration of $Co(NO_3)_2$ can be made so great that it effects the catalysis, but even at this elevated level, more than seven times higher than what is found to exist in solution, the majority of catalysis still derives from **Co_4PPOM**.

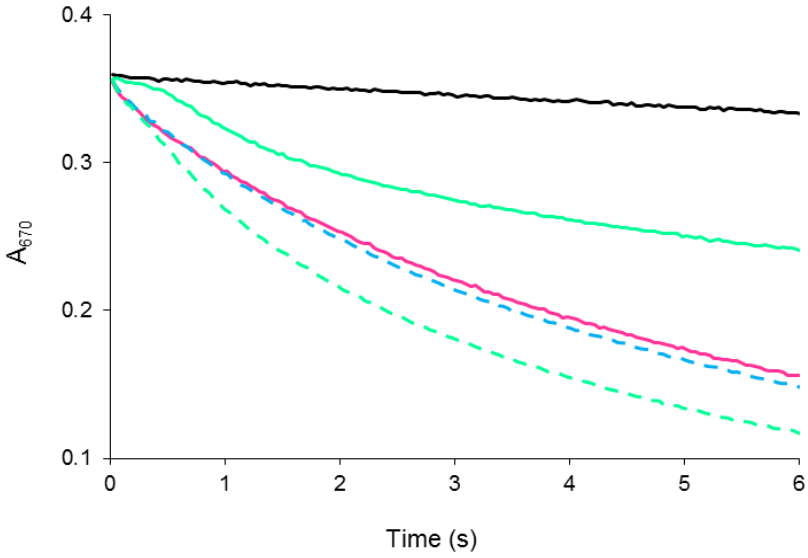

Figure 3-8. Kinetics of $[Ru(bpy)_3]^{3+}$ reduction in 80 mM sodium borate buffer at pH 8.0 and 25 °C, measured as the decrease in absorbance at 670 nm: No catalyst (black), 2.0 µM **Co_4PPOM** (pink), 0.5 µM $Co(NO_3)_2$ (solid teal), 2.0 µM **Co_4PPOM** in the presence of 0.10 µM $Co(NO_3)_2$ (blue dashed), 2.0 µM **Co_4PPOM** in the presence of 0.50 µM $Co(NO_3)_2$ (dashed teal)

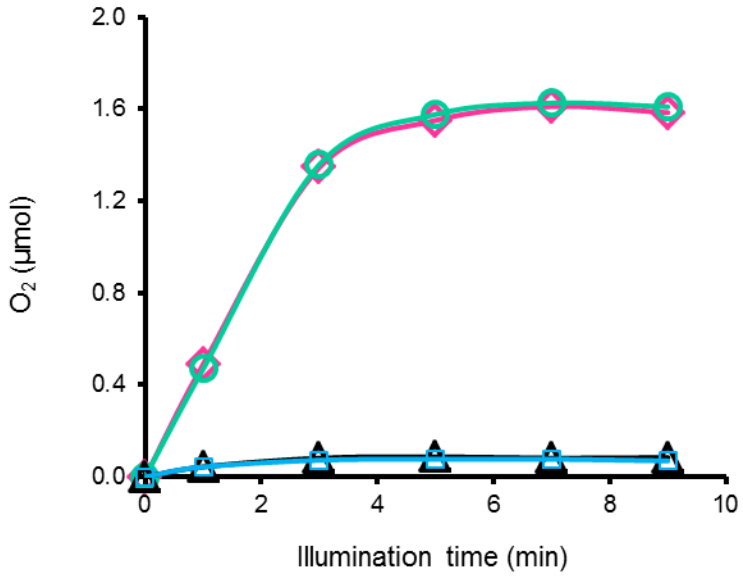

Figure 3-9. Kinetics of light-driven catalytic O_2 evolution from water catalyzed by **Co_4PPOM** and $Co(NO_3)_2$. Conditions: 5.0 mM $Na_2S_2O_8$, 1.0 mM $[Ru(bpy)_3]Cl_2$. 2.0 µM **Co_4PPOM** (teal) , 2.0 µM **Co_4PPOM** + 0.15 µM $Co(NO_3)_2$ (pink), 0.15 µM $Co(NO_3)_2$ (black) all in 120 mM borate buffer, and 0.15 µM $Co(NO_3)_2$ (blue) in 80 mM borate buffer. Initial pH = 8.0, total volume 2.0 mL.

3.3.2 Behavioral distinction between a molecular catalyst and decomposition product catalysts

Examining behavioral differences between each catalytically competent species under specific conditions provides further evidence to differentiate **Co_4PPOM** from Co_{app}, CoO_x, or other possible decomposition products. By analyzing differences in the kinetics of the dark reaction or the yields of the light-driven reaction, when changing only a single variable of the conditions, we can determine the identity of the catalytically active species. Several additional control experiments to compare the catalytic behavior of freshly prepared and aged solutions of **Co_4PPOM** and $Co(NO_3)_2$ were performed.

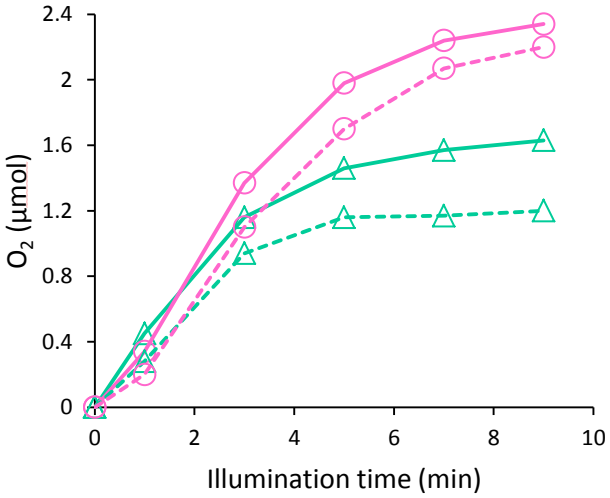

Figure 3-10. The kinetics of O_2 formation catalyzed by 2 µM **Co_4PPOM** (teal triangles) or 2 µM $Co(NO_3)_2$ (pink circles) in 80 mM borate buffers (dashed curves at pH 8 and solid curves at pH 9). Conditions: 1.0 mM $[Ru(bpy)_3]^{2+}$, 5.0 mM $Na_2S_2O_8$.

First, it has been established that these two species have quite different time profiles for O_2 formation and $[Ru(bpy)_3]^{3+}$ reduction. Similar findings were reported for the kinetics of Co^{2+}(aq) as a WOC.[81] Second, it was confirmed, that water oxidation by $Co(NO_3)_2$

exhibits an induction period, as observed by a characteristic sigmoidal-shape (teal curve, **Figure 3-8**), indicating that the initial $Co(NO_3)_2$ is a precursor of a catalytically active species. In contrast **Co_4PPOM** shows no induction period (pink solid and blue dashed curve **Figures 3-8**, **3-10**, and **3-11**).

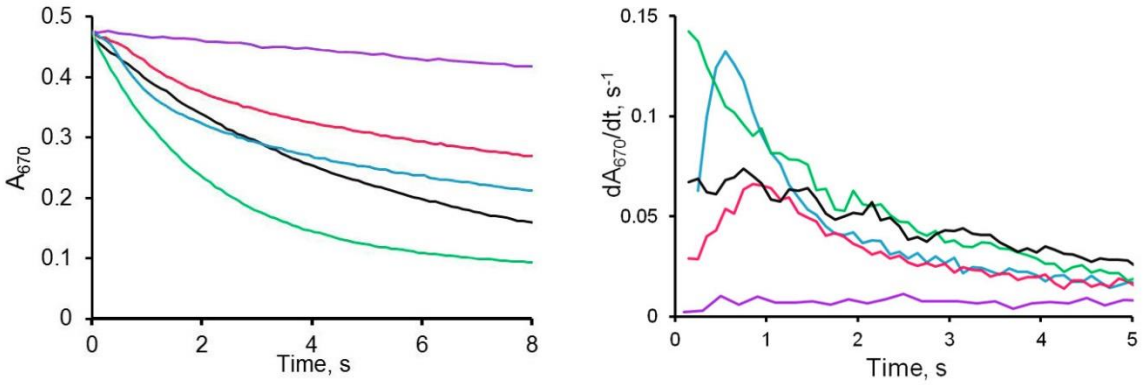

Figure 3-11. Left panel: stopped flow kinetics of catalytic $[Ru(bpy)_3]^{3+}$ reduction in 80 mM sodium borate buffer at pH 8.0 and 25 °C: No catalyst (purple), 1 and 3 µM **Co_4PPOM** (black and teal, respectively), 0.5 and 1.0 µM $Co(NO_3)_2$ (pink and blue, respectively). Right panel: the rate of catalytic $[Ru(bpy)_3]^{3+}$ reduction as a function of time in 80 mM sodium borate buffer at pH 8.0 and 25 °C: No catalyst (purple), 1 and 3 µM **Co_4PPOM** (black and teal respectively), 0.5 and 1.0 µM $Co(NO_3)_2$ (pink and blue, respectively).

Third, the pH dependence of **Co_4PPOM** and other species were compared. In general, different pH dependencies of O_2 yields are consistent with the presence of different catalytically active species during turnover. Therefore, the response of a catalytic system to pH change can and should be used to probe the nature of the catalyst in aqueous media. Here, the pH dependence of O_2 yields for **Co_4PPOM**, Co^{2+}(aq) and CoO_x catalysts were compared. As seen in **Table 3-4**, the activity of **Co_4PPOM** strongly depends on pH: lines 10 and 11 show that when the pH increases from 7.2 to 8.0, with all

other conditions held constant, the yield increases by over an order of magnitude. In contrast, the O_2 yield from both $Co(NO_3)_2$ and CoO_x is weakly dependent on pH: under the same conditions the yields increase by only about two- and three-fold respectively. The different dependences on pH provide further evidence that the catalytic activity observed from **Co_4PPOM** is not due to either Co^{2+}(aq) or CoO_x.

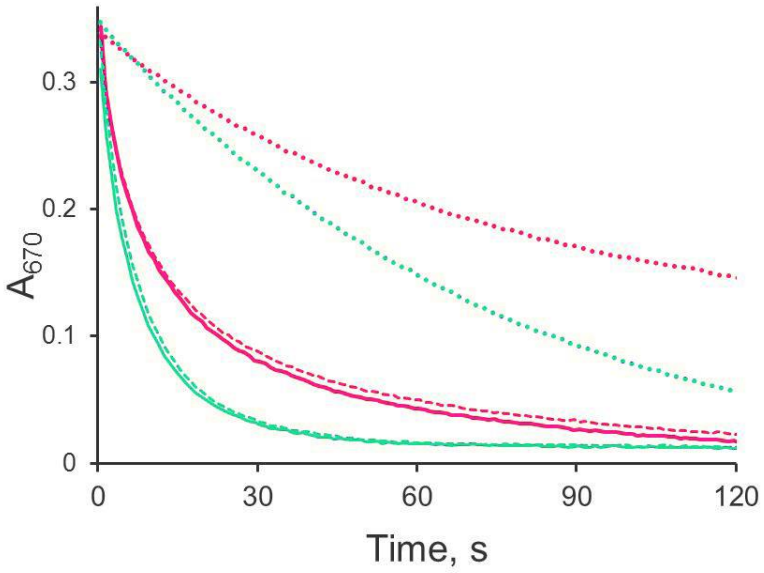

Figure 3-12. The reduction of 0.83 mM $[Ru(bpy)_3]^{3+}$ catalyzed by 5 µM **Co_4PPOM** freshly prepared (solid lines) and aged in buffer solutions for 1.5 h (dashed lines): 0.1 M sodium phosphate (pink lines) or borate buffer (teal lines) at pH 8. The self-decomposition of $[Ru(bpy)_3]^{3+}$ in the absence of the **Co_4PPOM** is in phosphate and borate (pink and teal dotted lines respectively).

Fourth, the behavioral dependence in different buffers was studied. The overall rate of **Co_4PPOM** loss is faster in NaP_i than in NaB_i as seen in high concentrations quantified by UV-Vis (**Figure 3-5**). The decrease in absorbance is also slower in the presence of CAPS buffer, where **Co_4PPOM** shows only slight decomposition even at pH 10.[69] The amount of Co_{app} quantified by ICP-MS and CAdSV at lower, catalytic

conditions corroborates this relationship (over 6 fold greater [Co_{app}] for both techniques in NaP_i over NaB_i, **Tables 3-2** and **3-3**). The effect of aging **Co_4PPOM** solutions in buffer on the catalytic activity under HG conditions was also examined. Data show that the kinetic curves for reduction of 0.83 mM $[Ru(bpy)_3]^{3+}$ by 2 μM **Co_4PPOM** are nearly identical for both freshly prepared and 1.5 h-aged solutions in 0.1 M NaP_i or NaB_i at pH 8.0 suggesting that any Co_{app} has little effect on catalytic activity (**Figure 3-12**). The photochemical reactions give similar results where the catalytic solutions in both NaB_i and NaP_i show only a minimal decrease in TON after several hours of aging (**Table 3-4** entries 2 and 3, 6 and 7 respectively).

In addition to the dependence on the nature of the buffer, the concentration of the buffer was also investigated as a fifth behavioral test. If the concentration of NaP_i is that in HG, the decrease in absorbance for **Co_4PPOM** is ~ 2.5 % compared to ~ 7.5 % when the concentration of NaP_i is increased to that used in SF (after 16 h of aging). A similar trend is observed in catalytic water oxidation activities; when the concentration of NaP_i is increased from 80 mM to 100 mM, the TON decreases from 125 ± 1 to 44 ± 3 (entries 6 and 10, **Table 3-4**). Importantly, **Co_4PPOM** and Co^{2+}(aq) show the opposite buffer-concentration dependence when NaB_i is used. When the concentration of NaB_i is increased from 80 mM to 120 mM with all other conditions held constant, the TON increases from 302 ± 1 to 399 ± 4 for **Co_4PPOM** (entries 2 and 4, **Table 3-4**), and decreases from 509 ± 5 to 423 ± 11 for Co^{2+}(aq) (entries 14 and 15, **Table 3-4**). Thus, the nature of buffer, its concentration, and pH of the solution are all critical parameters in the decomposition of **Co_4PPOM** and, in general, POM-metal oxide equilibria.

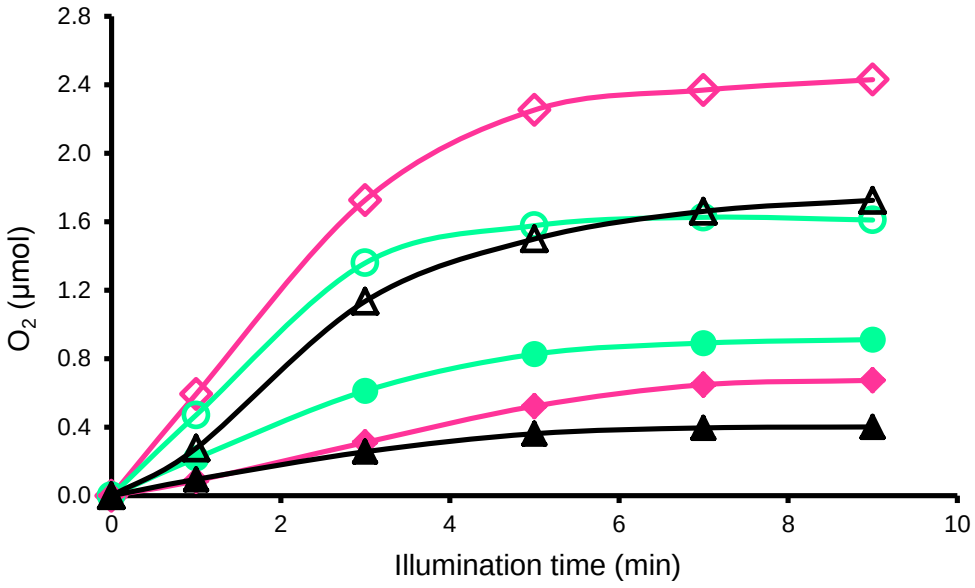

Figure 3-13. Kinetics of light-driven catalytic O_2 evolution from water catalyzed by **Co_4PPOM** and $Co(NO_3)_2$ in 0.12 M borate buffer at pH 8. Conditions: 5.0 mM $Na_2S_2O_8$, 1.0 mM $[Ru(bpy)_3]Cl_2$, 2.0 µM **Co_4PPOM** (teal) or 2.0 µM (black) or 8 µM $Co(NO_3)_2$ (pink). Initial pH = 8.0, total volume 2.0 mL, 120 mM borate buffer. The curves with solid icons are for the second run after addition of another portion of 5.0 mM $Na_2S_2O_8$ to bring the solution to its original concentration.

As a sixth behavioral metric, when the photochemical reactions were completed, a second identical molar amount of $Na_2S_2O_8$ was added. This provides a test of the reusability of the entire catalytic system (buffer, $[Ru(bpy)_3]Cl_2$, etc.) and not solely the catalyst. The addition of a second aliquot of $Na_2S_2O_8$ to the **Co_4PPOM** solution results in a 43.6 ± 2 % drop in O_2 yield relative to the first run (entries 4-5 in **Table 3-4** and **Figure 3-15**). The lower O_2 yield in the second runs results primarily from partial decomposition of the $[Ru(bpy)_3]Cl_2$ photosensitizer (**Figure 3-14**), and a slight decrease of pH from the water oxidation reaction itself. In contrast, $Co(NO_3)_2$ shows a dramatically deceased O_2 yield in the second run (76.1 ± 0.9 % drop relative to the first run, entries 15-16 in **Table 3-4** and **Figure 3-13**). Although 8 µM $Co(NO_3)_2$ (same Co equivalents as that of 2 µM

Co_4PPOM) gives a higher O_2 yield in the first run; the second run produces far less O_2 than for the **Co_4PPOM**-catalyzed reactions (75 ± 3 % drop relative to the first run, entries 17-18 in **Table 3-4** and **Figure 3-13**).

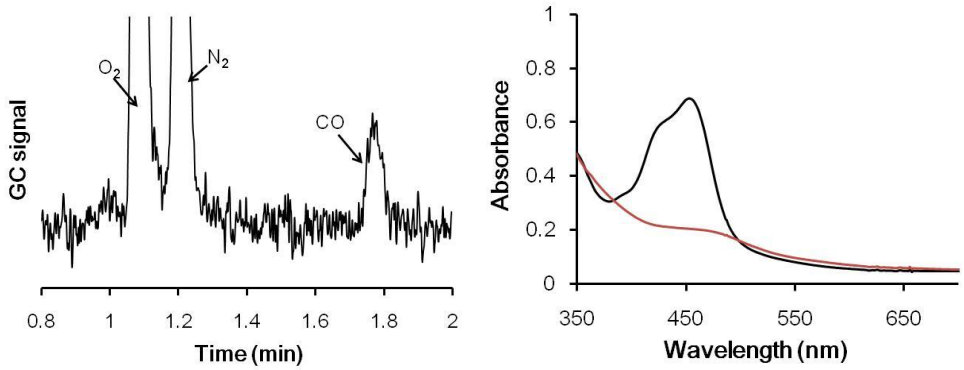

Figure 3-14. Left: the GC/TCD signal of gas products at the end of reaction. Right: the UV-vis absorbance of the reaction solution before (black) and after (red) photocatalytic water oxidation. Conditions: 5.0 mM $Na_2S_2O_8$, 50 μM $[Ru(bpy)_3]Cl_2$, 50 μM **Co_4PPOM** in 80 mM NaP_i pH = 8.0 buffer, reaction time: 11 min.

A seventh new probe addresses particle formation during water oxidation catalyzed by **Co_4PPOM**, and Co_{app} in separate reactions. Detecting the formation of nanoparticles has been well established as a crucial component in distinguishing homogeneous species from heterogeneous ones.[82] DLS studies of the post-water-oxidation catalytic solutions, confirm that no CoO_x particles result from water oxidation catalyzed by **Co_4PPOM** above the LoD, while those catalyzed by Co^{2+}(aq) do produce particles which are presumably CoO_x (**Figure 3-15**). This finding is consistent with the observation of others,[83] indicating that CoO_x is not the actual catalyst under HG turnover conditions

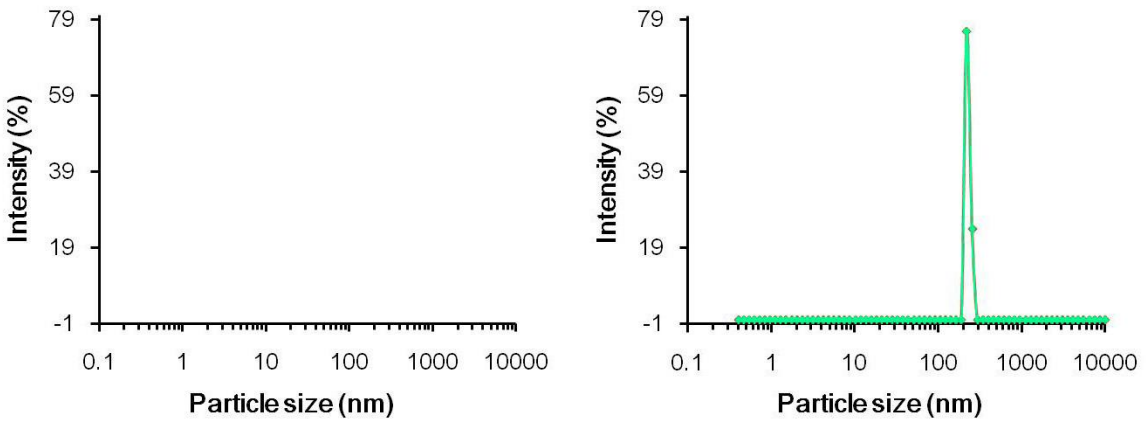

Figure 3-15. Particle size distribution (intensity %) obtained from dynamic light scattering measurement for post-reaction solutions containing 2 μM **Co_4PPOM** (left) or $Co(NO_3)_2$ (right) as catalyst, 1 mM $[Ru(bpy)_3]^{2+}$ in 80 mM borate buffer (pH = 8), 5.0 mM $Na_2S_2O_8$.

In summary, these collective experiments establish that when both Co_{app} and **Co_4PPOM** are present in solution, the vast majority of catalytic activity — assessed either by $[Ru(bpy)_3]^{3+}$ reduction, or by photochemical O_2 production, is accounted for by **Co_4PPOM**. Furthermore each catalyst exhibits unique kinetic behavior as a function of pH, buffer identity, and buffer concentration. These experiments should be helpful in many other investigations of POM catalysis, particularly in water, to identify the active catalyst. These include but are not limited to other WOC systems.

Table 3-4. Light-driven water oxidation activity of **Co_4PPOM**, Co^{2+}(aq) and amorphous CoO_x as a function of pH, buffer and buffer concentration.

Entry	Complex	Complex concentration (μM)	pH	Buffer (mM)	TON	O_2 yield (%)
1	**Co_4PPOM**	2	9.0	80 NaB_i	410±4	32.8±0.3
2	**Co_4PPOM**	2	8.0	80 NaB_i	302±1	24.2±0.1
3	**Co_4PPOM**$^{\|}$	2	8.0	80 NaB_i	290±4	23.2±0.2
4	**Co_4PPOM**	2	8.0	120 NaB_i	399±4	31.9±0.4
5*	**Co_4PPOM**	2	7.6	120 NaB_i	226±4	18±0.3
6	**Co_4PPOM**	2	8.0	80 NaP_i	125±1	9.9±0.1
7	**Co_4PPOM**$^{\|}$	2	8.0	80 NaP_i	130±2	10.4±0.2
8‡	**Co_4PPOM**	50	8.0	80 NaP_i	0.35±0.11	0.71±0.22
9‡	**Co_4PPOM**$^{\|}$	50	8.0	80 NaP_i	0.38±0.02	0.75±0.04
10	**Co_4PPOM**	2	8.0	100 NaP_i	44±3	3.6 ± 0.2
11	**Co_4PPOM**	2	7.2	100 NaP_i	4.3±0.1	0.34±0.01
12	**Co_4PPOM**	2	6.2	100 NaP_i	2.8±0.2	0.23±0.02
13	$Co(NO_3)_2$	2	9.0	80 NaB_i	596±8	47.7±0.6
14	$Co(NO_3)_2$	2	8.0	80 NaB_i	509±5	40.8±0.5
15	$Co(NO_3)_2$	2	8.0	120 NaB_i	423±11	33.9±0.9
16*	$Co(NO_3)_2$	2	7.6	120 NaB_i	100±1	8.1±0.1
17	$Co(NO_3)_2$	8	8.0	120 NaB_i	600±11	48±1
18*	$Co(NO_3)_2$	8	7.6	120 NaB_i	160±11	12.8±1.1
19	$Co(NO_3)_2$	2	8.0	80 NaP_i	7.7±0.2	0.61±0.01
20	$Co(NO_3)_2$	2	8.0	100 NaP_i	6.4± 0.4	0.51±0.04
21	$Co(NO_3)_2$	2	7.2	100 NaP_i	3.4±0.1	0.27±0.01
22	$Co(NO_3)_2$	2	6.2	100 NaP_i	0.5±0.04	0.04±0.01
23	CoO_x†	8§	9.0	80 NaB_i	40±3	3.2±0.1
24	CoO_x†	8§	8.0	80 NaB_i	144±2	11.5±0.1
25	CoO_x†	8§	8.0	100 NaP_i	2.6±0.6	0.19±0.02
26	CoO_x†	8§	7.2	100 NaP_i	0.78±0.08	0.07±0.01
27	CoO_x†	8§	6.2	100 NaP_i	0.25±0.01	0.02±0.001

Conditions unless otherwise noted: 1 mM $Ru(bpy)_3^{2+}$, 5 mM $Na_2S_2O_8$, 455 nm LED light, $^{\|}$Aged 3h in the corresponding buffer solution. *Catalyst reusability test: 2.38 mg $Na_2S_2O_8$ added for the second run. ‡SSB conditions (50 μM $[Ru(bpy)_3]^{2+}$ and 50 μM **Co_4PPOM**). †CoO_x was prepared electrochemically. §Not soluble, suspension obtained after 10 min of sonication, 8 μM equivalents of Co^{2+} used for catalytic reaction. Errors are calculated as standard deviation from multiple runs.

3.4 Discussion

3.4.1 Equilibrium aspects of POM systems

Molecular catalysts represent a growing portion of water oxidation studies. While molecular WOCs have been and are now typically coordination complexes or organometallic compounds with one or more transition metals, several POM WOCs have been reported recently as noted in **Chapter 1**.[59] POMs, metal oxides, and soluble hydrated metal cations constitute equilibrium systems; under some conditions (pH, ionic strength, buffer and buffer concentration) the metal oxides are more stable, and the POMs convert to metal oxides; under other conditions, the POMs are more stable and metal oxides and hydroxides convert to the POMs.[84] There are examples over the full pH range (0 – 14) where metal oxides convert to POMs and thus the former are less stable thermodynamically than the latter: at pH 14, the oxide Nb_2O_5 converts fully to the POM, $[Nb_6O_{19}]^{8-}$,[85] and at pH 0, many metal oxides will dissolve and form POMs.[86,87] Thus a POM system is ideal for the rigorous analysis presented in this paper as it is likely that some other species besides the initial POM will exist in solution. It has been well established that **Co_4PPOM** is hydrolytically unstable above pH 7.5-8.0 in NaP_i.[68-70] As a consequence seven control experiments were conducted in HG demonstrating that the catalytic water oxidation derives form **Co_4PPOM** and not from Co^{2+}(aq) or metal oxide CoO_x as elaborated above. The present work further affirms that despite some decomposition, **Co_4PPOM** is absolutely the dominant species in solution under HG conditions, including the time scale of the reactions.[65] Experiments reproduced by others,[88] involve the chelation of Co^{2+}(aq) leading to quantitative formation of

$[Co(bpy)_3]^{2+}$, where bpy = 2,2'-bipyridine (($\log\beta_3 = 16.02$[76]) and complete suppression of CoO_x formation provided strong evidence that Co^{2+}(aq) is not the WOC under the HG conditions.[65]

3.4.2 Analysis of previous Co_4PPOM studies

A series of studies examining the same catalyst, **Co_4PPOM** arrive at apparently different conclusions. The first of these studies by Hill reported homogeneous water oxidation activity of the compound in both dark[65] and light-driven[80] systems, and provided seven lines of evidence for a soluble catalyst under their conditions (these and all relevant conditions listed in **Table 3-1**). Since then, several other groups have analyzed these works,[48,56,58,89-97] reported additional stability studies,[69,70] or used **Co_4PPOM** for water oxidation.[88,91] Thus further analysis of this catalyst and the various systems it has been reported in were required.

A subsequent publication, SF, demonstrated convincingly that **Co_4PPOM**, in an electrochemical system, decomposes into a heterogeneous Co-containing film responsible for the water oxidation activity.[75] However, these were electrocatalytic, rather than homogeneous chemically driven experiments. This difference, coupled with a 156-fold higher **Co_4PPOM** concentration and longer aging times, are most likely key factors that lead to formation of CoO_x in catalytically significant quantities. Additionally, it was observed that **Co_4PPOM** aged in sodium phosphate buffer decomposes to release Co^{2+}(aq) in amounts that quantitatively account for all of the observed water oxidation activity within the standard error. As stated in SF, the conditions used in the SF and HG studies differ and conclusions from one work might not apply to the other.[75] While all the

catalytic water oxidation studies by **Co_4PPOM** and other multi-cobalt POM WOCs,[88,98] use NaP_i or NaB_i buffers, the most detailed thermodynamic hydrolytic (speciation) studies use either no buffer[70] or HEPES, PIPES and CAPS buffers.[69] Potential confusion in catalytic water oxidation by POMs very often arises from neglecting the specific effects of the buffer molecules on both POM speciation in water and POM-catalyzed water oxidation. Both the buffer and the buffer concentration must be kept relatively constant in POM studies if meaningful comparisons are to be made, particularly near the pH where the POM becomes hydrolytically unstable with respect to metal oxide. As discussed above, the equilibria involving a POM, soluble hydrated metal cations, and metal oxides, is dependent on concentrations of all soluble species present in the equilibrium, and these are frequently perturbed by the buffer.[69] The SF study brought this home in the case of **Co_4PPOM**, by showing that at a concentration of 500 μM, the absorbance at 580 nm (λ_{max}) in pH 8.0 NaP_i decreases by about 5 % over 3 h. In NaB_i, we observe a decrease of 1.7 % over 16 h in agreement with SF (**Figure 3-5**), and as described above, it was also found that in either buffer the concentration of Co_{app} under photocatalytic conditions is extremely small. Thus, while it has been shown that **Co_4PPOM** releases some Co_{app}, these sub-micromolar quantities of Co species formed by **Co_4PPOM** equilibria cannot account for the O_2 yields observed.

A third publication, SSB, examined this system by nanosecond flash photolysis detailing that Co^{2+}(aq) was not involved in the catalysis either as a catalyst or as a precursor to CoO_x. These nanosecond flash photolysis experiments dictate that quite different experimental conditions ($[Ru(bpy)_3]^{2+}$: **Co_4PPOM** = 1:1[83,99]) than those of HG ($[Ru(bpy)_3]^{n+}$: **Co_4PPOM** = 470:1[65] or 200:1[80]) are used (**Table 3-1**). Under these

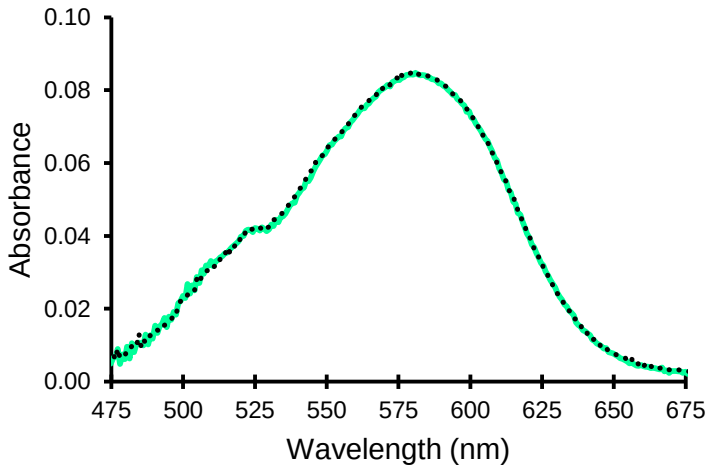

Figure 3-16. Stopped flow mixing of 80 mM sodium phosphate buffer at pH 8.0 (final concentration 40 mM), and 1000 µM **Co_4PPOM** in water (final concentration 500 µM) at 25 °C. Teal, initial spectrum; black dashed, after 10 minutes.

conditions, it was reported that scavenging of the photo-generated $[Ru(bpy)_3]^{3+}$ (or hole scavenging) by **Co_4PPOM** in NaP_i buffer increases with aging time (rapidly in the first 1-8 minutes and continuing to 90 min) of **Co_4PPOM** solutions. From this experiment it was concluded that **Co_4PPOM** is not the true WOC and that no CoO_x forms under these water oxidation conditions, therefore another decomposition product of **Co_4PPOM** must be the active catalyst. Certainly it appears that a new species must form, but our stopped flow data show that there is no significant change in the UV-vis spectra of **Co_4PPOM** in NaP_i buffer from 2 s to 8 minutes (**Figure 3-16**). Thus, the effect of **Co_4PPOM** aging seen by SSB is too fast to be the process observed in this work or SF. Additionally almost no effect of aging **Co_4PPOM** in NaB_i buffer was observed up to 22 h in SSB.[83] If the hypothesis in SSB (i.e. some **Co_4PPOM** decomposition product and not **Co_4PPOM** itself is the actual WOC) is correct, then one should see higher O_2 yields in NaP_i buffer than in NaB_i buffer, unless the decomposition products exhibit drastically different activity in the

two buffers. However, the exact opposite trend is observed experimentally: water oxidation activity in the presence of 2 μM **Co_4PPOM** is threefold higher in NaB_i buffer than that in NaP_i buffer (**Figure 3-9** and entries 2-3, 6-7 in **Table 3-4**).

This study in SSB did not actually involve measuring water oxidation (O_2 evolution). New experimental evidence in this work comparing O_2 formation under SSB and HG conditions show that there is no effect within experimental error of **Co_4PPOM** solution aging on catalytic water oxidation activity (entries 6-9 in **Table 3-4**, black and grey curves in **Figure 3-17**). As noted above, the possible decomposition products proposed by SSB[100] could not account for observed catalytic activity in the amounts they are produced. Interestingly, it is reported here that the O_2 yield under SSB experimental conditions is negligible with approximately 96 % decrease in O_2 yield from HG to SSB conditions, and is independent of aging time (entries 2, 8-9 in **Table 2** and **Figure 3-17**). Thus, the conditions required for nanosecond flash photolysis cannot accurately probe those required for successful catalytic water oxidation. As a possible explanation, we reproducibly see an increase in carbon monoxide from *bpy* ligand oxidation under SSB conditions by gas chromatography, indicating that the bleach recovery observed by SSB is not solely from the hole-scavenging process, i.e. oxidation of **Co_4PPOM** (left panel in **Figure 3-14**). The UV-Vis spectra show that the photosensitizer, $[Ru(bpy)_3]^{2+}$, has been almost completely degraded after 11 minutes of irradiation (right panel in **Figure 3-14**).

It was also reported that $[Ru(bpy)_3]^{3+}$ does not have sufficient potential to oxidize **Co_4PPOM**, or to promote water oxidation catalyzed by **Co_4PPOM**, thus **Co_4PPOM** itself could not be the active catalyst. Electrochemical studies in SSB show an increase in anodic current at ca. 1.3 V (vs. Ag/AgCl) with aging time, data similar to that of SF and

their later work.[67] However, the electrochemical work in SF and HG makes a strong case that the catalytic current observed at ca. 1.1 V results from CoO_x films, not from **Co_4PPOM**. Recently, Finke also explored the electrochemical activity of 2.5 μM **Co_4PPOM** at 1.4 V but concluded that the observed O_2 evolution could not be distinguished as originating from either **Co_4PPOM** or decomposition products.[67] Compounding the difficulty in electrochemical studies of **Co_4PPOM**, as shown by HG, SF and others[101] is that the cobalt-based redox processes in molecular **Co_4PPOM** are voltammetrically silent in aqueous media.[102] As such, the driving forces for redox processes involving $[Ru(bpy)_3]^{3+}$ and other soluble species in **Co_4PPOM** -catalyzed water oxidation studies conditions, are not accessible by voltammetry and remain unknown.

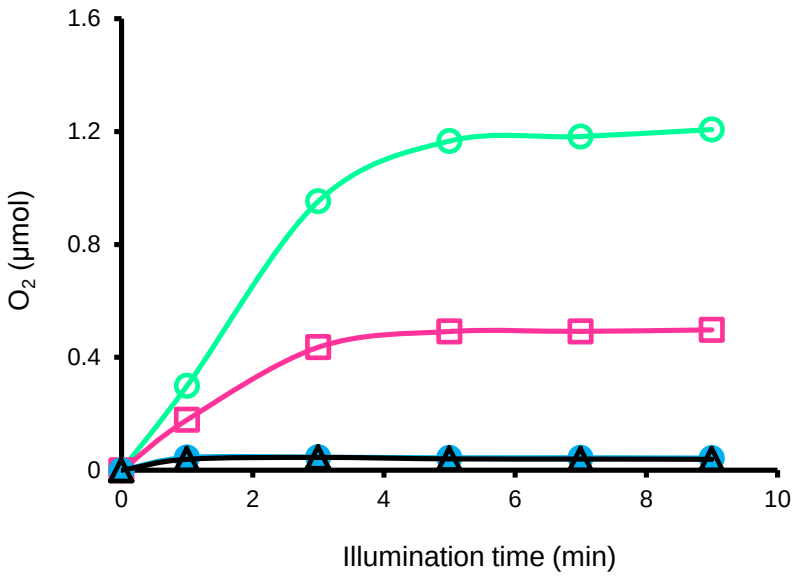

Figure 3-17. Kinetics of light-driven catalytic O_2 evolution as function of buffer and reactant concentration ratio. Conditions: and 5.0 mM $Na_2S_2O_8$. With 1.0 mM $[Ru(bpy)_3]Cl_2$, 2.0 μM **Co_4PPOM** in 80 mM NaB_i (teal) or 80 mM NaP_i (pink), and 50 μM $[Ru(bpy)_3]Cl_2$, 50 μM **Co_4PPOM**, 80 mM NaP_i fresh solution (black) and aged for 3 h (blue) all pH = 8.0. Note: black and grey curves are obtained under the SSB conditions.

3.5 Conclusions

It is frequently challenging to determine whether a given complex or material acts as a heterogeneous or homogeneous catalyst, particularly under oxidizing conditions where POMs and metal oxides are frequently the thermodynamic products. The situation is further complicated when possible catalyst decomposition products are soluble species and known catalysts. Pinpointing all species that may result due to dissociation or other decomposition of a dissolved WOC can be problematical. Based on conflicting reports in the literature, and the nature of POM systems, the WOC **Co_4PPOM** was chosen as an ideal system for rigorous study using new techniques to determine the nature of the catalytically active species, and to quantify decomposition products. Supplementing the techniques reported in the initial HG study, several additional experiments are reported here that distinguish homogeneous WOCs, from their corresponding WOC hydrolysis products (Co^{2+}(aq) and CoO_x in this case). Some of these experiments are of general use in distinguishing these three types of WOCs. A new procedure entails extracting the catalyst from the aqueous phase where water oxidation takes place with a hydrophobic organic solvent containing a hydrophobic quaternary ammonium cation, THpA, in toluene. POMs are extracted quantitatively from the water into toluene; whereas, hydrated metal cations and metal oxides are not extracted at all. This procedure clearly distinguishes the initial catalyst from its possible hydrolysis products.

The amount of Co_{app} present in a range of experiments involving **Co_4PPOM** was quantified at micromolar concentrations using two complementary techniques, cathodic adsorptive stripping voltammetry and $THpA^+$/toluene extraction followed by ICP-MS. Both techniques found the amount of Co_{app} to be 0.07 ± 0.01 μM under catalytic

conditions with 2 μM **Co_4PPOM**. Control experiments show that this amount of Co_{app}, approximated by $Co(NO_3)_2$, results in a negligible increase either in catalytic reduction of $[Ru(bpy)_3]^{3+}$ (dark reactions) or O_2 production (light-driven reactions). Thus the amount of Co_{app} or CoO_x formed from **Co_4PPOM**, cannot account for the observed O_2 yields.

While the POM-metal oxide equilibrium can lie on the side of POM or the metal oxide, for all the studies of **Co_4PPOM** as a WOC thus far (basic buffered aqueous solutions), this POM is thermodynamically unstable towards hydrolysis. As a consequence, we have systematically examined the kinetic stability (specifically Co^{2+} (aq) loss from **Co_4PPOM** and CoO_x particle formation) as a function of time and the four main variables that also impact thermodynamic stability (pH, ionic strength, buffer, and buffer concentration). In addition, the WOC activity was assessed by altering the above four variables over a wide range, including the experimental conditions in HG, SF and SSB. These collective studies establish the crucial role of these four variables in POM stability and reactivity. More importantly, the nature of the oxidation: a soluble oxidant versus applied potential (electrochemical) is paramount in addressing stability. A central corollary here is that catalytic studies of molecular species, especially POM WOCs, under one set of experimental conditions should be compared only with extreme caution, if at all, to those under other conditions.

3.6 References

(1) Chow, J.; Kopp, R. J.; Portney, P. R. *Science* **2003**, *302*, 1528.

(2) Lewis, N. S.; Nocera, D. G. *Proc. Natl. Acad. Sci.* **2006**, *103(43)*, 15729.

(3) Gray, H. B. *Nature Chem.* **2009**, *1*, 7.

(4) Eisenberg, R.; Gray, H. B. *Inorg. Chem.* **2008**, *47*, 1697.

(5) Young, K. J.; Martini, L. A.; Milot, R. L.; III, R. C. S.; Batista, V. S.; Schmuttenmaer, C. A.; Crabtree, R. H.; Brudvig, G. W. *Coord. Chem. Rev.* **2012**, *256*, 2503.

(6) Kanan, M. W.; Surendranath, Y.; Nocera, D. G. *Chem. Soc. Rev.* **2009**, *38*, 109.

(7) Concepcion, J. J.; Jurss, J. W.; Brennaman, M. K.; Hoertz, P. G.; Patrocinio, A. O. T.; Iha, N. Y. M.; Templeton, J. L.; Meyer, T. J. *Acc. Chem. Res.* **2009**, *42*, 1954.

(8) Gersten, S. W.; Samuels, G. J.; Meyer, T. J. *J. Am. Chem. Soc.* **1982**, *104*, 4029.

(9) Hurst, J. K. *Coord. Chem. Rev.* **2005**, *249*, 313.

(10) McDaniel, N. D.; Coughlin, F. J.; Tinker, L. L.; Bernhard, S. *J. Am. Chem. Soc.* **2008**, *130*, 210.

(11) Muckerman, J. T.; Polyansky, D. E.; Wada, T.; Tanaka, K.; Fujita, E. *Inorg. Chem.* **2008**, *47*, 1787.

(12) Hull, J. F.; Balcells, D.; Blakemore, J. D.; Incarvito, C. D.; Eisenstein, O.; Brudvig, G. W.; Crabtree, R. H. *J. Am. Chem. Soc.* **2009**, *131*, 8730.

(13) Masaoka, S.; Sakai, K. *Chem. Lett.* **2009**, *38*, 182.

(14) McCool, N. S.; Robinson, D. M.; Sheats, J. E.; Dismukes, G. C. *J. Am. Chem. Soc.* **2011**, *133*, 11446.

(15) Bernet, L.; Lalrempuia, R.; Ghattas, W.; Mueller-Bunz, H.; Vigara, L.; Llobet, A.; Albrecht, M. *Chem. Commun.* **2011**, *47*, 8058.

(16) Chen, Z.; Concepcion, J. J.; Meyer, T. J. *Dalton Trans.* **2011**, *40*, 3789.

(17) Fillol, J. L.; Codolà, Z.; Garcia-Bosch, I.; Gómez, L.; Pla, J. J.; Costas, M. *Nature Chem.* **2011**, *3*, 807.

(18) Murakami, M.; Hong, D.; Suenobu, T.; Yamaguchi, S.; Ogura, T.; Fukuzumi, S. *J. Am. Chem. Soc.* **2011**, *133*, 11605.

(19) Wasylenko, D. J.; Ganesamoorthy, C.; Borau-Garcia, J.; Berlinguette, C. P. *Chem. Commun.* **2011**, *47*, 4249.

(20) Roeser, S.; Fàrrs, P.; Bozoglian, F.; Martínez-Belmonte, M.; Benet-Buchholz, J.; Llobet, A. *ChemSusChem* **2011**, *4*, 197.

(21) An, J.; Duana, L.; Sun, L. *Faraday Discuss.* **2012**, *155*, 267.

(22) Kaveevivitchai, N.; Zong, R.; Tseng, H.-W.; Chitta, R.; Thummel, R. P. *Inorg. Chem.* **2012**, *51*, 2930.

(23) Hong, D.; Jung, J.; Park, J.; Yamada, Y.; Suenobu, T.; Lee, Y.-M.; Nam, W.; Fukuzumi, S. *Energy Environ. Sci.* **2012**, *5*, 7606.

(24) Bernardini, G.; Wedd, A. G.; Zhao, C.; Bond, A. M. *Proc. Natl. Acad. Sci.* **2012**, *109*, 11552.

(25) Zhang, M.-T.; Chen, Z.; Kang, P.; Meyer, T. J. *J. Amer. Chem. Soc.* **2013**, *135*, 2048.

(26) Joya, K. S.; Subbaiyan, N. K.; D'Souza, F.; Groot, H. J. M. d. *Angew. Chem. Int. Ed.* **2012**, *51*, 9601.

(27) Youngblood, W. J.; Lee, S.-H. A.; Maeda, K.; Mallouk, T. E. *Acc. Chem. Res.* **2009**, *42*, 1966.

(28) Shafirovich, V. Y.; Khannanov, N. K.; Strelets, V. V. *Nouveau J. Chim.* **1980**, *4*, 81.

(29) Harriman, A.; Pickering, I. J.; Thomas, J. M.; Christensen, P. A. *J. Chem. Soc., Faraday Trans. 1 F* **1988**, *84*, 2795.

(30) Kanan, M. W.; Nocera, D. G. *Science* **2008**, *321*, 1072.

(31) Jiao, F.; Frei, H. *Angew. Chem. Int. Ed.* **2009**, *48*, 1841.

(32) Robinson, D. M.; Go, Y. B.; Greenblatt, M.; Dismukes, G. C. *J. Am. Chem. Soc.* **2010**, *132*, 11467.

(33) Carraro, M.; Sartorel, A.; Toma, F. M.; Puntoriero, F.; Scandola, F.; Campagna, S.; Prato, M.; Bonchio, M. *Top. Curr. Chem.* **2011**, *303*, 121.

(34) Gerken, J. B.; McAlpin, J. G.; Chen, J. Y. C.; Rigsby, M. L.; Casey, W. H.; Britt, R. D.; Stahl, S. S. *J. Am. Chem. Soc.* **2011**, *133*, 14431.

(35) Pijpers, J. J. H.; Winkler, M. T.; Surendranath, Y.; Buonassisi, T.; Nocera, D. G. *Proc. Natl. Acad. Sci.* **2011**, *108*, 10056.

(36) Sivasankar, N.; Weare, W. W.; Frei, H. *J. Am. Chem. Soc.* **2011**, *133*, 12976.

(37) Wang, C.; Xie, Z.; deKrafft, K. E.; Lin, W. *J. Am. Chem. Soc.* **2011**, *133*, 13445.

(38) Wang, D.; Jiang, H.; Zong, X.; Xu, Q.; Ma, Y.; Li, G.; Li, C. *Chem. Eur. J.* **2011**, *17*, 1275.

(39) Steinmiller, E. M. P.; Choi, K.-S. *Proc. Natl. Acad. Sci.* **2009**, *106*, 20633.

(40) Zidki, T.; Zhang, L.; Shafirovich, V.; Lymar, S. V. *J. Am. Chem. Soc.* **2012**, *134*, 14275.

(41) Higashi, M.; Domen, K.; Abe, R. *J. Am. Chem. Soc.* **2012**, *134*, 6968.

(42) Youngblood, W. J.; Lee, S.-H. A.; Kobayashi, Y.; Hernandez-Pagan, E. A.; Hoertz, P. G.; Moore, T. A.; Moore, A. L.; Gust, D.; Mallouk, T. E. *J. Am. Chem. Soc.* **2009**, *131*, 926.

(43) Chen, Z.; Concepcion, J. J.; Hull, J. F.; Hoertz, P. G.; Meyer, T. J. *Dalton Trans.* **2010**, *39*, 6950.

(44) Shevchenko, D.; Anderlund, M. F.; Thapper, A.; Styring, S. *Energy Environ. Sci.* **2011**, *4*, 1284.

(45) Barnett, S. M.; Goldberg, K. I.; Mayer, J. M. *Nature Chem.* **2012**, *4*, 498.

(46) Gonçalves, R. H.; Leite, L. D. T.; Leite, E. R. *ChemSusChem* **2012**, *5*, 2341.

(47) Toma, F. M.; Sartorel, A.; Iurlo, M.; Carraro, M.; Parisse, P.; Maccato, C.; Rapino, S.; Gonzalez, B. R.; Amenitsch, H.; Ros, T. D.; Casalis, L.; Goldoni, A.; Marcaccio, M.; Scorrano, G.; Scoles, G.; Paolucci, F.; Prato, M.; Bonchio, M. *Nature Chem.* **2010**, *2*, 826.

(48) Yamada, Y.; Yano, K.; Hong, D.; Fukuzumi, S. *Phys. Chem. Chem. Phys.* **2012**, *14*, 5753.

(49) Risch, M.; Klingan, K.; Ringleb, F.; Chernev, P.; Zaharieva, I.; Fischer, A.; Dau, H. *ChemSusChem* **2012**, *5*, 542.

(50) Anton, D. R.; Crabtree, R. H. *Organometallics* **1983**, *2*, 855.

(51) Widegren, J. A.; Finke, R. G. *J. Mol. Catal. A: Chem.* **2003**, *198*, 317.

(52) Whitesides, G. M.; Hackett, M.; Brainard, R. L.; Lavalleye, J.-P. P. M.; Sowinski, A. F.; Izumi, A. N.; Moore, S. S.; Brown, D. W.; Staudt, E. M. *Organometallics* **1985**, *4*, 1819.

(53) Kuznetsov, A. E.; Geletii, Y. V.; Hill, C. L.; Morokuma, K.; Musaev, D. G. *J. Am. Chem. Soc.* **2009**, *131*, 6844.

(54) Quiñonero, D.; Kaledin, A. L.; Kuznetsov, A. E.; Geletii, Y. V.; Besson, C.; Hill, C. L.; Musaev, D. G. *J. Phys. Chem. A* **2010**, *114*, 535.

(55) Sartorel, A.; Miro, P.; Salvadori, E.; Romain, S.; Carraro, M.; Scorrano, G.; Valentin, M. D.; Llobet, A.; Bo, C.; Bonchio, M. *J. Am. Chem. Soc.* **2009**, *131*, 16051.

(56) Car, P.-E.; Guttentag, M.; Baldridge, K. K.; Albertoa, R.; Patzke, G. R. *Green Chem.* **2012**, *14*, 1680.

(57) Zhu, G.; Glass, E. N.; Zhao, C.; Lv, H.; Vickers, J. W.; Geletii, Y. V.; Musaev, D. G.; Song, J.; Hill, C. L. *Dalton Trans.* **2012**, *41*, 13043.

(58) Tanaka, S.; Annaka, M.; Sakai, K. *Chem. Commun.* **2012**, *48*, 1653.

(59) Lv, H.; Geletii, Y. V.; Zhao, C.; Vickers, J. W.; Zhu, G.; Luo, Z.; Song, J.; Lian, T.; Musaev, D. G.; Hill, C. L. *Chem. Soc. Rev.* **2012**, *41*, 7572.

(60) Geletii, Y. V.; Botar, B.; Kögerler, P.; Hillesheim, D. A.; Musaev, D. G.; Hill, C. L. *Angew. Chem. Int. Ed.* **2008**, *47*, 3896.

(61) Geletii, Y. V.; Huang, Z.; Hou, Y.; Musaev, D. G.; Lian, T.; Hill, C. L. *J. Am. Chem. Soc.* **2009**, *131*, 7522.

(62) Besson, C.; Musaev, D. G.; Lahootun, V.; Cao, R.; Chamoreau, L.-M.; Villanneau, R.; Villain, F.; Thouvenot, R.; Geletii, Y. V.; Hill, C. L.; Proust, A. *Chem. Eur. J.* **2009**, *15*, 10233.

(63) Besson, C.; Huang, Z.; Geletii, Y. V.; Lense, S.; Hardcastle, K. I.; Musaev, D. G.; Lian, T.; Proust, A.; Hill, C. L. *Chem. Commun.* **2010**, 2784.

(64) Sartorel, A.; Carraro, M.; Scorrano, G.; Zorzi, R. D.; Geremia, S.; McDaniel, N. D.; Bernhard, S.; Bonchio, M. *J. Am. Chem. Soc.* **2008**, *130*, 5006.

(65) Yin, Q.; Tan, J. M.; Besson, C.; Geletii, Y. V.; Musaev, D. G.; Kuznetsov, A. E.; Luo, Z.; Hardcastle, K. I.; Hill, C. L. *Science* **2010**, *328*, 342.

(66) Finke, R. G.; Droege, M. W.; Domaille, P. J. *Inorg. Chem.* **1987**, *26*, 3886.

(67) Preprint provided by author. Stracke, J. J.; Finke, R. G. *ACS Catal.*, **2013**, *3*, 1209.

(68) Finke, R. G.; Droege, M.; Hutchinson, J. R.; Gansow, O. *J. Am. Chem. Soc.* **1981**, *103*, 1587.

(69) Lieb, D.; Zahl, A.; Wilson, E. F.; Streb, C.; Nye, L. C.; Meyer, K.; Ivanović-Burmazović, I. *Inorg. Chem.* **2011**, *50*, 9053.

(70) Ohlin, C. A.; Harley, S. J.; McAlpin, J. G.; Hocking, R. K.; Mercado, B. Q.; Johnson, R. L.; Villa, E. M.; Fidler, M. K.; Olmstead, M. M.; Spiccia, L.; Britt, R. D.; Casey, W. H. *Chem. Eur. J.* **2011**, *17*, 4408.

(71) Swierk, J. R.; Mallouk, T. E. *Chem. Soc. Rev.* **2013**, *42*, 2357.

(72) Ghosh, P. K.; Brunschwig, B. S.; Chou, M.; Creutz, C.; Sutin, N. *J. Am. Chem. Soc.* **1984**, *106*, 4772.

(73) Klemperer, W. G. In *Inorg. Synth.*; Ginsberg, A. P., Ed.; John Wiley and Sons, Inc.: New York, 1990; Vol. 27, p 71.

(74) Krolicka, A.; Bobrowski, A.; Kalcher, K.; Mocak, J.; Svancara, I.; Vytras, K. *Electroanalysis* **2003**, *15*, 1859.

(75) Stracke, J. J.; Finke, R. G. *J. Am. Chem. Soc.* **2011**, *133*, 14872.

(76) Del Piero, S.; Di Bernardo, P.; Fedele, R.; Melchior, A.; Polese, P.; Tolazzi, M. *Eur. J. Inorg. Chem.* **2006**, *2006*, 3738.

(77) Quoting from SF: "whether it is just aqueous Co^{2+}, a Co(II)-POM fragment, or conceivably some other Co(II)-containing species".

(78) Katsoulis, D. E.; Pope, M. T. *J. Am. Chem. Soc.* **1984**, *106*, 2737.

(79) Performed by Galbraith Laboratories, Inc. Knozville, TN, USA.

(80) Huang, Z.; Luo, Z.; Geletii, Y. V.; Vickers, J.; Yin, Q.; Wu, D.; Hou, Y.; Ding, Y.; Song, J.; Musaev, D. G.; Hill, C. L.; Lian, T. *J. Am. Chem. Soc.* **2011**, *133*, 2068.

(81) Vickers, J.; Lv, H.; Zhuk, P. F.; Geletii, Y. V.; Hill, C. L. *MRS Proceedings* **2012**, *1387*, mrsf11.

(82) Schley, N. D.; Blakemore, J. D.; Subbaiyan, N. K.; Incarvito, C. D.; D'Souza, F.; Crabtree, R. H.; Brudvig, G. W. *J. Am. Chem. Soc.* **2011**, *133*, 10473.

(83) Natali, M.; Berardi, S.; Sartorel, A.; Bonchio, M.; Campagna, S.; Scandola, F. *Chem. Commun.* **2012**, *48*, 8808.

(84) Weinstock, I. A.; Barbuzzi, E. M. G.; Wemple, M. W.; Cowan, J. J.; Reiner, R. S.; Sonnen, D. M.; Heintz, R. A.; Bond, J. S.; Hill, C. L. *Nature* **2001**, *414*, 191.

(85) Flynn, C. M., Stucky, G. D. *Inorg. Chem.* **1969**, *8*, 178.

(86) Hill, C. L. In *Comprehensive Coordination Chemistry-II: From Biology to Nanotechnology*; Wedd, A. G., Ed.; Elsevier Ltd.: Oxford, UK, 2004; Vol. 4, p 679.

(87) Pope, M. T. In *Comprehensive Coordination Chemistry II: From Biology to Nanotechnology*; Wedd, A. G., Ed.; Elsevier Ltd.: Oxford, UK, 2004; Vol. 4, p 635.

(88) Goberna-Ferrón, S.; Vigara, L.; Soriano-López, J.; Galán-Mascarós, J. R. *Inorg. Chem.* **2012**, *51*, 11707.

(89) Joya, K. S.; Vallés-Pardo, J. L.; Joya, Y. F.; Eisenmayer, T.; Thomas, B.; Buda, F.; de Groot, H. J. M. *ChemPlusChem* **2013**, *78*, 35.

(90) Wasylenko, D. J.; Palmer, R. D.; Schott, E.; Berlinguette, C. P. *Chem. Commun.* **2012**, *48*, 2107.

(91) Wu, J.; Liao, L.; Yan, W.; Xue, Y.; Sun, Y.; Yan, X.; Chen, Y.; Xie, Y. *ChemSusChem* **2012**, *5*, 1207.

(92) Woolerton, T. W.; Sheard, S.; Chaudhary, Y. S.; Armstrong, F. A. *Energy Environ. Sci.* **2012**, *5*, 7470.

(93) Limburg, B.; Bouwman, E.; Bonnet, S. *Coord. Chem. Rev.* **2012**, *256*, 1451.

(94) Anxolabéhère-Mallart, E.; Costentin, C.; Fournier, M.; Nowak, S.; Robert, M.; Savéant, J.-M. *J. Am. Chem. Soc.* **2012**, *134*, 6104.

(95) Du, P.; Eisenberg, R. *Energy Environ. Sci.* **2012**, *5*, 6012.

(96) Crabtree, R. H. *Chem. Rev.* **2012**, *112*, 1536.

(97) Soriano-López, J.; Goberna-Ferrón, S.; Vigara, L.; Carbó, J. J.; Poblet, J. M.; Galán-Mascarós, J. R. *Inorg. Chem.* **2013**, *52*, 4753.

(98) Zhu, G.; Geletii, Y. V.; Song, J.; Zhao, C.; Glass, E. N.; Bacsa, J.; Hill, C. L. *Inorg. Chem.* **2012**, *52*, 1018.

(99) Sartorel, A.; Bonchio, M.; Campagna, S.; Scandola, F. *Chem. Soc. Rev.* **2013**, *42*, 2262.

(100) Quoting SSB: "As to the nature of such an active product, free aqueous Co^{2+} (an obvious candidate on the way to cobalt oxide formation) is ruled out by control experiments performed with $Co(NO_3)_2$, where no appreciable $[Ru(bpy)_3]^{3+}$ reduction takes place in this time scale. Therefore, the most likely hypothesis is that of an earlier decomposition product, possibly a fragment of the original [**Co_4PPOM**] anion of 2:1 Co:POM stoichiometry."

(101) Gao, S.; Li, T.; Li, X.; Cao, R. *Mater. Lett.* **2006**, *60*, 3622.

(102) Balula, Maria S.; Gamelas, José A.; Carapuça, Helena M.; Cavaleiro, Ana M. V.; Schlindwein, W. *Eur. J. Inorg. Chem.* **2004**, *2004*, 619.

Chapter 4

Collecting Meaningful Early-time Kinetic Data in Homogeneous Catalytic Water Oxidation with a Sacrificial Oxidant

James W. Vickers, Jordan M. Sumliner, Hongjin Lv, Mike Morris, Yurii V. Geletii and Craig L. Hill. *Phys. Chem. Chem. Phys*., **2014**, *16*, 11942-11949 - Reproduced by permission of the PCCP Owner Societies.

4.1 Introduction

Experimental design of apparatuses to quantify the performance of water oxidation catalysts (WOCs) can be challenging as with the multi-variable optimization detailed in **Chapter 2**. As another experimental difficulty, the product requiring quantification (O_2) is abundant in air. Apparatuses widely vary between groups in this field, meaning that there is no clear best method, and each laboratory set-up has its limitations which can result in systematic errors. These apparatuses are also limited by what type of information they are able to collect; systems designed to quantify O_2 production do not allow for the monitoring of sacrificial oxidant consumption and vice-versa. By virtue of the experimental design, simultaneous monitoring of O_2 formation and oxidant consumption has not been easy. Most kinetic data for WOC systems are the result of experiments and experimental setups separate from the actual reactions where oxygen is quantified. Early work in this field involved mixing the WOC in solution with a sacrificial oxidant in submerged vessels by cannula transfer and monitoring O_2 final yield by sampling of the reaction vessel headspace with GC, whereas sacrificial oxidant consumption kinetics were obtained using a stopped-flow apparatus. Other groups have reported evaluating WOCs by a variety of mixing methods, including injecting solutions into one another by pipette or syringe.[1-14] Heavily linked to the experimental design is the O_2 detection method, which also varies from group to group as each one has inherent strengths and weaknesses. Here a new experimental design that takes advantage of detection method strengths while avoiding the weaknesses in the pursuit of a more accurate mechanistic understanding of WOCs is reported.

A reaction mechanism is a working hypothesis based on experimental results that is used to predict a rate law. However, if a mechanism agrees with the experimental results, this does not mean that the mechanism is correct. Different reaction mechanisms can result in the same rate law with respect to one or more of the reactants. However, the number of possible mechanisms can be restricted and ideally reduced to just one by comprehensive kinetic studies. Complicating the process, the concentrations of reagents are not measured directly in most cases; therefore a correct interpretation of raw kinetic data is imperative. The new experimental design reported here is utilized to describe the interpretation of kinetic data for the reaction of catalytic water oxidation by the most commonly used stoichiometric oxidant, $[Ru(bpy)_3]^{3+}$. This new method of following WOC reactions has been used to evaluate several catalysts.[15, 16] These reactions are relatively fast at neutral pH values (typical time scales are seconds) and the determination of both O_2 evolution and $[Ru(bpy)_3]^{3+}$ consumption for the same reaction at the same time is reported. The ability to follow both reactant and product O_2 with time on short timescales is unprecedented. Additional problems arise with quantification of $[Ru(bpy)_3]^{3+}$ concentration by UV-vis spectrophotometry including the formation of precipitate involving the WOC are addressed below as well.

4.2 Experimental materials and methods

4.2.1 Synthesis

$[Ru(bpy)_3]Cl_2$, sodium persulfate, $Co(NO_3)_2{\cdot}6H_2O$, and all other reagents were obtained from commercial sources. $[Ru(bpy)_3]Cl_2$ was recrystallized prior to use as detailed in **Chapter 2**. $[Ru(bpy)_3](ClO_4)_3$, $Na_{10}[Co_4(H_2O)_2(PW_9O_{34})_2]$ (**Co_4PPOM**),[13]

and $Rb_8K_2[(Ru_4O_4(OH)_2(H_2O)_4)(\gamma\text{-}SiW_{10}O_{36})_2]$ (**Ru_4SiPOM**)[11] were prepared as previously described in **Chapter 2**. $Na_{10}[Co_4(H_2O)_2(VW_9O_{34})_2]$ (**Co_4VPOM**) and $K_{10}H_2[Ni_5(OH)_6(OH_2)_3(SiW_9O_{33})_2]$ (**Ni_5SiPOM**) were prepared as reported elsewhere.

4.2.2 Instruments

Water oxidation with $[Ru(bpy)_3]^{3+}$ was performed using a Hi-Tech KinetAsyst Stopped Flow SF-61SX2 instrument equipped with a diode array detector operating in wavelength range 400-700 nm. In a typical experiment one of the syringes was filled with a $Ru(bpy)_3^{3+}$ solution, and the other with a buffered solution of WOC. The consumption of $Ru(bpy)_3^{3+}$ was followed by a decrease in absorbance at 670 nm (ε_{670} = 420 M^{-1} cm^{-1}) with optical path length l = 10 mm. Detailed analysis of kinetic data was performed using both Copasi 4.7 (Build 34).[17]

4.2.3 Fast mixing system

Quantification of O_2 was performed using A Hi-Tech Scientific SF-61SX2 mixing apparatus. Stock solutions at twice the desired final concentrations were deareated with Ar in round bottom flasks before being injected into the mixer with 1010 TLL Gastight Hamilton syringes. One of the feeding syringes was filled with a $[Ru(bpy)_3]^{3+}$ solution and the other with a freshly prepared solution of WOC in buffer. The mixing apparatus was connected with PEEK tubing to an Ocean Optics FOXY-FLOW-CELL fitted with an oxygen probe. All joints were sealed with Teflon tape and DAP BLUESTIK adhesive putty. Oxygen measurements were made using an Ocean Optics Neofox Phase Measurement System with a FOXY-R probe and FOXY-AF-MG coating. The probe was

calibrated using a two point curve (0 and 20.9%). Repeated shots were performed until the oxygen reading was constant for three shots. The mixer is then purged with deaerated water before the procedure is repeated at least twice more.

4.2.4 Continuous-flow system

The continuous-flow system is pictured in **Scheme 4-1**. Separate solutions of $[Ru(bpy)_3]^{3+}$ in dilute HCl and WOC in buffer were deaerated with Ar in 50 mL vials which feed directly into separate 5 mL syringe pumps. The syringe pumps were controlled with FIA Labs software allowing for movement of the valve and adjusting flow speed, and are connected reservoirs of Ar deaerated solution. At the beginning of a run, 5 mL of the solutions were drawn into the syringes and simultaneously pumped into a Y-joint where they are quickly mixed. A similar fast mixing procedure has been reported.[18] The mixed solution then flowed through a length of PEEK tubing, which is proportional to the reaction time. The reacted solution then flowed through a Z-cell with 1 cm path-length and optical glass windows. Fiber optics were attached to the cell and run to an Ocean Optics UV-vis 2000+ and a LS-1 tungsten lamp respectively. The solution then passed through a short length of tubing to a T-cell with a FOXY-R oxygen sensing probe and finally to waste. All joints were sealed with Teflon tape and DAP BLUESTIK adhesive putty.

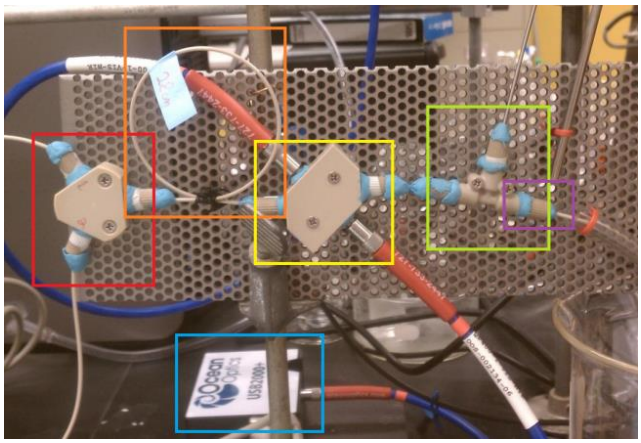

Scheme 4-1. Continuous flow system comprising (from left to right) two syringe pumps with variable pump volume (out of picture), a Y-mixing joint (red), variable loop of PEEK tubing (orange), a Z-cell with optical glass windows connected to fiber optics (yellow) connected to a tungsten lamp and Ocean Optics UV-vis (blue), and Ocean Optics FOXY optical oxygen probe in a T-cell (green). Teflon tape and DAP Blue Stik adhesive putty used to seal joints (violet).

4.3 Results and discussion

First, the importance of fast mixing of stock solutions for a reliable determination of O_2 yield for the processes with a reaction time shorter than 1-3 s are discussed. A reliable technique for fast-mixing was applied to analyze the WOCs **Co_4VPOM** and **Ni_5SiPOM**.[15, 16] Second, a continuous flow technique to follow the kinetics of O_2 formations for the fast water oxidation reactions is described. Under minimally optimized conditions a resolution shorter than 2 s was achieved. Finally, typical problems in interpretation of raw kinetic data are discussed.

4.3.1 Fast mixing of solutions

Catalytic WOC reactions can be quite fast, especially at basic pH values. For example, when $[Ru(bpy)_3]^{3+}$ is the stoichiometric oxidant, consumption of $[Ru(bpy)_3]^{3+}$ >

20% is achieved in less than 2 s when **Co_4PPOM** is used under conditions in **Figure 4-1**. Therefore, fast and thorough mixing of stock solutions is required to achieve a homogeneous solution on a timescale short enough to allow for accurate kinetic measurements. Commonly, one solution is simply injected into another without special care for fast or uniform mixing.[1-14] In these cases high local concentrations of reagents cannot be avoided due to inadequate mixing. Under previous stoichiometric oxidant procedure the injection lasts at least 0.5 s, necessitated to avoid contamination by air. After injection an uneven distribution of color is clearly visible for a short time (the mixing time is estimated to be about 1 s).[13] This is a problem that has plagued the water oxidation literature.

In our recent work at elevated pH, we use a fast mixing unit from a stopped flow instrument with a mixing time of about 1 ms to ensure fast and consistent mixing.[15] The feeding syringes are filled with deaerated stock solutions, and are pumped through a stopped-flow mixer to a holding chamber where they are stored until the reaction is complete. The mixed solution then flows through a T-joint with O_2 sensor (the same as that used in the continuous flow set up below). This requires approximately 10-15 shots to obtain a stable reading.

As reported in other work, a Φ_{CY} of 0.59 is reported when 2 μM **Co_4VPOM** is used as a WOC under conditions listed within.[16] The reported Φ_{CY} was calculated as in **Chapter 2**, **Equation 2-4** and based on the reaction in **Equation 2-2** which is a function of the sacrificial electron acceptor $Na_2S_2O_8$. This is in good agreement with the yield obtained from the fast mixing system under identical conditions by **Equation 2-8** which is based on the reaction in **Equation 2-1** and is a function of the sacrificial oxidant

$[Ru(bpy)_3]^{3+}$. The value was obtained to be 0.62 with a difference between the two values of 4.2 % suggesting good agreement. Conditions: 1.0 mM $[Ru(bpy)_3]^{3+}$, 80 mM sodium borate buffer at pH 9.0, 298 K. These equations are reproduced below for convenience.

$$4\,[Ru(bpy)_3]^{3+} + 2\,H_2O \xrightarrow{\phi_C,\mathbf{Co_4PPOM}} 4\,[Ru(bpy)_3]^{2+} + O_2 + 4\,H^+ \quad \textbf{(2-1)}$$

$$2\,S_2O_8{}^{2-} + 2\,H_2O + 2\,h\upsilon \xrightarrow{\Phi_{CY},\Phi_{QY}} 4\,SO_4{}^{2-} + O_2 + 4\,H^+ \quad \textbf{(2-2)}$$

$$\Phi_{CY} = 2\frac{[O_2]_f}{[Na_2S_2O_8]_0} \quad \textbf{(2-4)}$$

$$\text{Yield} = \frac{4[O_2]_f}{[Ru(bpy)_3]^{3+}{}_0} \quad \textbf{(2-8)}$$

This same technique was used to analyze the compound **Ni_5SiPOM**, however in this case it was used only to confirm the production of O_2 from the dark conditions (**Equation 2-1**) as a yield of only 5% was reported in the light-driven system.

4.3.2 Measurements of O_2 concentration

Measurements of O_2 formation in the present study were obtained with a luminescent oxygen sensor. Optical oxygen sensors do not consume oxygen, do not require frequent calibration and are convenient to use. They function via the quenching of a luminescent species by triplet oxygen, thus the presence of $[Ru(bpy)_3]^{2+}$ in solutions gives a false positive due to spectral overlap. Therefore the probe is coated to prevent light leaking which has the negative effect of increasing the response time to about 30 seconds. Since no head space is present in the setups described here, we did not need to

consider the mole fraction of O_2 in the gas phase. The calibrations of the optical probes are stable regardless of media, stirring speed and other variable experimental conditions.[19-21] Despite their wide usage in the literature,[3, 4, 8, 19] Clark style electrodes have known disadvantages.[4, 8, 19, 21, 22] They consume oxygen, and therefore their signal is proportional to the rate of O_2 diffusion past the oxygen permeable membrane, through the electrolyte solution and to the electrodes where O_2 is reduced to OH^-. As a result, the signal depends on multiple factors including the stirring speed, hydrodynamics of the sensor geometry, and is prone to drift from surface contamination and change in the alkalinity of the electrolyte over time.[23] Thus, the calibration should be done under exactly the same conditions over the narrow range of O_2 concentrations. Micro electrodes can be used to obtain faster response time, at the expense of lower measured currents, and still have a response time of 2-3 seconds. One shared disadvantage of both approaches is that they are temperature dependent, and when only small amounts of O_2 are produced, control of the temperature is critical. Gas chromatographic analysis of the reactor head space remains the ultimate technique to confirm the presence of O_2 and to quantify the amount of oxygen leaked from air into the reactor, but again, the response time of this technique is too slow for monitoring kinetics. Finally, it is worth mentioning that manometric measurements of O_2 formation seem to be close to ideal, but in most cases the overall yield of O_2 is too small to detect the change in gas pressure. Here we employ the Ocean Optics optical luminescent oxygen sensor, FOXY probe.

4.3.3 Continuous-flow system

Monitoring of the fast kinetics of both O_2 yield and consumption of oxidant remains an experimental challenge. Here we employ the Ocean Optics luminescent optical oxygen sensor and for O_2 measurements and UV-vis spectroscopy to follow the consumption as a decrease of absorbance at 670 nm. For the continuous flow system described in this work, the reaction time is the ratio of the loop volume (orange square in **Scheme 4-1**) and the flow rate, **Equation 4-1**.

$$\text{Reaction Time (s)} = \frac{\text{Volume } (\mu\text{L})}{\text{Flow Rate } (\frac{\mu\text{L}}{\text{s}})} \qquad (\mathbf{4\text{-}1})$$

The desired reaction time can be achieved by varying the flow rate and the loop volume. For the pictured configuration the shortest reaction time achievable is 0.75 s and the variable flow rate of the pumps allows for two orders of magnitude change in reaction time. Because the two pumps contain a total of 10 mL of solution, the O_2 probe and UV-Vis are able to continuously observe the reaction time of 0.75 s continuously for 10 s. While this is still slightly faster than the response time of the coated optical probe, multiple experiments can be run in immediate succession, thus eliminating any concerns regarding the response time of the FOXY probe.

Furthermore, the continuous flow system presented here is able to collect both O_2 kinetic data, and $[Ru(bpy)_3]^{3+}$ consumption kinetics for the same reaction at the same time. Previous studies were limited to examining the reactions at similar conditions but variation in mixing time and method persisted, limiting quantitative comparison. All experimental details of the two methods of measurement in the continuous flow system

are identical, however there exists a slight delay that is proportional to flow rate between the UV-vis measurement and the FOXY probe. This delay effectively makes the reaction time observed by the FOXY probe slightly longer than the UV-vis. While the length of tubing connecting these two sensors is short (**Scheme 4-1**) it does produce a modest delay of at most approximately 1.8 s for the slowest flow rates which, in this case, is about 2% of the total reaction time.

4.3.4 System validation

A validation of the continuous-flow system was conducted to ensure that results obtained with this system are applicable to kinetic data collected by traditional stopped-flow technique. The continuous-flow technique was performed as described above. Here **Ru_4SiPOM**, was employed as the catalyst. The configuration of the continuous-flow system utilized an 164 cm length of PEEK tubing where the reaction is carried out (orange box, **Scheme 4-1**) with an internal area of 4.56 x 10^3 cm^2 and thus a volume of 0.75 mL. The individual pump speeds were varied from 500 to 10 µL/s which when using two pumps produces double the flow rate. In this configuration, these flow rates correspond to reaction times from 1.5 to 75 s respectively. The full UV-Vis spectra of these separate runs from the continuous flow system are presented in **Figure 4-1**. The absorbance of each run at 670 nm plotted as a function of the reaction time was compared to a reaction under the same conditions collected by traditional stopped-flow technique in **Figure 4-2**. Visual comparison of results from the two techniques suggests good agreement between them.

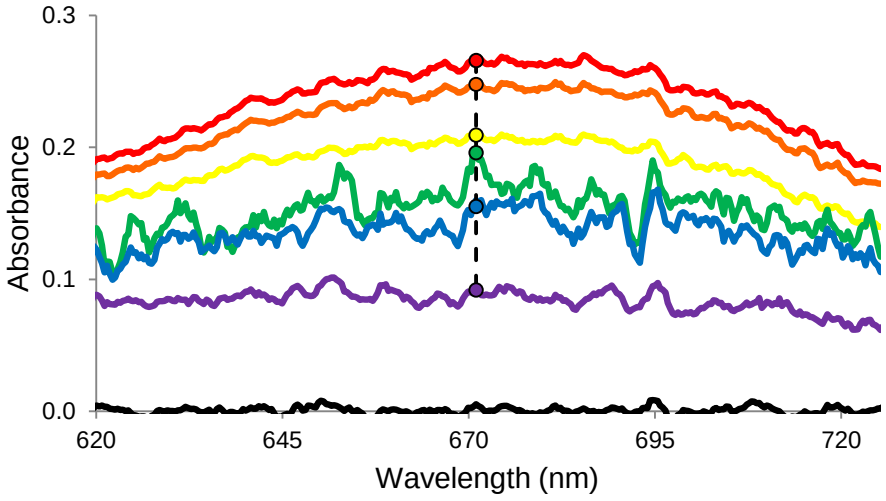

Figure 4-1. UV-Vis spectra from continuous-flow system. Final flow rates are 1000 (red), 500 (orange), 200 (yellow), 100 (green), 50 (blue), and 20 (purple) µL/s. Data points highlighted at 670 nm. Conditions: 1 mM $[Ru(bpy)_3]^{3+}$, 60 mM NaP_i pH = 7.2, 5 µM **Ru_4SiPOM**. Control in absence of $[Ru(bpy)_3]^{3+}$ (black).

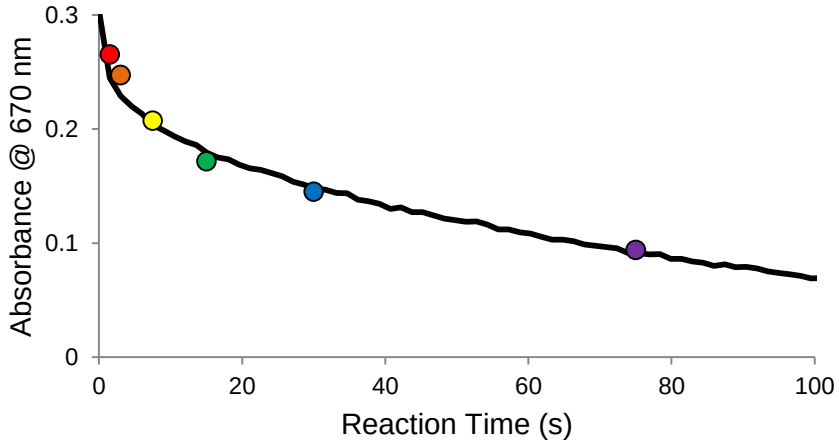

Figure 4-2. Absorbance at 670 nm from separate runs of continuous-flow system. Final flow rates are 1000 (red), 500 (orange), 200 (yellow), 100 (green), 50 (blue), and 20 (purple) µL/s. Black curve: absorbance at 670 nm with stopped-flow technique. Conditions in both systems: 1 mM $[Ru(bpy)_3]^{3+}$, 60 mM NaP_i pH = 7.2, 5 µM **Ru_4SiPOM**.

4.3.5 Measurements of $[Ru(bpy)_3]^{3+}$ concentration

While it does have limitations, $[Ru(bpy)_3]^{3+}$ is a common sacrificial oxidant for WOC studies, the most common primary oxidant when the WOC is a POM, and even more so if $[Ru(bpy)_3]^{2+}$ in a light driven system is included. A table with the conditions of various POM WOC studies can be found in **Equation 2-4** [24] and a recent review examines common primary oxidants in WOC studies in general.[25]

The spectrum of $[Ru(bpy)_3]^{3+}$ has a broad maximum at λ = 670 nm with ε = 420 $M^{-1}cm^{-1}$, which makes UV-vis spectroscopy an ideal technique to study the kinetics of its consumption. It is often assumed that the concentration of $[Ru(bpy)_3]^{3+}$ is directly proportional to the absorbance at 670 nm based on Beer's law. However, $[Ru(bpy)_3]^{2+}$ also has a small absorbance at 670 nm (ε_{670} = 20 $M^{-1}cm^{-1}$) which can become substantial in high concentrations. Decomposition products of $[Ru(bpy)_3]^{3+}$ often absorb near 670 nm as well, exhibiting higher absorption than that of $[Ru(bpy)_3]^{2+}$.[26] Even the WOC itself can also absorb light at this wavelength which is obvious when **Ru_4SiPOM** is used, and while **Co_4PPOM** has a very low molar absorptivity at this wavelength, little is known about the spectra of its higher oxidation states during turnover. Without consideration of these overlapping components, this could affect the relationship between $[Ru(bpy)_3]^{3+}$ and the absorbance, especially at high conversion. The initial rates determined as $d[Ru^{3+}]/dt = d(A_{670}/\varepsilon l)/dt$ are less sensitive to the absorbance of reaction products. Therefore, one could expect that the reaction rate law can be determined from a dependence of initial rates on catalyst and $[Ru(bpy)_3]^{3+}$ concentrations. However, in numerous cases the initial rate cannot be determined due to unique kinetic features of a given WOC, as evident from the data in **Figure 4-3**. The initial rates for the reaction

catalyzed by **Ru_4SiPOM** are very high and strongly depend on trace amounts of $[Ru(bpy)_3]^{2+}$ present in solution as has been previously elaborated.[27] A similar scenario is operable when Co^{2+} (aq) is employed as the catalyst: there is an induction period which has been addressed in several recent publications.[28, 29] No special features are seen for the system with **Co_4PPOM** in **Figure 4-1** (pink curve, the conditions are the same as in recently published paper).[10] Thus, at short time scales it is quite clear that the kinetic curve cannot be approximated by a straight line. Only the fitting of whole kinetic curves "A_{670} vs. time" could provide valuable information on kinetics of $[Ru(bpy)_3]^{3+}$ consumption.

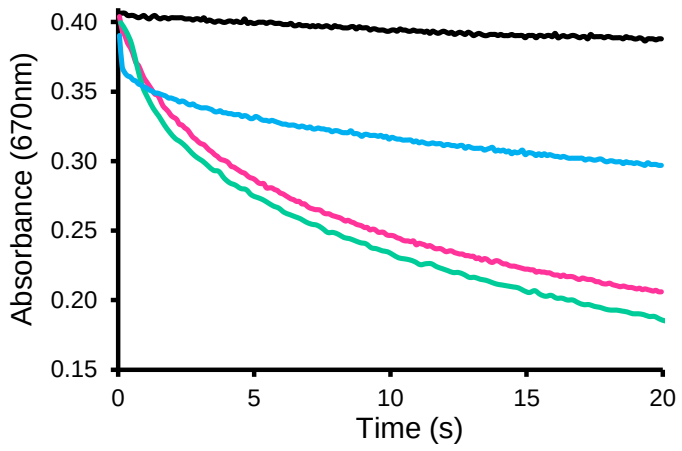

Figure 4-3. Kinetic curves of decrease in absorbance at 670 nm obtained by stopped-flow technique. Conditions: 25 ºC, 1.0 mM $[Ru(bpy)_3]^{3+}$, 40 mM NaP_i, pH = 8.0, no catalyst (black), 3 µM **Ru_4SiPOM** (blue), 3 µM **Co_4PPOM** (pink) and 5 µM $Co(NO_3)_2$ (teal).

Recently Stracke and Finke collected the kinetics of both $[Ru(bpy)_3]^{3+}$ consumption (absorbance at 675 nm) and O_2 formation (by a custom made Clark microelectrode) for the reaction of water oxidation by $[Ru(bpy)_3]^{3+}$ in 30 mM phosphate buffer (pH 6.5-7.8) catalyzed by **Co_4PPOM.**[10] The reaction rate law was determined

based on measurement of initial reaction rates. The stock solutions were mixed by pipette injection, and the absorbance was measured each second using a diode-array UV-vis spectrophotometer. The initial rate was measured at ~10% conversion typically within the first 10 s. Our measurements under the same standard experimental conditions but using a stopped flow technique revealed that the initial part of the kinetic curves cannot be approximated by a straight line, **Figure 4-4**. The reaction within the initial 3 s is almost twice as fast as the rate determined in the time range 3-10 s. This seems to also be true under other experimental conditions. In the procedure described by Stracke and Finke the kinetic measurements most likely start 2-3 seconds after the beginning of the reaction. Consequently, instrumental limitations only permitted measurements after this amount of time. The beginning of the kinetic curve might be due to an establishment of steady state conditions.

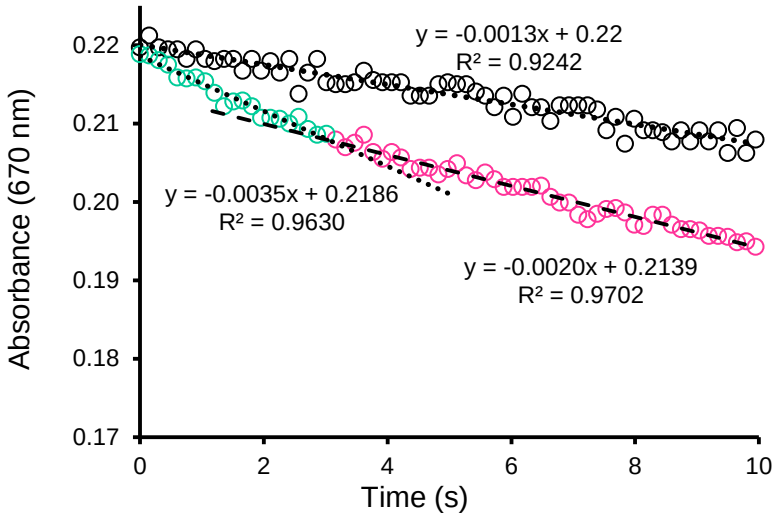

Figure 4-4. Kinetic curves of decrease in absorbance at 670 nm obtained by stopped-flow technique. Conditions: 25 ºC, 0.5 mM $[Ru(bpy)_3]^{3+}$, 0.1 mM $[Ru(bpy)_3]^{2+}$, 30 mM NaP_i, pH = 7.2 without catalyst (black) and with 1.0 μM **Co_4PPOM** 1-3 seconds (teal) 3-10 seconds (pink). The solution of Ru^{3+}/Ru^{2+} (pH~3) was mixed with the solution of the catalyst in buffer.

4.3.6 The effect of precipitation on the reaction kinetics

Previously, it was reported that an initially homogeneous mixture of $[Ru(bpy)_3]^{3+}$ with **Co_4PPOM** became cloudy before reaction completion.[13] Such behavior indicates that the solubility of the POM complex with $[Ru(bpy)_3]^{2+}$ is lower than that with $[Ru(bpy)_3]^{3+}$. This property has been used to precipitate POM complexes from solution by adding more $[Ru(bpy)_3]^{2+}$.[13] Recently, the solubility constant of $(\mathbf{Co_4PPOM})_2([Ru(bpy)_3]^{2+})_3$ has been determined in 30 mM sodium phosphate (NaP_i) buffer: $K_{sp} = (8 \pm 7) \times 10^{-25}$ (M^5).[10] In the presence of 0.5-1.0 mM $[Ru(bpy)_3]^{2+}$ the concentration of **Co_4PPOM** was estimated to be very low, ~ 10^{-7} M. Based on this value, kinetics data were analyzed assuming that **Co_4PPOM** in solution is in equilibrium with the insoluble complex.[10] However, the process of precipitation is often kinetically controlled and strongly dependent on ionic strength. For a relatively fast reaction, the post-reaction solution could be homogeneous but supersaturated. Under such conditions, the low solubility of the reaction products might not affect the reaction kinetics. Experimentally, precipitation is visible as an increase of background absorbance in UV-vis spectra due to light scattering. Here, we confirm that the reaction kinetics followed by absorbance at 670 nm strongly depend on the sequence of reagent mixing. This effect is best seen at higher catalyst concentration and is shown in **Figure 4-5**. In this experiment, one feeding syringe was filled with fresh $[Ru(bpy)_3]^{3+}$ solution and the second one with **Co_4PPOM** premixed with $[Ru(bpy)_3]^{2+}$ in phosphate buffer. The second solution was aged about 4 hours before reaction. Both the initial and final absorbencies are significantly higher when catalyst was used (teal dashed line) than in the uncatalyzed

reaction (black line). When both $[Ru(bpy)_3]^{3+}$ and $[Ru(bpy)_3]^{2+}$ were in the first feeding syringe, and **Co_4PPOM** was not premixed with $[Ru(bpy)_3]^{2+}$, the rate of precipitation was slower than the reaction, and no significant increase in background absorbance was detected (teal black line). Thus, a correct design of the experiment minimizes the effect of low product solubility. In some systems catalyst decomposition may result in formation of catalytically active nanoparticles which may visually appear homogeneous. Developing methods for differentiating between homogeneous and heterogeneous catalysts formed during a reaction is an ongoing concern in the field of homogeneous catalysis,[30-32] and was recently described for this specific system.[10, 29, 33, 34]

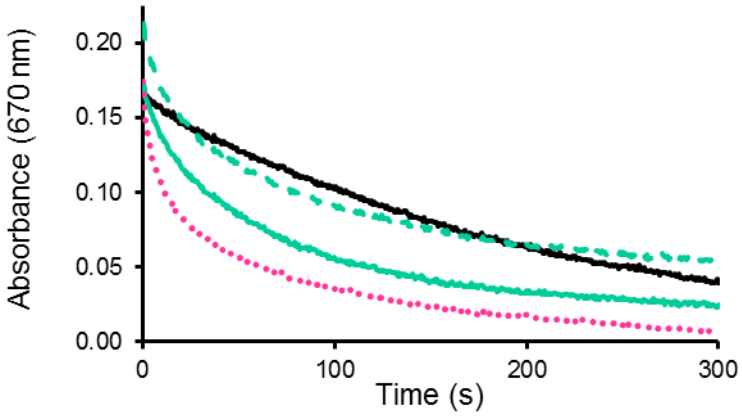

Figure 4-5. Kinetic curves of decrease in absorbance at 670 nm obtained by stopped-flow technique. Conditions: 25 ºC, 0.4 mM $[Ru(bpy)_3]^{3+}$, 0.1 mM $[Ru(bpy)_3]^{2+}$, 30 mM NaP_i, pH = 7.2 without catalyst (black) and with 3.0 µM **Co_4PPOM** (teal and pink lines). The solution of $[Ru(bpy)_3]^{3+}$ (pH~3) was mixed with the solution of **Co_4PPOM** and $[Ru(bpy)_3]^{2+}$ in buffer aged 4 hours (dashed teal). The solution of $[Ru(bpy)_3]^{3+}$ and $[Ru(bpy)_3]^{2+}$ (pH~3) was mixed with the solution of **Co_4PPOM** in buffer aged 5-15 min (solid teal). **Co_4PPOM** added to $[Ru(bpy)_3]^{3+}$ with no initial $[Ru(bpy)_3]^{2+}$ (dotted pink).

4.3.7 Simplified reaction mechanism

In order to precisely describe the experimental kinetics data, a reaction mechanism may include numerous steps. Some of them are kinetically insignificant but required to maintain a reaction stoichiometry, charge balance, etc. As a general rule the number of steps in a mechanism should be minimal. Some reactions in a mechanism are not necessarily elementary and may proceed in several simpler steps, however, these are very fast and are described by apparent reaction rate constants.

In stoichiometric water oxidation, $[Ru(bpy)_3]^{3+}$ is a commonly used oxidant with a standard oxidation potential 1.21 V (NHE).[25, 35] It is relatively stable under acidic conditions, but in neutral and basic conditions $[Ru(bpy)_3]^{3+}$ undergoes self-decomposition, with the rate dependent on pH and the nature and concentration of buffer, as shown in **Equation 4-2**. The decay kinetics are first order and the rate constant k_2 is 0.0014 s^{-1} in Na_2SiF_6-$Na_2B_4O_7$ at pH ca 5.5,[36] 0.02 and 0.05 s^{-1} in borate buffer at pH 8 and 9, respectively.[37, 38] This is for a generic reaction (**Equation 4-2**) where one or more of the bpy ligands are oxidized one or more times; some of the bpy ligand is fully oxidized to CO_2, however, the products are largely $[Ru(bpy)_3]^{2+}$ with the yield up to 98% based on initial $[Ru(bpy)_3]^{3+}$. Sutin *et al.* have identified at least eight separate products in previous work.[26] Despite this previous work, little is known about the importance of these reactions and the rates relative to water oxidation.

$$Ru^{3+} \xrightarrow{k_2} \text{products} \qquad \textbf{(4-2)}$$

Where Ru^{3+} is $[Ru(bpy)_3]^{3+}$, and Ru^{2+} is $[Ru(bpy)_3]^{2+}$. In the presence of WOC four oxidative equivalents of Ru^{3+} are used to oxidize water in **Equation 4-3**.

$$4\,Ru^{3+} + 2\,H_2O \xrightarrow{k_3} 4\,Ru^{2+} + O_2 + 4\,H^+ \qquad (\mathbf{4\text{-}3})$$

The simplified mechanism of catalytic water oxidation is given in **Eqs 4-8**:

$$Ru^{3+} + cat(0) \xrightarrow{k_4} Ru^{2+} + cat(1) \qquad (\mathbf{4\text{-}4})$$

$$Ru^{3+} + cat(1) \xrightarrow{k_5} Ru^{2+} + cat(2) \qquad (\mathbf{4\text{-}5})$$

$$Ru^{3+} + cat(2) \xrightarrow{k_6} Ru^{2+} + cat(3) \qquad (\mathbf{4\text{-}6})$$

$$Ru^{3+} + cat(3) \underset{k_{-7}}{\overset{k_7}{\rightleftharpoons}} Ru^{2+} + cat(4) \qquad (\mathbf{4\text{-}7})$$

$$cat(4) + 2\,H_2O \xrightarrow{k_8} cat(0) + O_2 + 4\,H^+ \qquad (\mathbf{4\text{-}8})$$

where "i" in cat(i) is the number of electrons removed from the resting oxidation state of a catalyst. The first three reactions are assumed to be fast and the [cat(0)], [cat(1)], [cat(2)], [cat(3)], [cat(4)] to be steady state. Under these assumptions, and taking into account the mass balance for total catalyst concentration [cat], the rate law of $[Ru(bpy)_3]^{3+}$ consumption is in **Equation 4-9**, for which a detailed derivation is provided (see **Appendix A**):

$$\frac{-d[Ru^{3+}]}{dt} = k_2[Ru^{3+}] + \frac{4k_8k_7[Ru^{3+}][cat]}{(k_7[Ru^{3+}] + k_{-7}[Ru^{2+}] + k_8)} \qquad (\mathbf{4\text{-}9})$$

For illustration purposes we simplify **Equation 4-9**. If $k_7[Ru^{3+}] + k_{-7}[Ru^{2+}] << k_8$ then the reaction in **Equation 4-7** is the rate limiting step and the reaction rate laws are **Equations 4-10a** and **4-10b**:

$$\frac{-d[Ru^{3+}]}{dt} = k_2[Ru^{3+}] + 4k_7[Ru^{3+}][cat] \quad \textbf{(4-10a)}$$

$$\frac{d[O_2]}{dt} = k_7[Ru^{3+}][cat] \quad \textbf{(4-10b)}$$

In this case the O_2 yield per consumed Ru^{3+} is **Equation 11**:

$$\frac{-d[O_2]}{d[Ru^{3+}]} = \frac{k_7[cat]}{(k_2 + 4k_7[cat])} \quad \textbf{(4-11)}$$

At high concentration of the catalyst the contribution of the reaction in **Equation 4-2** is negligible and O_2 yield should be equal to (1/4) $[Ru^{3+}]_o$. However, this scenario is not consistent with experimental data where, as mentioned above, yields are still well below 100% based on $[Ru^{3+}]_o$. If instead, $(k_{-7}[Ru^{2+}] + k_7[Ru^{3+}]) >> k_8$, the reaction in **Equation 4-7** is equilibrated, $K_7 = k_7/k_{-7}$, and rate laws are **Equations 4-12a and 4-12b**:

$$\frac{-d[Ru^{3+}]}{dt} = k_2[Ru^{3+}] + \frac{4k_8K_7[Ru^{3+}][cat]}{([Ru^{2+}] + K_7[Ru^{3+}])} \quad \textbf{(4-12a)}$$

$$\frac{d[O_2]}{dt} = \frac{k_8K_7[Ru^{3+}][cat]}{([Ru^{2+}] + K_7[Ru^{3+}])} \quad \textbf{(4-12b)}$$

$$\frac{-d[O_2]}{d[Ru^{3+}]} = \frac{k_8K_7[cat]}{(([Ru^{2+}] + K_7[Ru^{3+}])(k_2 + 4k_8K_7[cat]))} \quad \textbf{(4-13)}$$

Taking into account that $[Ru^{2+}] \approx ([Ru^{3+}]_o - [Ru^{3+}])$, **Equation 4-13** can be simplified to **Equation 4-14**, which after integration gives **Equation 4-15**:

$$\frac{-d[O_2]}{d[Ru^{3+}]} = \frac{k_8 K_7 [cat]}{(k_2[Ru^{3+}]_o + k_2 (K_7 - 1)[Ru^{3+}] + 4k_8 K_7 [cat])} \quad \textbf{(4-14)}$$

$$\frac{[O_2]}{[Ru^{3+}]_o} = \frac{k_8 K_7 [cat]}{k_2 [Ru^{3+}]_o (K_7 - 1)} \ln\left(\frac{K_7 k_2 [Ru^{3+}]_o + 4k_8 K_7 [cat]}{(k_2[Ru^{3+}]_o + k_2 (K_7 - 1)[Ru^{3+}] + 4k_8 K_7 [cat])}\right) \quad \textbf{(4-15)}$$

Basic analysis of **Equation 4-15** reveals that O_2 is strongly dependent on [cat] and weakly dependent on $[Ru^{3+}]_o$, which is again, not consistent with experimental data. This inconsistency between the kinetic model above, and experimental results indicate that another pathway for $[Ru(bpy)_3]^{3+}$ consumption exists and it must be the pathway of $[Ru(bpy)_3]^{3+}$ decomposition involving the catalyst, thus the model must be expanded to incorporate additional $[Ru(bpy)_3]^{3+}$ decomposition steps. Recently a similar conclusion has been made.[10]

In deriving **Equation 4-14** it was assumed that $[Ru^{2+}] \approx [Ru^{3+}]_o - [Ru^{3+}]$. The yield, Y, of $[Ru^{2+}]$ per $[Ru^{3+}]_o$ in **Equation 4-3** in the absence of catalyst is about 95%. Therefore, it would be reasonable to assume that $[Ru^{2+}] \approx [Ru^{3+}]_o - Y\,[Ru^{3+}]$. In this case the modified **Equation 4-15** predicts that O_2 yield per $[Ru^{3+}]_o$ reaches 95% at high catalyst concentrations.

4.3.8 Selectivity of the catalyst

At high catalyst concentration the O_2 yield based on $[Ru^{3+}]_o$ concentration, $4x[O_2]/[Ru^{3+}]_o$ should be 100%, but experimentally determined yields are much lower; 48

% for **Co_4PPOM** as seen in **Figure 4-6**. A similar phenomenon was observed for **Co_4VPOM**, **Ni_5SiPOM** as reported above, and IrO_2 catalyst.[36] The lower than expected O_2 yield can be explained by a catalytic oxidation of bpy ligand in the $Ru^{3+/2+}$ complexes, which is explored in-depth by Sutin *et al.*[26] For the purpose of illustration and simplicity we assume that the bpy ligand is oxidized solely by cat(4) as it is the strongest oxidant in the system (**Equation 4-16**), although it is possible that another oxidation state of the catalyst could be involved. We also considered the scenario where bpy is oxidized in the $[Ru(bpy)_3]^{3+}$ species, but this appeared to be inconsistent with experimental data.

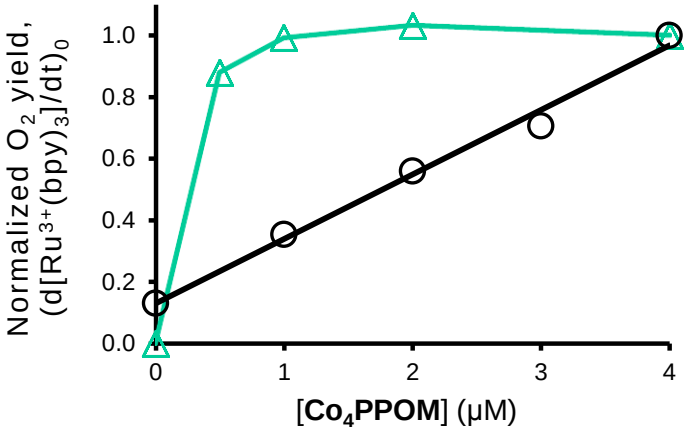

Figure 4-6. Normalized O_2 yield (teal triangles) and initial rates of $[Ru^{3+}]$ consumption (black circles) in the reaction of water oxidation by 1.0 mM $[Ru^{3+}]$ in 80mM sodium borate buffer at pH 8.0. Where 4 x $[O_2]/[Ru^{3+}]_o$ = 0.48 ± 0.05 at 4 μM **Co_4PPOM**.

$$Ru^{2+} + \text{cat(4)} \xrightarrow{k_{16}} [Ru(bpy')(bpy)_2]^{2+} + \text{cat(2)} \qquad \textbf{(4-16)}$$

where bpy' is a product of bpy oxidation. Such a product is more oxidizable than the initial bpy and therefore triggers a sequence of oxidation reactions up to CO_2 formation

as has been quantified previously.[29] For simplicity, these reactions can be written as **Equation 4-17**, since the identity of the products is largely unimportant here.

$$n\,Ru^{3+} + [Ru(bpy')(bpy)_2]^{2+} \xrightarrow{k_{17}} n\,Ru^{2+} + \text{products} \qquad (\mathbf{4\text{-}17})$$

After taking into account the reactions in **Equations 4-16** and **4-17** and assuming fast equilibration in **Equation 4-6**, the rate laws are in **Equations 4-18a** and **4-18b**, and O_2 yield in **Equation 4-19**:

$$\frac{-[Ru^{3+}]}{dt} = \frac{K_7[Ru^{3+}][cat]\,(4k_8 + nk_{16}[Ru^{2+}])}{([Ru^{2+}] + K_7[Ru^{3+}])} \qquad (\mathbf{4\text{-}18a})$$

$$\frac{d[O_2]}{dt} = \frac{k_8 K_7[Ru^{3+}][cat]}{([Ru^{2+}] + K_7[Ru^{3+}])} \qquad (\mathbf{4\text{-}18b})$$

$$\frac{-d[O_2]}{d[Ru^{3+}]} = \frac{1}{\left(4 + \frac{nk_{16}[Ru^{2+}]}{k_8}\right)} \qquad (\mathbf{4\text{-}19})$$

The validity of **Equation 4-19** has been qualitatively confirmed by the data obtained using the continuous flow technique, **Figure 4-7**.

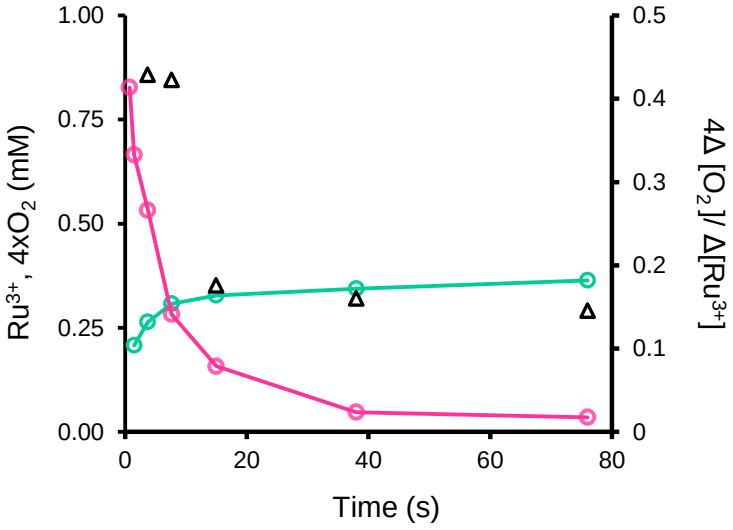

Figure 4-7. Kinetics of 1.2 mM $[Ru(bpy)_3]^{3+}$ consumption (pink) and $4xO_2$ formation (teal) in 60 mM NaP_i at pH 7.2 in the presence of 8 μM **Ru_4SiPOM** and selectivity ($4x\Delta[O_2]/\Delta[Ru^{3+}]$, black) collected by the continuous flow technique.

Indeed, with accumulation of $[Ru(bpy)_3]^{2+}$, the ratio $\Delta[O_2]/\Delta[Ru^{3+}]$ quickly decreases with time. This is consistent with two competitive reactions involving cat(4); the desired water oxidation in **Equation 4-8**, and destructive $[Ru(bpy)_3]^{2+}$ ligand oxidation in **Equation 4-16**. The catalytic oxidation of bpy ligand is also observed in the reaction catalyzed by **Co_4PPOM**: the final O_2 is half of the theoretical value and is independent of catalyst concentration (**Figure 4-7**). However, the kinetic data do indicate that the same reactive intermediate is involved in both the water and ligand-oxidation reactions. This, in turn, means that the selectivity of the catalyst is controlled primarily by the relative reactivity of this intermediate in **Equation 4-8** and **Equation 4-16** where the selectivity is a function of $[Ru^{2+}]$, k_{16}, and k_8 as indicated by **Equation 4-19**. The initial rates of $[Ru(bpy)_3]^{3+}$ consumption are reproducible and do not strongly depend on traces of $[Ru(bpy)_3]^{2+}$ (**Figure 4-3**), in contrast to **Ru_4SiPOM**. This would be consistent with

Equation 4-7 being the rate-limiting step. In this case the rate law should be **Equation 4-20**:

$$\frac{-d[Ru]^{3+}}{dt} = 4k_7[Ru^{3+}][cat] \qquad (\mathbf{4\text{-}20})$$

Indeed, the initial rates are linearly proportional to [cat] (**Figure 4-6**), but the kinetics of $[Ru(bpy)_3]^{3+}$ consumption measured as the decrease of absorbance at 670 nm is not exponential (**Figure 4-8**). As discussed above this deviation from exponential decay could arise from increase of absorbance by reaction products.

Since the equation describing the dependence of $[Ru^{3+}]$ versus time cannot be derived in this case, we performed a digital simulation using Copasi software[17] and the mechanism consists only of **Equations 4-4 - 4-8**, and **16**. The simulation demonstrated that the absorbance of $[Ru(bpy)_3]^{3+}$, $[Ru(bpy)_3]^{2+}$, and $[Ru(bpy')(bpy)_2]^{2+}$ should be taken into account to obtain an agreement with experimental data, as discussed above. The simulation gave $4[O_2]/[Ru^{3+}] = 0.52$, which is an excellent agreement with experimental value 0.48. The validity of the model is further demonstrated by good agreement between theoretical and experimental kinetic trials (**Figure 4-8**). The parameters for simulation are given in **Figure 4-4**. Thus, a thorough analysis of limited amount of kinetic data could provide solid evidence for the reaction mechanism. Note that the above reaction mechanism does not require taking precipitation of the catalyst into account. Inhibition of the reaction by $[Ru(bpy)_3]^{2+}$ is explained by the reversibility of **Equation 4-7**.

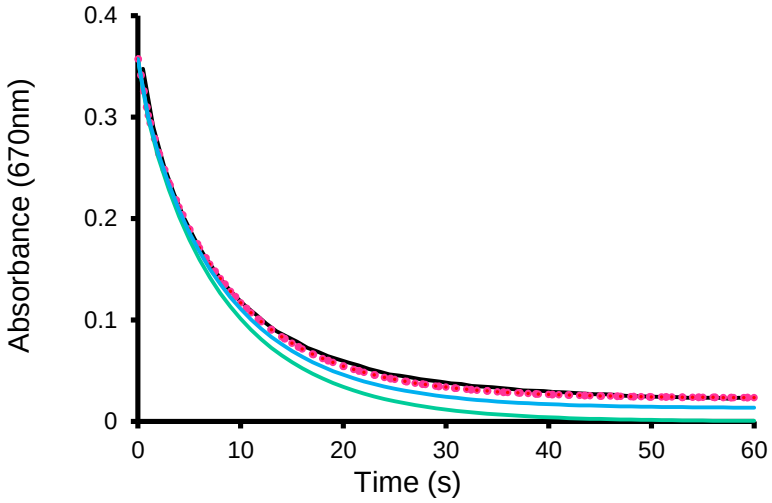

Figure 4-8. The experimental (black) and simulated kinetics of absorbance decrease at 670 nm. Conditions: 0.85 mM Ru^{3+}, 2 µM **Co_4PPOM**, 80 mM NaB_i buffer at pH 8.0, 25 °C. Parameters used in simulation: $k_4 = k_5 = k_6 = 10^9$ $M^{-1}s^{-1}$, $k_7 = 10^5$ $M^{-1}s^{-1}$, $k_{-7} = 10^7$ $M^{-1}s^{-1}$ $k_8 = 10^5$ s^{-1} $k_{16} = 6x10^7$ $M^{-1}s^{-1}$, $\varepsilon(Ru^{3+}) = 420$ $M^{-1}cm^{-1}$, $\varepsilon(Ru^{2+}) = 20$ $M^{-1}cm^{-1}$, $\varepsilon([Ru(bpy')(bpy)_2]^{2+}) = 50$ $M^{-1}cm^{-1}$. Pink dotted line: all three extinction coefficients were used. Blue line: $\varepsilon(Ru^{3+})$ and $\varepsilon(Ru^{2+})$ were used. Teal line: only $\varepsilon(Ru^{3+})$ was used.

4.4 Conclusions

Through our work with WOCs we have come to identify some shortcomings of our own experimental design and those reported in the literature. When O_2 is measured by mixing solutions of $[Ru(bpy)_3]^{3+}$ as a stoichiometric oxidant with catalyst in buffer, the reaction occurs so quickly that a fast and through mixing is crucial for obtaining meaningful kinetic data. Furthermore, some WOCs have unique early time kinetics which can be obscured by slow mixing, or missed entirely. To this end we developed a system which meets these requirements to facilitate accurate O_2 measurements that reflect the performance of the catalyst and the not speed of mixing. Although this does not produce kinetics data, the accurate final O_2 yield of the dark reaction is still of great use. We have previously been limited by the long instrumental delay required for O_2 quantification in

attempts to collect O_2 production kinetics. Thus a second system – dubbed continuous flow – was constructed that by-passes the delay and allows for full kinetic measurement of O_2 production. It also allows for the monitoring of the consumption of $[Ru(bpy)_3]^{3+}$ by UV-vis for same reaction at the same time. This has not been previously reported and nullifies concerns about uniform experimental design when the reactions are separated. Applying data collected from these techniques to a kinetic model which reflects several known side reactions has provided insight to not only the speed of the catalyst, but also the ratio of water oxidation to non-oxygen-producing side reactions. This metric is referred to herein as "selectivity". Knowledge about selectivity is absolutely crucial when considering a WOC for incorporation into a device where lifetime of the system is more important than simply the stability of the catalyst. Finally, the kinetic model was shown to demonstrate good agreement with experiment in terms of kinetic profiles and O_2 yields (compare 0.52 and 0.48 respectively for **Co_4PPOM** and **Figure 4-8**).

4.5 References

(1) McDaniel, N. D.; Coughlin, F. J.; Tinker, L. L.; Bernhard, S. *J. Am. Chem. Soc.* **2008**, *130*, 210.

(2) Muckerman, J. T.; Polyansky, D. E.; Wada, T.; Tanaka, K.; Fujita, E. *Inorg. Chem.* **2008**, *47*, 1787.

(3) Hull, J. F.; Balcells, D.; Blakemore, J. D.; Incarvito, C. D.; Eisenstein, O.; Brudvig, G. W.; Crabtree, R. H. *J. Am. Chem. Soc.* **2009**, *131*, 8730.

(4) Masaoka, S.; Sakai, K. *Chem. Lett.* **2009**, *38*, 182.

(5) Fillol, J. L.; Codolà, Z.; Garcia-Bosch, I.; Gómez, L.; Pla, J. J.; Costas, M. *Nature Chem.* **2011**, *3*, 807.

(6) Roeser, S.; Fàrrs, P.; Bozoglian, F.; Martínez-Belmonte, M.; Benet-Buchholz, J.; Llobet, A. *ChemSusChem* **2011**, *4*, 197.

(7) An, J.; Duana, L.; Sun, L. *Faraday Discuss.* **2012**, *155*, 267.

(8) Kaveevivitchai, N.; Zong, R.; Tseng, H.-W.; Chitta, R.; Thummel, R. P. *Inorg. Chem.* **2012**, *51*, 2930.

(9) Murakami, M.; Hong, D.; Suenobu, T.; Yamaguchi, S.; Ogura, T.; Fukuzumi, S. *J. Am. Chem. Soc.* **2011**, *133*, 11605.

(10) Stracke, J. J.; Finke, R. G. *ACS Catal.* **2014**, *4*, 79.

(11) Geletii, Y. V.; Botar, B.; Kögerler, P.; Hillesheim, D. A.; Musaev, D. G.; Hill, C. L. *Angew. Chem. Int. Ed.* **2008**, *47*, 3896.

(12) Goberna-Ferrón, S.; Vigara, L.; Soriano-López, J.; Galán-Mascarós, J. R. *Inorg. Chem.* **2012**, *51*, 11707.

(13) Yin, Q.; Tan, J. M.; Besson, C.; Geletii, Y. V.; Musaev, D. G.; Kuznetsov, A. E.; Luo, Z.; Hardcastle, K. I.; Hill, C. L. *Science* **2010**, *328*, 342.

(14) Sartorel, A.; Carraro, M.; Scorrano, G.; Zorzi, R. D.; Geremia, S.; McDaniel, N. D.; Bernhard, S.; Bonchio, M. *J. Am. Chem. Soc.* **2008**, *130*, 5006.

(15) Zhu, G.; Glass, E. N.; Zhao, C.; Lv, H.; Vickers, J. W.; Geletii, Y. V.; Musaev, D. G.; Song, J.; Hill, C. L. *Dalton Trans.* **2012**, *41*, 13043.

(16) Lv, H.; Song, J.; Geletii, Y. V.; Vickers, J. W.; Sumliner, J. M.; Musaev, D. G.; Kögerler, P.; Zhuk, P. F.; Bacsa, J.; Zhu, G.; Hill, C. L. *J. Am. Chem. Soc.* **2014**, *136*, 9268.

(17) Hoops, S.; Sahle, S.; Gauges, R.; Lee, C.; Pahle, J.; Simus, N.; Singhal, M.; Xu, L.; Mendes, P.; Kummer, U. *Bioinformatics* **2006**, *22*, 3067.

(18) Zidki, T.; Zhang, L.; Shafirovich, V.; Lymar, S. V. *J. Am. Chem. Soc.* **2012**, *134*, 14275.

(19) Shahriari, M. R.; Zhous, Q.; G.H. Sigel, J.; Stokess, G. In *"Porous Fiber Optic Sensor for Monitoring Underground Water Contaminants", Symposium Proceedings of Field Screening Methods for Hazardous Waste Site Investigations, First International Symposium,* Las Vegas, NV, October 1988, p 43.

(20) Wang, W.; Reimers, C. E.; Shahriari, M. R.; Morris, M. J. *Sea Technology* **March 1999**, *40*, 69.

(21) Alla, S.; Solanki, R.; Mattley, Y. D.; Dabhi, H.; Shahriari, M. R. In *Nanoporous thin film platform for biophotonic sensors, Proc. SPIE, Optical Fibers and Sensors for Medical Diagnostics and Treatment Applications IX, 717304* San Jose, CA., February 20, 2009; Vol. 7173.

(22) Huang, H.; Leung, D. Y. C.; Ye, D. *J. Mater. Chem.* **2011**, *21*, 9647.

(23) Ramamoorthy, R.; Dutta, P. K.; Akbar, S. A. *J. Mater. Sci.* **2003**, *38*, 4271.

(24) Sumliner, J. M.; Vickers, J. W.; Lv, H.; Geletii, Y. V.; Hill, C. L. In *Molecular Water Oxidation Catalysts: A Key Topic for New Sustainable Energy Conversion Schemes*; Llobet, A., Ed.; John Wiley & Sons, Ltd.: 2014; Vol. First Edition, p 211.

(25) Parent, A. R.; Crabtree, R. H.; Brudvig, G. W. *Chem. Soc. Rev.* **2013**, *42*, 2247.

(26) Ghosh, P. K.; Brunschwig, B. S.; Chou, M.; Creutz, C.; Sutin, N. *J. Am. Chem. Soc.* **1984**, *106*, 4772.

(27) Geletii, Y. V.; Besson, C.; Hou, Y.; Yin, Q.; Musaev, D. G.; Quinonero, D.; Cao, R.; Hardcastle, K. I.; Proust, A.; Kögerler, P.; Hill, C. L. *J. Am. Chem. Soc.* **2009**, *131*, 17360.

(28) Vickers, J.; Lv, H.; Zhuk, P. F.; Geletii, Y. V.; Hill, C. L. *MRS Proceedings* **2012**, *1387*, mrsf11.

(29) Vickers, J. W.; Lv, H.; Sumliner, J. M.; Zhu, G.; Luo, Z.; Musaev, D. G.; Geletii, Y. V.; Hill, C. L. *J. Am. Chem. Soc.* **2013**, *135*, 14110.

(30) Anton, D. R.; Crabtree, R. H. *Organometallics* **1983**, *2*, 855.

(31) Whitesides, G. M.; Hackett, M.; Brainard, R. L.; Lavalleye, J.-P. P. M.; Sowinski, A. F.; Izumi, A. N.; Moore, S. S.; Brown, D. W.; Staudt, E. M. *Organometallics* **1985**, *4*, 1819.

(32) Widegren, J. A.; Finke, R. G. *J. Mol. Catal. A: Chem.* **2003**, *198*, 317.

(33) Stracke, J. J.; Finke, R. G. *ACS Catal.* **2013**, *3*, 1209.

(34) Stracke, J. J.; Finke, R. G. *J. Am. Chem. Soc.* **2011**, *133*, 14872.

(35) Juris, A.; Balzani, V.; Barigelletti, F.; Campagna, S.; Belser, P.; Zelewsky, A. V. *Coord. Chem. Rev.* **1988**, *84*, 85.

(36) Hara, M.; Waraksa, C. C.; Lean, J. T.; Lewis, B. A.; Mallouk, T. E. *J. Phys. Chem. A* **2000**, *104*, 5275.

(37) Lv, H.; Rudd, J. A.; Zhuk, P. F.; Lee, J. Y.; Constable, E. C.; Housecroft, C. E.; Hill, C. L.; Musaev, D. G.; Geletii, Y. V. *RSC Adv.* **2013**, *3*, 20647.

(38) Evangelisti, F.; Car, P.-E.; Blacque, O.; Patzke, G. R. *Catal. Sci. Technol.* **2013**, *3*, 3117.

Appendix A

Derivation of Equation 4-9:

From the text:

$$Ru^{3+} \xrightarrow{k_2} \text{products} \qquad \textbf{(4-2)}$$

In the presence of WOC four oxidative equivalents of Ru^{3+} are used to oxidize water in **Equation 2-1**.

$$4\,Ru^{3+} + 2\,H_2O \xrightarrow{k_3} 4\,Ru^{2+} + O_2 + 4\,H^+ \qquad \textbf{(2-1)}$$

The simplified mechanism of catalytic water oxidation is given in **Equations 4-4 - 4-8** from **Chapter 4**:

$$Ru^{3+} + cat(0) \xrightarrow{k_4} Ru^{2+} + cat(1) \qquad \textbf{(4-4)}$$
$$Ru^{3+} + cat(1) \xrightarrow{k_5} Ru^{2+} + cat(2) \qquad \textbf{(4-5)}$$
$$Ru^{3+} + cat(2) \xrightarrow{k_6} Ru^{2+} + cat(3) \qquad \textbf{(4-6)}$$
$$Ru^{3+} + cat(3) \underset{k_{-7}}{\overset{k_7}{\rightleftharpoons}} Ru^{2+} + cat(4) \qquad \textbf{(4-7)}$$
$$cat(4) + 2\,H_2O \xrightarrow{k_8} cat(0) + O_2 + 4\,H^+ \qquad \textbf{(4-8)}$$

where "i" in cat(i) is the number of electrons removed from the resting oxidation state of a catalyst. The first three reactions are assumed to be fast and the [cat(0)], [cat(1)], [cat(2)], [cat(3)], [cat(4)] to be steady state. Under these assumptions and taking into account the mass balance for total catalyst concentration [cat] the rate law of Ru^{3+} consumption is in **Equation 4-9**:

$$\frac{-d[Ru^{3+}]}{dt} = k_2[Ru^{3+}] + \frac{4k_8k_7[Ru^{3+}][cat]}{(k_7[Ru^{3+}] + k_{-7}[Ru^{2+}] + k_8)} \qquad \textbf{(4-9)}$$

Derivation of **Equation 4-9**:

$$\frac{-d[Ru^{3+}]}{dt} = k_2[Ru^{3+}] + k_4[Ru^{3+}][cat(0)] + k_5[Ru^{3+}][cat(1)] + k_6[Ru^{3+}][cat(2)] + k_7[Ru^{3+}][cat(3)] - k_{-7}[Ru^{2+}][cat(4)] \quad \textbf{(A-1)}$$

Steady state condition with respects to cat(i):

$$i = 1;\ k_4[cat(0)][Ru^{3+}] = k_5[cat(1)][Ru^{2+}] \quad \textbf{(A-2)}$$

$$i = 2;\ k_5[cat(1)][Ru^{3+}] = k_6[cat(2)][Ru^{2+}] \quad \textbf{(A-3)}$$

$$i = 3;\ k_6[cat(2)][Ru^{3+}] - k_7[cat(3)][Ru^{3+}] + k_{-7}[cat(4)][Ru^{2+}] = 0; \quad \textbf{(A-4)}$$

$$i = 4;\ k_7[cat(3)][Ru^{3+}] - k_{-7}[cat(4)][Ru^{2+}] - k_8[cat(4)] = 0 \quad \textbf{(A-5)}$$

From these equations, we obtain:

$$k_8[cat(4)] = k_6[cat(2)][Ru^{3+}],\ k_6[cat(2)][Ru^{3+}] = k_5[cat(1)][Ru^{3+}] = k_4[cat(0)][Ru^{3+}] \quad \textbf{(A-6)}$$

thus,

$$\frac{-d[Ru^{3+}]}{dt} = k_2[Ru^{3+}] + k_7[Ru^{3+}][cat(3)] - k_{-7}[Ru^{2+}][cat(4)] + 3k_8[Ru^{3+}][cat(4)] \quad \textbf{(A-7)}$$

The mass balance with respect to the catalyst gives:

$$[cat(0)]\left(1 + \frac{k_4}{k_5} + \frac{k_5}{k_6}\right) + [cat(3)] + [cat(4)] = [cat] \quad \textbf{(A-8)}$$

where

$$\frac{k_4}{k_5} \approx \frac{k_5}{k_6} \approx 1 \quad \textbf{(A-9)}$$

Equation A-6 can be re-arranged to:

$$[cat(0)] = [cat(4)]\left(\frac{k_8}{k_4[Ru^{3+}]}\right) \quad \textbf{(A-10)}$$

If the reactions 4-4 through 4-6 are fast, or $k_8 << k_4[Ru^{3+}]$, then [cat(4)] >> [cat(0)], [cat(4)] >> [cat(1)], and [cat(4)] >> [cat(2)]. In this case the mass balance in **Equation A-8** is simplified to:

$$[cat(3)] = [cat] - [cat(4)] \quad \textbf{(A-11)}$$

Inserted into **Equation A-5** from above gives:

$$k_7[cat(3)][Ru^{3+}] = k_{-7}[cat(4)][Ru^{2+}] + k_8[cat(4)] \quad \textbf{(A-12)}$$

$$k_7([cat] - [cat(4)])[Ru^{3+}] = k_{-7}[cat(4)][Ru^{2+}] + k_8[cat(4)] \quad \textbf{(A-13)}$$

$$[cat(4)] = \frac{k_7[Ru^{3+}][cat]}{(k_7[Ru^{3+}] + k_{-7}[Ru^{2+}] + k_8)} \quad \textbf{(A-14)}$$

Inserting this into **Equation A-7**:

$$\frac{-d[Ru^{3+}]}{dt} = k_2[Ru^{3+}] + k_7[Ru^{3+}]([cat] - [cat(4)]) - k_{-7}[Ru^{2+}][cat(4)] + 3k_8[Ru^{3+}][cat(4)] \quad \textbf{(A-15)}$$

$$\frac{-d[Ru^{3+}]}{dt} =$$

$$k_2[Ru^{3+}] + k_7[Ru^{3+}][cat] - k_7[Ru^{3+}][cat(4)] - k_{-7}[Ru^{2+}][cat(4)] + 3k_8[Ru^{3+}][cat(4)] \quad \textbf{(A-16)}$$

$$\frac{-d[Ru^{3+}]}{dt} = k_2[Ru^{3+}] + k_7[Ru^{3+}][cat] - k_7[Ru^{3+}]\left(\frac{k_7[Ru^{3+}][cat]}{(k_7[Ru^{3+}] + k_{-7}[Ru^{2+}] + k_8)}\right) - k_{-7}[Ru^{2+}]\left(\frac{k_7[Ru^{3+}][cat]}{(k_7[Ru^{3+}] + k_{-7}[Ru^{2+}] + k_8)}\right) + 3k_8[Ru^{3+}]\left(\frac{k_7[Ru^{3+}][cat]}{(k_7[Ru^{3+}] + k_{-7}[Ru^{2+}] + k_8)}\right)$$

(**A-17**)

Rearrangement of **Equation A-17** produces **Equation A-18** (which is **Equation 4-9** from the text):

$$\frac{-d[Ru^{3+}]}{dt} = k_2[Ru^{3+}] + \left(\frac{4k_8k_7[Ru^{3+}][cat]}{(k_7[Ru^{3+}] + k_{-7}[Ru^{2+}] + k_8)}\right) \quad \textbf{(4-9)}$$